

S U P P L E M E N T O

A L V O L U M E X X I , S E R I E X

D E L


N U O V O C I M E N T O

A C U R A D E L L A S O C I E T À I T A L I A N A D I F I S I C A

1 9 6 1

3° Trimestre

N I C O L A Z A N I C H E L L I E D I T O R E
B O L O G N A



Digitized by the Internet Archive
in 2024

SUPPLEMENTO
AL VOLUME XXI, SERIE X, DEL
NUOVO CIMENTO
A CURA DELLA SOCIETÀ ITALIANA DI FISICA

1961

3° Trimestre

N. 1

**The Track Density of a Charged Particle
in a Photographic Emulsion.**

C. CANDLER

South Australian Institute of Technology - Adelaide

(ricevuto il 22 Marzo 1961)

Summary. — In the track formed by a charged particle passing through a photographic emulsion, the curve relating the number of grains per unit length dN/dR to the rate of energy loss dE/dR is important. R is the residual range, and dN/dR is commonly written g . Hitherto based on experiment alone, this curve is shown to fit the equation of a photographic monolayer, $(s dE/dR)^P = g/(g_s - g)$. Here g_s is the linear saturation density, P the photon number and s the reaction cross-section of a silver halide crystal. Experiment shows that P differs little from unity. The characteristic of a plate exposed to a large number of α -particles fits the Poisson equation $D/D_s = 1 - \exp[-sE]$. This equation has been long accepted, but it is not easily explained.

1. — A track as a monolayer.

In the track formed by a charged particle passing through a photographic emulsion the number of silver grains formed per unit path length dN/dR is a much studied quantity, for it provides a key to the mass, charge and velocity of the particle. Here R is the residual range, and dN/dR is commonly written g .

g is determined by the rate dE/dR at which the incident particle loses energy in passing through the emulsion. Curves relating dN/dR and dE/dR have been published for two nuclear emulsions Kodak NT4 and Ilford C2 ^(1,2)

⁽¹⁾ G. F. POWELL, P. H. FOWLER and D. H. PERKINS: *The Study of Elementary Particles by the Photographic Method* (1959).

⁽²⁾ C. E. K. MEES: *The Theory of the Photographic Process* (1954), p. 307.

but no one seems to have noticed that in theory each curve is the characteristic of a monolayer, or that both fit the exposure equation of a Schumann's plate:

$$(1) \quad (sE')^P = D/(D_s - D).$$

Here D is the density produced by an exposure E' in photons per unit area, s is the reaction cross-section of a silver halide crystal, and the photon number

P is the number of photons required to fertilize a crystal.

First noticed ⁽³⁾ as describing the grain counts of SHEPPARD, TRIVELLI and LOVELAND ⁽⁴⁾, this equation is now recognized as covering a wide field ⁽⁵⁾. For not only does it describe the characteristic of a Schumann's plate recorded by BAKER ⁽⁶⁾ at several wavelengths between 197 and 480m μ , but also the X-ray characteristics of a normal coating (Fig. 1, Table I) recorded by BROILLI and KIESSIG ⁽⁷⁾. More important in the present context, it describes the characteristic of a Schumann's plate exposed to high speed electrons (Fig. 2, Table II) by BECKER and KIPP-

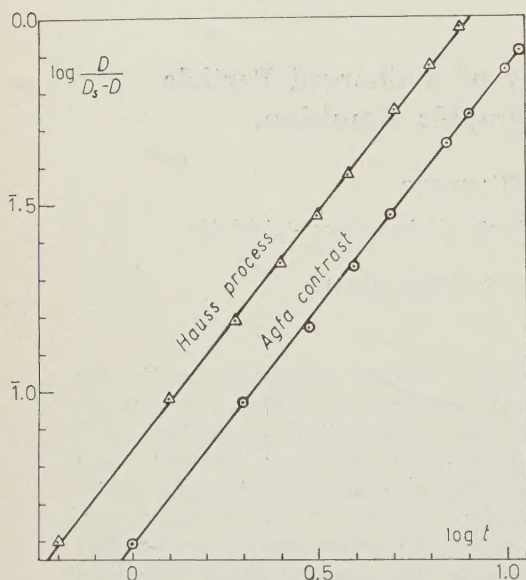


Fig. 1. - Two plates, Agfa Contrast and Hauss Process, exposed to X-rays of wavelength 1.54 Å by BROILLI and KIESSIG in 1934.

TABLE I. - Parameters of two plates exposed to X-rays of wavelength 1.54 Å by BROILLI and KIESSIG. The fog and saturation densities were not recorded, and the values chosen are those which best make $\log \{D/(D_s - D)\}$ linear.

	D_s	D_f	P
Agfa contrast	2.3	.014	1.27
Hauss Process	3.3	.023	1.27

⁽³⁾ C. CANDLER: *Austral. Journ. Phys.*, **13**, 419 (1960).

⁽⁴⁾ S. E. SHEPPARD, A. P. H. TRIVELLI and R. P. LOVELAND: *Journ. Franklin Inst.*, **200**, 51 (1952).

⁽⁵⁾ C. CANDLER: *Zeits. Wiss. Phot.*, in press.

⁽⁶⁾ E. A. BAKER: *Proc. Roy. Soc. Edinburgh*, **48**, 118 (1928).

⁽⁷⁾ H. BROILLI and H. KIESSIG: *Zeits. Phys.*, **87**, 425 (1934).

HAN⁽⁸⁾. A charged particle fertilizes a photographic plate chiefly by producing high speed electrons⁽¹⁾, so the law which describes high speed

TABLE II. — *The parameters of a Schumann's plate exposed to high speed electrons by BECKER and KIPPHAN in 1931. The fog and saturation densities were not recorded.*

kV	D_s	D_f	P	$\log s$
18	4.5	.06	1.37	2.38
29	4.5	.02	1.37	2.85
39	4.5	.13	1.37	2.94
54	4.5	.14	1.37	2.96

electrons should logically describe the track of an ionized particle. In a track the exposure reaching a crystal is equal to the rate at which the incident particle loses energy, so the photographic exposure E' of eq. (1) is properly replaced by dE/dR ; while in unit length of track the fraction of the crystals fertilized is g/g_s , where g_s is the saturation density or the number of crystals fertilized on long exposure, so g/g_s replaces D/D_s :

$$(2) \quad (s \, dE/dR)^P = g/(g_s - g).$$

The experimental proof of this law is that $\log g/(g_s - g)$ is linear in $\log E$ in both the nuclear emulsions studied by POWELL⁽¹⁾ (Fig. 3, Table III). As neither curve reaches saturation, g_s must be obtained by extrapolation, a convenient equation being

$$(3) \quad g_s = \{g_2(g_1 + g_3) - 2g_1g_3\} / \{g_2 - g_1g_3/g_2\},$$

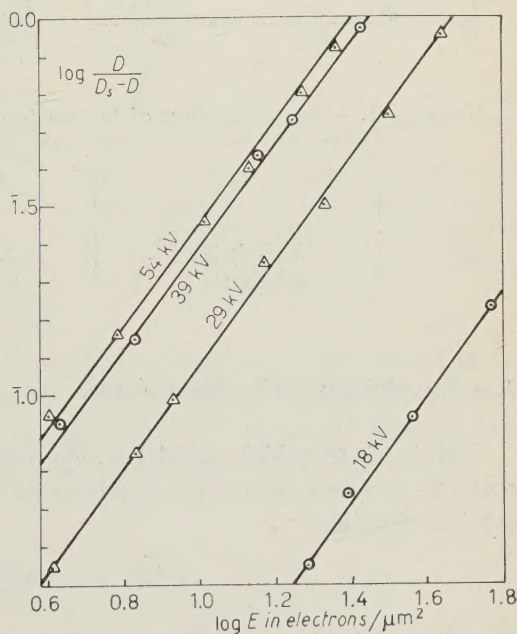
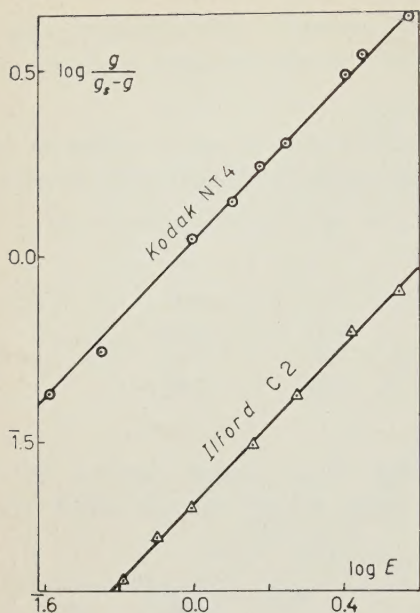


Fig. 2. — A Schumann's plate exposed to high speed electrons by BECKER and KIPPHAN in 1931. The energy of the electrons in kV is written beside each line.

(8) A. BECKER and E. KIPPHAN: *Ann. Phys.*, **10**, 15 (1931).



where g_1 , g_2 and g_3 are the linear densities at points equally spaced along the axis of $\log(dE/dR)$.

In both curves the value of P differs little from unity, and this nicely confirms Powell's ⁽¹⁾ argument that fertilization follows a single absorption.

Fig. 3. - Two nuclear emulsions, Kodak NT4 and Ilford C2, studied by POWELL.

TABLE III. - The parameters of two nuclear emulsion plates studied by POWELL.

	g_s	P
Kodak NT4	2.75	1.05
Ilford C2	2.57	1.04

2. - The alpha-particle characteristic.

The track of a high speed particle must be distinguished from a plate exposed to a large number of α -particles for the characteristic of the latter satisfies the equation

$$D/D_s = 1 - \exp[-sE].$$

Found empirically by KINOSHITA ⁽⁹⁾, and many times confirmed ⁽¹⁰⁻¹³⁾ this is the Poisson equation of an event triggered by a single pulse.

⁽⁹⁾ S. KINOSHITA: *Proc. Roy. Soc. London*, A **83**, 432 (1910).

⁽¹⁰⁾ T. SVEDBERG and H. ANDERSSON: *Phot. Journ.*, **61**, 325 (1921).

⁽¹¹⁾ W. MEIDINGER: *Die theor. Grundlagen der phot. Prozesse* (1932).

⁽¹²⁾ J. H. WEBB: *Journ. Opt. Soc. Amer.*, **38**, 312 (1948).

⁽¹³⁾ C. E. K. MEES: *supra* 180 (1954).

The reason why the α -particle characteristic is to be distinguished from the track cannot lie in the reaction occurring in a single crystal. In any sequence of reactions, however, only the slowest affects the rate, and thus the relationship between the reactants and products; and here the slowest is the arrival of α -particles. Unfortunately this argument seems to imply that a plate exposed to X-rays of sufficiently low intensity should also satisfy the Poisson law, and no experiments are known which support this prediction. Quite the contrary, for when TELLEZ-PLASENCIA ⁽¹⁴⁾ reviewed some eight equations based on the Poisson law, he concluded that none would explain the X-ray characteristics unless it contained a number of arbitrary constants; but just possibly the measurements were made at too high an intensity.

Alternatively one may argue that an α -particle not only produces hundreds of silver atoms in each grain, but fertilizes many grains through secondary electrons. If this is the «event» of Poisson theory, the Poisson law should apply, whatever the internal mechanism. But if this is the reason, should not the Poisson law govern the linear density along a track?

Neither of these explanations is likely to convince the sceptical. While KINOSHITA ⁽⁹⁾ appears to have obtained his curve empirically, later workers probably expected to confirm the Poisson law. Mistakes occasioned by prejudice are not unknown in the history of physics, and as the two curves are closely alike (Fig. 4), they may perhaps have been confused. A fresh experiment would therefore be welcome.

3. - The photon number.

The photon number is the mean number of photons required to fertilize a crystal of silver halide. In the visible P usually lies between 1.8 and 2.4, but values as low as 1.44 in Sheppard's Seed Graflex emulsion and as high as 3.6 in a Kodak B-10 plate are well established.

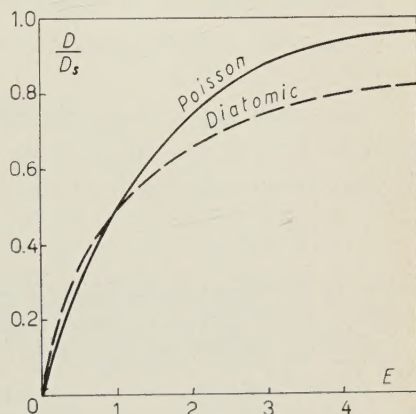


Fig. 4. - The Poisson and diatomic characteristics for $P=1$ with the values of the reaction cross-sections adjusted so that the two curves intersect, when $D/D_s = \frac{1}{2}$.

⁽¹⁴⁾ H. TELLEZ-PLASENCIA: *Sci. Ind. Phot.*, **29**, 297 (1958).

When the frequency of the incident radiation is increased, P is often invariant over an octave or two (^{6,15-17}), but between the ultra-violet and the X-ray region P falls from roughly 2 to roughly unity, presumably because at higher energies one photon produces two trapped electrons, and trapped electrons are the active agents in the reaction process.

Neither in the visible nor in the X-ray region does the evidence suggest that P is precisely integral in any emulsion examined, so there is no justification for supposing that the empirical photon numbers of 1.05 in Kodak NT4 and 1.04 in Ilford C-2 plates differ from unity because of some experimental error.

* * *

I am much indebted to the Director of the Institute, the late Mr. R. W. PARSONS and to the Head of the Physics Department, Mr. G. H. HASKARD for their encouragement in this work.

(¹⁵) C. CANDLER: *Spectrochim. Acta*, **8**, 262 (1956).

(¹⁶) C. CANDLER: *App. Spectroscopy*, **13**, 97 (1959).

(¹⁷) H. J. HÜBNER and H. OHZU: *Zeits. angew. Phys.*, **11**, 460 (1960).

RIASSUNTO

Per la traccia formata da una particella con carica che attraversa un'emulsione fotografica, è importante la curva che esprime la relazione fra il numero di grani per unità di lunghezza dN/dR con il tasso di perdita di energia dE/dR , R è il range residuo e dN/dR è indicato comunemente con g . Si mostra questa curva, sinora basata solo su esperimenti, si adatta all'equazione di un singolo strato fotografico, $(s dE/dR)^P = g/(g_s - g)$. Qui g_s è la densità di saturazione lineare, P il numero di fotoni ed s la sezione d'urto reattiva di un cristallo di alogenuro d'argento. Le prove sperimentali dimostrano che P differisce poco dall'unità. La caratteristica di una lastra esposta ad un gran numero di particelle α segue l'equazione di Poisson $D/D_s = 1 - \exp[-sE]$. Questa equazione è accettata da molto tempo, ma non è facilmente spiegabile.

Optical Measurements on Neon Flash-Tubes.

H. COXELL, M. A. MEYER (*), P. S. SCULL and A. W. WOLFENDALE

Department of Physics, Durham Colleges, University of Durham - Durham

(ricevuto il 1° Aprile 1961)

Summary. — The light output from neon flash-tubes traversed by ionizing particles has been studied under a wide range of experimental conditions. It is shown that there is sufficient reproducibility in the intensity of the light output of the tubes in an array for accurate estimates to be made of the number of tubes flashing from the total amount of light emitted. An obvious application of this technique is to the study of cosmic ray showers (extensive air showers); the need to photograph the array of flash-tubes is removed and the recording of a single pulse from a photomultiplier system is substituted. When used in conjunction with « after-flashing » the photomultiplier method can be used to give an array of flash-tubes some measure of internal selection of events, for example photographs may be taken only when many flash-tubes have been traversed by ionizing particles.

1. — Introduction.

The neon flash-tube was first introduced by CONVERSI and GOZZINI ⁽¹⁾ and developed mainly by CONVERSI and co-workers ^(2,3) and by the Durham

(*) On leave from University of Potchefstroom, Transvaal, South Africa.

(1) M. CONVERSI and A. GOZZINI: *Nuovo Cimento*, **2**, 189 (1955).

(2) M. CONVERSI, S. FOCARDI, C. FRANZINETTI, A. GOZZINI and P. MURTAS: *Suppl. Nuovo Cimento*, **4**, 234 (1955).

(3) G. BARSANTI, M. CONVERSI, S. FOCARDI, G. P. MURTAS, C. RUBBIA and G. TORELLI: *Proc. Geneva Conference* (1956).

group (⁴⁻⁶). It consists of a glass tube, filled with neon gas to a pressure of the order of an atmosphere, which is mounted between parallel conducting electrodes. If a high voltage pulse is applied across the electrodes within a few microseconds of the traversal of the tube by an ionizing particle then there is a high probability that the tube will emit a flash of light. This flash, having the wavelength of the predominant red neon lines, has sufficient intensity to be easily seen by the naked eye or recorded by a photographic plate. A knowledge of the characteristics of the flash of light—its intensity and duration—are important both from the point of view of our understanding of the mechanism of the operation of the flash-tube and for possible applications of optical measurements to specific experiments. The most obvious application is to use a photomultiplier to integrate the intensity of light from an array of tubes and to give an output pulse accurately related to the number of discharged tubes.

The measurements made on the flash-tubes can be divided into two main groups: those dealing with the properties of single tubes and those concerned with the properties of arrays of tubes. In the first group there are such measurements as the variation in intensity from one pulse to the next, the polar diagram and the variation with parameters of the pulse. To some extent the properties of arrays of tubes can be predicted from the behaviour of single tubes but there are also problems peculiar to the case of arrays. These problems, which have a bearing on the application of optical measurements, will be discussed in detail.

2 - The experimental arrangement.

The arrangement consisted of a light-tight container in which was mounted the tube (or tubes) and the photo-multiplier system. This latter comprised an EMI photo-multiplier, Type 6095, followed by a cathode-follower; the pulses were recorded on a Solartron Oscilloscope (Type CD 643.5 or 513.2). Accurate measurements of the polar diagram were afforded by using distances between the flash-tubes and the multiplier of up to 4 m.

The tubes used in the measurements were of internal diameter 1.5 cm, wall thickness 1 mm and of two lengths: 115 cm and 27 cm. The gas filling was commercial neon (see COXELL *et al.* (⁶), referred to as I) to a pressure of 65 cm. These tubes were specially developed for experiments on extensive

(⁴) M. GARDENER, S. KISDNASAMY, E. RÖSSLE and A. W. WOLFENDALE: *Proc. Phys. Soc.*, B **70**, 687 (1957).

(⁵) F. ASHTON, S. KISDNASAMY and A. W. WOLFENDALE: *Nuovo Cimento*, **8**, 615 (1958).

(⁶) H. COXELL and A. W. WOLFENDALE: *Proc. Phys. Soc.*, **75**, 378 (1960).

air showers and their properties will be described in detail by COXELL *et al.* (to be published).

A radioactive source (10 mc ^{60}Co) was used to provide the initiating ionization in the case of measurements on single tubes. For the measurements on the array of tubes cosmic rays were used; these were selected by a 4-fold Geiger telescope consisting of a pair of crossed counters above the array and a pair below.

The high voltage pulsing system was of the type described in I. For most of the work the pulse applied to the plates was derived from a circuit in which a single condenser was discharged through a trigatron and the resulting pulse amplified by a pulse transformer. The magnitude of the pulse was varied by varying the tapping on an impedance connected across the output of the pulse transformer.

The lack of linearity of the multiplier system was found by various standard procedures and an accurate calibration curve determined.

3. — The characteristics of single tubes.

Of the many factors affecting the intensity of the flash, only the more important have been studied. These are: the position along the length of the tube of the trajectory of the ionizing particle, the magnitude of the applied high voltage pulse, and the angle with respect to the axis of the tube at which the intensity is measured. Also included are the variation in intensity from one tube to another and the variation for one tube from one pulse to the next.

3'1. The position of the ionizing particle. — The form of the discharge was studied by operating in the counter telescope a composite array of tubes in which unpainted tubes were placed at right angles to a normal array of painted tubes. Plate I shows two photographs taken with this arrangement. The layers of tubes above and below the unpainted tubes give the direction of the «triggering» particle and the two unpainted tubes show the pattern of the discharge. It will be seen that the discharge takes the form of streamers and it is found that these streamers occupy the whole of the length of the tube between the electrodes. A feature of some interest is the absence of any obviously brighter streamer in the immediate region of the particle trajectory.

The latter observation differs from that of FUKUI and MIYAMOTO (private communication), who observed a bright discharge column on the path of the particle. This difference, which is thought to arise from differences in pulse characteristics, will be discussed in a later paper which will examine the mechanism of the discharge in some detail.

Studies have also been made of the discharge using a radioactive source. In particular the intensity of the flash emitted through the end window of a normal painted tube has been found as a function of the position of the source along the tube. An interesting result is that there is a variation, amounting to 22 % difference in intensity when the source is at one end of a 115 cm tube and then at the other, the intensity being higher when the source is at the far end. This result indicates that the discharge is brighter in the region of the

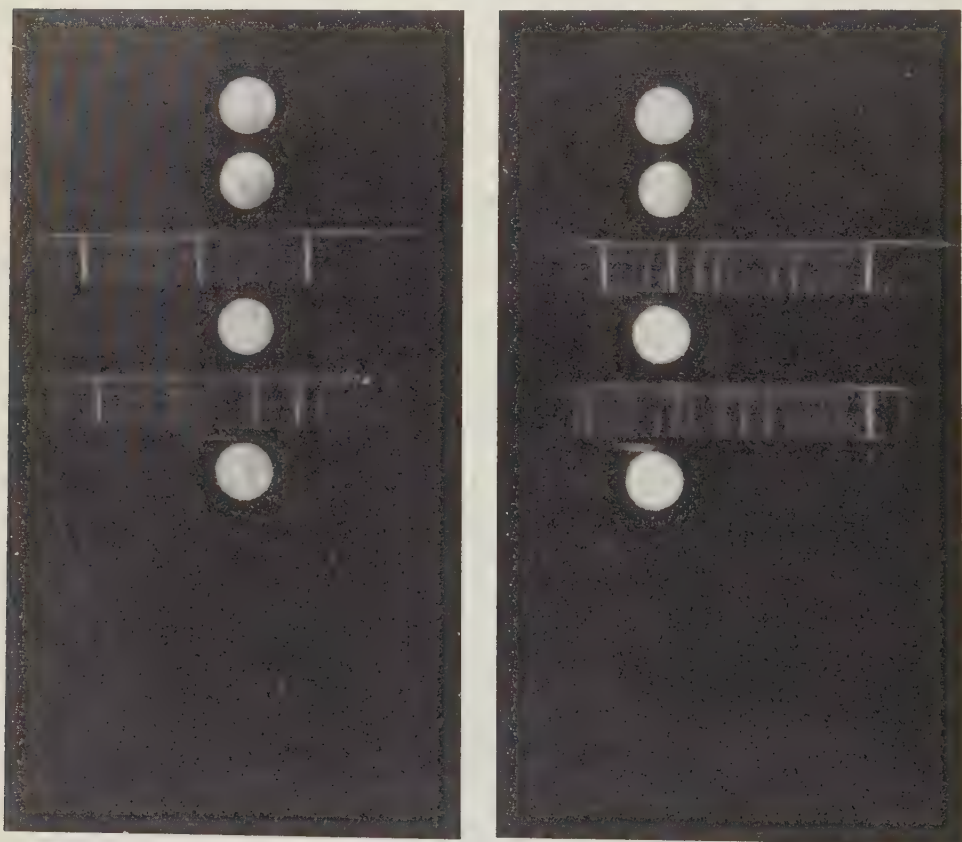


PLATE I. - Photographs of the discharges.

source and that an enhancement in intensity arises from internal reflexions, which are more effective when the source is at the far end of the tube.

The variation in intensity is too small for it to be used in practice to indicate the position of the trajectory with any precision. Likewise, the uncertainty in our other results arising from this effect is very small, particularly so for the radioactive source measurements where the source was always placed in a standard position.

3'2. *The variation in intensity from one pulse to the next.* — This variation is obviously of importance for, if large fluctuations in intensity occur for a single tube, there is no prospect of making useful quantitative observations on the light output of arrays of tubes.

The longer tubes were used for this investigation and many measurements of the pulse height from the photo-multiplier were made on each of 45 tubes. The differences from the mean for each tube were found and all the differences were combined to give the distribution shown in Fig. 1. It will be noted that the differences between the means of each tube are not included; a discussion of these is given in Section 3'3. Many tubes were taken so that a truly representative distribution should be found.

After correction for the error in measuring the pulse heights the standard deviation (σ_1) of a single reading from the mean is found to be 5.1%.

The variation in the actual intensity of the flash is presumably appreciably less, and perhaps much less, than this, since σ_1 includes « noise » from other sources, such as variations in gain of photomultiplier, oscilloscope and amplifiers.

No detectable change in σ_1 was found for variations of the interval of time between pulses, above about 2 s. Measurements were not made below 2 s.

It is concluded that the discharge mechanism is essentially reproducible and that quantitative use of light intensity measurements should be possible.

3'3. *The variation in intensity from one tube to the next.* — Constancy of intensity for a particular tube from one pulse to the next is not sufficient if there are big variations amongst the tubes. Variations are expected to arise from differences in the « quality » of the end window of the tube, which affects the amount of light emerging from it, and differences in gas filling. The mean intensity was found for each of 45 tubes taken from 6 different batches. By batch of tubes is meant a group of tubes (usually 60) filled at the same time on the high vacuum system. The results are shown in Fig. 2.

It is evident that there is a significant variation between batches as well as a variation within a batch. The resulting standard deviation for all the tubes from the overall mean is calculated to be

$$\sigma_2 = 17 \% .$$

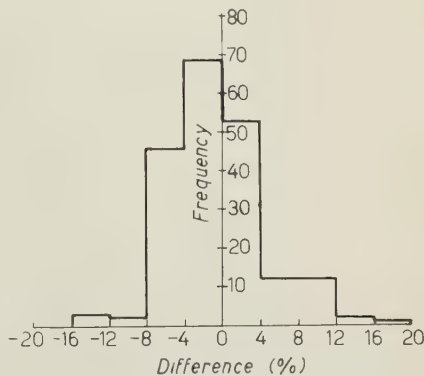


Fig. 1. — Pulse to pulse variation.

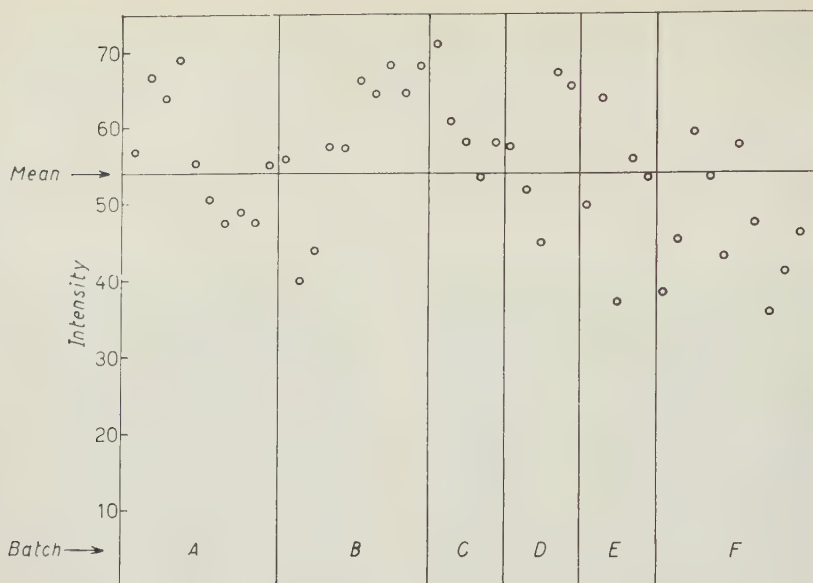


Fig. 2. - Variation of intensity from tube to tube.

This value could no doubt be reduced by using greater care in the glass blowing and filling technique but for most applications σ_2 is not too large.

3.4. *The polar diagram.* - In a practical arrangement using the photo-multiplier method to select events a multiplier will be «looking» at an array

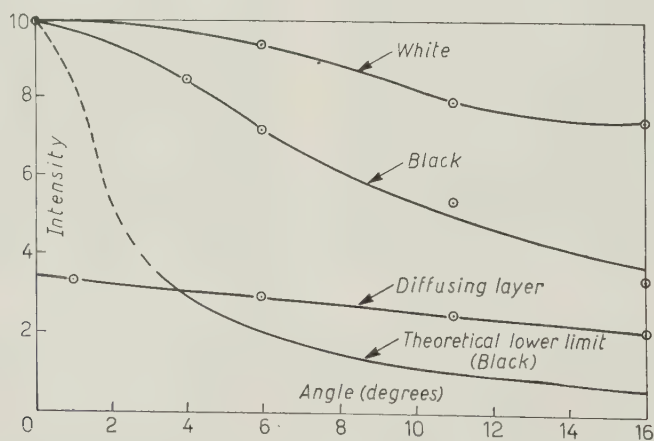


Fig. 3. - Polar diagram for short tube.

of tubes and the recorded light from each tube will make a different angle to the tube axis. Measurements were made of the polar diagram in the plane

perpendicular to the direction of the field (horizontal plane) for both short and long tubes with the results shown in Fig. 3 and 4. The geometrical arrangement is shown in the inset of Fig. 4. The separation of the photomultiplier and tube, d , was made sufficiently great for the smearing of the distribution, due to the finite angle subtended by the photocathode, to be small. Thus for the long tube a value of $d = 425$ cm was used.

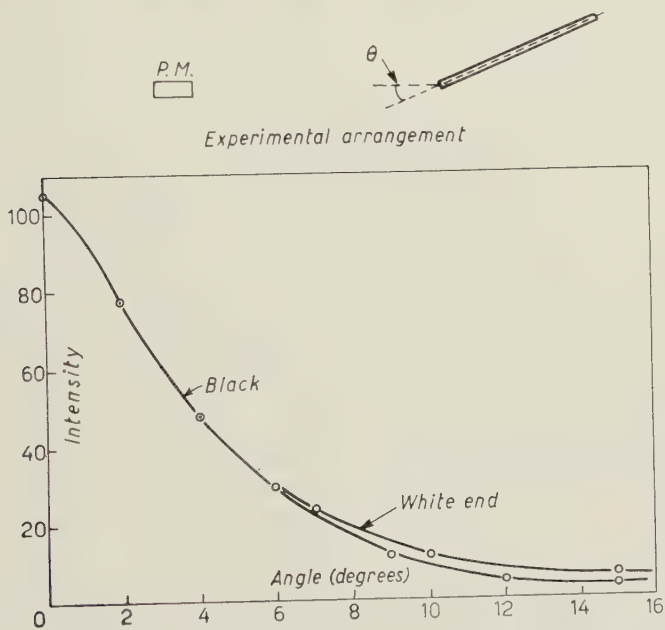


Fig. 4. - Polar diagram for long tube.

As might be expected the fall-off in intensity with angle is quite rapid, particularly for the long tube. A similar, though rather less rapid, fall-off was found in the vertical plane. This presumably arises from the fact that the elementary discharges (Plate I) are vertical streamers and therefore have themselves polar diagrams showing a less marked variation in the vertical direction.

A lower limit to the expected variation can be determined by disregarding the filamentary character of the discharge and assuming a uniform cylinder of emitting gas. Further assumptions are that reflexions and self-absorption are unimportant. The variation in intensity is then given by

$$I_{\theta}/I_0 = V_{\theta}/V_0,$$

where V_0 is the volume of the cylinder and V_{θ} is the volume visible through the circular window when viewed at the angle θ . It can easily be shown that

$$V_{\theta}/V_0 = (4/3\pi)(r/l) \operatorname{ctg} \theta \quad \text{for } \theta > \theta_0,$$

where $2r$ is the internal diameter of the tube and $2l$ is the length between the electrodes, assuming, as is always the case, that the front of the tube is flush with the front of the electrodes.

The theoretical variation, normalized to the intensity at $\theta = 0^\circ$ is shown in Fig. 3 for the short tubes. The observed intensity is obviously much greater than the « theoretical » value and reflexions are presumably mainly responsible. The effect of reflexion can be increased further, and the polar diagram improved, by painting the outside of the tube white. The result for a short tube, painted white along its entire length, is shown in Fig. 3. At angles above 5° most of the enhancement presumably comes from the first 20 cm of the tube and the long tubes used in studies of extensive air showers were stripped of black paint for this length and painted white, with a further overlying coat of black to prevent the transmitted light from discharging adjacent tubes. The result is shown in Fig. 4. The improvement amounts to about 50% at $\theta = 12^\circ$. This is a useful factor for photographic recording but the resulting distribution for the long tubes is still too sharply peaked if photo-multiplier measurements are to be made on an array with a maximum angle of 10° or so.

A big improvement in polar diagram results from the use of a translucent diffusing surface; a thin layer of tissue paper on the front of the tube gives polar diagrams of the form shown. The reduction in forward intensity is not important for photomultiplier measurements since the absolute intensity is still high.

3.5. *Variation of the light output with field strength.* — Of the parameters of the high voltage pulse likely to vary in practice the height is the most important. Studies have accordingly been made of the variation of intensity at a particular angle ($\theta = 0^\circ$) with field strength. The results for the long tubes are shown in Fig. 5. Those for the short tubes are very similar.

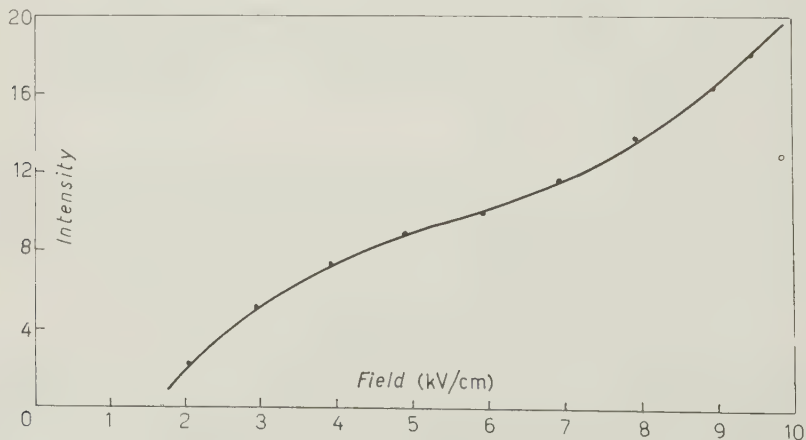


Fig. 5. — Variation of intensity with field strength.

The variation in light output at low field strengths is rather similar to that of pulse height in a Geiger counter. There is an initial region where the intensity (counter pulse height) is proportional to the field strength above threshold, followed by a falling rate of rise. At field strengths above 6 kV/cm, however, the rate of rise increases for the flash-tube.

3'6. After-flashing characteristics. — By «after-flashing» is meant the repeated flashing of a tube under a succession of high voltage pulses. This phenomenon is useful in that it gives an array of tubes a «memory». Thus, selection of events could be made on the basis of the number, or geometry, of flashed tubes occurring under the first high voltage pulse and a camera shutter opened and a second pulse applied only for the selected events.

The probability of a tube flashing a second time has been found as a function of the time interval between the pulses. An array of flash-tubes was controlled by the Geiger telescope and pairs of photographs were taken with a stereoscopic camera. One lens of the camera was covered by a solenoid-operated shutter which was opened between the two high voltage pulses. Thus one photograph showed only those flashes that occurred when the second pulse was applied and the other showed flashes from both pulses. The results of this experiment are shown in Fig. 6; the «half-life» is seen to be about 90 ms.

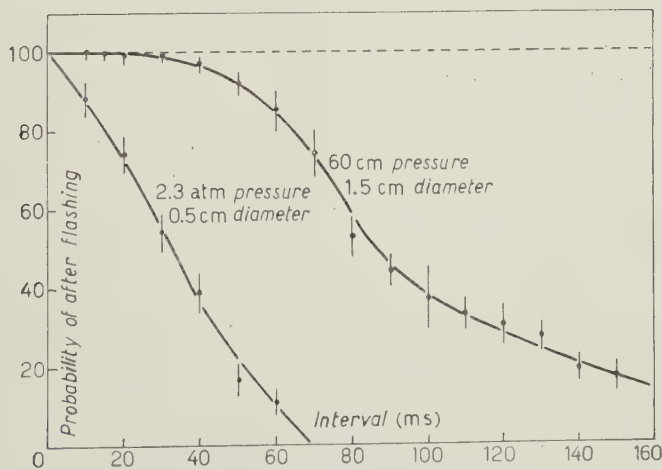


Fig. 6. — After-flashing probabilities.

Since the after-flashing probability has a bearing on the mechanism of the flash-tube, measurements were also made on tubes of another diameter and pressure. These are shown in Fig. 6.

4. - The detailed structure of the light pulse.

4.1. *The profile of the light pulse.* - Measurements were made of the variation of the intensity of the flash with time *i.e.* the profile of the light pulse. These measurements were made for both high voltage pulses derived from single condenser discharges and from a delay line via a hydrogen thyratron.

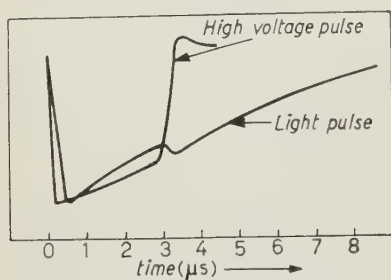


Fig. 7. - Profiles of pulses.

The latter circuit produces a nearly rectangular voltage pulse and these results will be considered since they are more fundamental. The results for a rectangular high voltage pulse of $3\ \mu\text{s}$ duration are shown in Fig. 7. The intensity is seen to rise rapidly to a maximum value and then fall with a time constant of some $5\ \mu\text{s}$, the fall being interrupted at the instant of cessation of the voltage pulse.

There are several effects which can contribute to the lengthening of the light pulse. These are: thermal relaxation, emission during recombination of positive and negative ions and metastable atoms. Similar « after glows » have been observed by CRAGGS and MEEK⁽⁷⁾ for sparks passing between metal electrodes in different gases. These authors attributed the after glow in argon to the effect of metastables and it is likely that this is the main cause here in the case of neon.

Confirmation comes from the work of JESSE and SADAUSKIS⁽⁸⁾ which shows that the half-life of metastable neon atoms is $7.5\ \mu\text{s}$ at one atmosphere pressure. A more detailed comparison is not possible since the light profile has a large initial contribution from non-metastable atoms and in addition the half-life given above may not be strictly applicable to the type of discharge considered here.

A possible explanation of the second peak in the light profile is that when the applied voltage is removed, electrons, which were held on the glass wall by the pulse, return to the gas and cause an increase in the rate of recombination and hence emission of photons.

4.1 *The number of photons emitted in the light pulse.* - An attempt has been made to estimate the number of photons emitted in the discharge in two ways—using photographic and photomultiplier techniques.

In both methods the intensity of the flash is measured on the axis of the

(7) J. D. CRAGGS and J. M. MEEK: *Proc. Roy. Soc., A* **186**, 241 (1946).

(8) W. P. JESSE and J. SADAUSKIS: *Phys. Rev.*, **100**, 1755 (1955).

tube. It is reasonable to assume that reflexions do not contribute appreciably to the intensity on the axis so that the total number of photons emitted is $4\pi N_0$, where N_0 , the number emitted per unit solid angle, is determined from the forward intensity.

With the photographic method N_0 is found from a knowledge of the number of photons required to give the degree of blackening on the photographic film. The result, which has only order of magnitude accuracy, is that the number of photons emitted when a pulse of 7 kV/cm is applied is 10^{12} for the case of a tube between 25 cm electrodes. This corresponds to $2 \cdot 10^{10}$ photons/cm³.

The photomultiplier method is rather more accurate. This relies on a knowledge of the calibration in terms of pulse height per photon incident on the photocathode, and the number of photons in the pulse was derived from the area under the pulse profile (Fig. 7). The result is a value close to 10^{12} photons for the whole tube under the same conditions as for the photographic method. The consistency of the two estimates is reassuring.

5. — The characteristics of arrays of tubes.

5.1. *Reasons for studying the characteristics.* — A study of the optical properties of arrays of tubes gives little information towards our understanding of the mechanism of the flash-tube but it is important if an application of the photomultiplier method to selection of events is envisaged. As mentioned in the Introduction an obvious application is to the field of extensive showers. If it could be arranged that the output pulse of the photomultiplier be accurately related to the number of discharged tubes then, for example, the density spectrum of showers could be studied by recording the pulse heights on a pulse height analyzer.

At present, most studies of showers are made using scintillation counters or Čerenkov detectors. Scintillation counters have a limitation, however, in that they determine essentially the energy lost by particles in the scintillator material and not the number of particles directly. Thus the signal from one slow proton cannot be distinguished from that from many fast electrons. Similarly, Čerenkov detectors have a disadvantage: the thickness necessary to give a signal of sufficient magnitude is usually so great (*e.g.* 50 cm water) that there is significant interference with the particle flux being measured. Thus, low energy electrons are absorbed and γ -rays converted, and the relationship between the output signal and the number of particles is not linear. With an array of flash-tubes however, provided that the density of particles is not so high that the statistical correction, introduced by the probability of more than one particle passing through a tube, is not too great, a closer relationship exists between output signal and number of particles. Up to

now the objection to the use of flash-tubes has been the need to photograph the flashes and the consequent time of analysis in counting up the number of flashes. The proposed method eliminates this difficulty

5'2. *Factors affecting the characteristics.* — The intensity of the integrated flash of light from an array of tubes is not uniquely related to the number of tubes discharged for the reasons discussed in Section 2, *e.g.* the irreproducibility from tube to tube and pulse to pulse. Further, the intensity of the integrated flash is not proportional to the number of discharged tubes because of the finite output impedance of the circuit producing the high voltage pulse. Thus, the intensity of the single flashes falls as the number of discharged tubes increases. It is therefore necessary to perform experiments on practical arrays of tubes, the object of which is to find the accuracy with which a single measurement of pulse height gives the number of tubes discharged. The results of these experiments will be described in the next section.

5'3. *The variation of integrated intensity with number of discharged tubes.* — An array of 25 long tubes, 5 layers of 5 tubes in each, was operated in an electrode system of length 25 cm and triggering pulses were derived from a simple counter system which selected cosmic ray showers. The flashes were

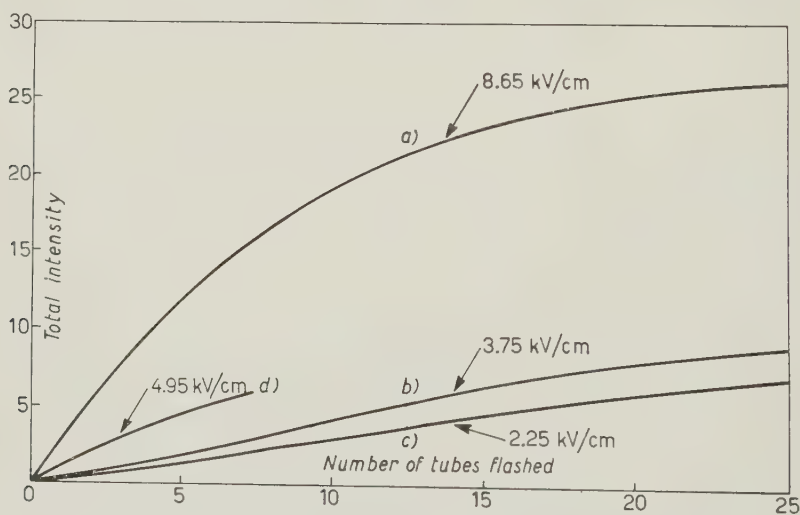


Fig. 8. — Variation of intensity with number of tubes flashed.

photographed and a separate camera recorded the height of the pulse from the photo-multiplier.

The first observations were made with the normal high-voltage system in which the high-voltage pulse applied to the electrodes is derived from a tapping

on the impedance across the output of the pulse transformer. The variation of integrated light intensity with number of discharged tubes is shown in Fig. 8, curve (a). It is noticeable that a departure from linearity sets in at a very small number (4) and that at high numbers the rate of increase is very small. This small rate of rise, coupled with the inherent fluctuations in the intensity, means that the accuracy with which a single photomultiplier pulse defines the number of discharged tubes is low.

As would be expected, an improvement arises if the output impedance of the high voltage pulse generator is reduced. Measurements were taken without the pulse transformer and using a very low terminating impedance; the results are shown in Fig. 8, curves (b) and (c). The linearity is seen to be greatly increased and it is thought to be adequate for most applications.

It should, in principle, be possible to select events in which more than n tubes had flashed by demanding that the intensity of the flash (from the height of the photomultiplier pulse) should be greater than an appropriate value. This value would be the intensity, Fig. 8, corresponding to $n + \frac{1}{2}$ tubes. In fact, due to the various fluctuations already discussed, some events with fewer than n tubes will be selected and some with more than n will be missed.

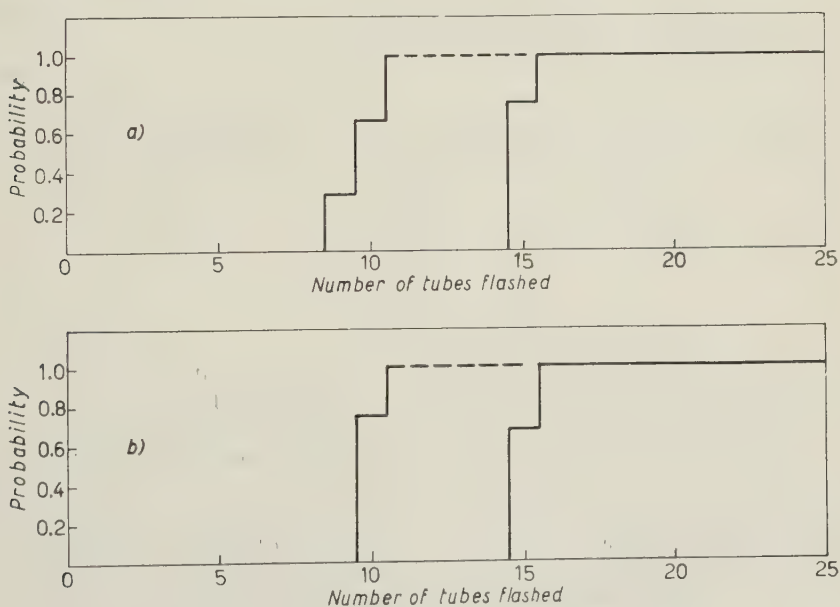


Fig. 9. - The discriminator characteristics.

Fig. 9 shows the histograms found for $n=9$ and 14 with the array operated under the conditions represented by Fig. 8 (b) and (c). It is immediately apparent that the form of these discriminator characteristics is quite satisfactory.

5'4. *Application of optical measurements to studies of extensive air showers.* —

The experiments described have shown that a measurement of the intensity of the flash of light from an array of flash-tubes is an accurate measure of the number of tubes flashing. Use can be made of this either by eliminating the photographic recording of the flashes completely and recording only pulse heights from a photomultiplier or by using the photomultiplier as a selection device and photographing only events having more (or less) than a particular number of discharged tubes. In the latter method a succession of high-voltage pulses would be applied and a camera shutter would be operated by the selection device.

The biggest problem in applying the technique is to allow for the sharply peaked polar diagram of the tubes. It seems likely that the best solution is to work with a considerable path length (via mirrors) and cover the front of the tubes with a translucent material.

* * *

The authors wish to thank Professor G. D. ROCHESTER F.R.S., for the facilities of his laboratory and for his interest in the work. We are grateful to Drs. M. G. THOMPSON and J. L. LLOYD for many useful suggestions.

One of us (M.A.M.) wishes to thank the Nuffield Foundation for the award of a Fellowship and the South African Council for Scientific and Industrial Research for a bursary.

Two of us (H.C. and P.S.S.) are grateful to the Department of Scientific and Industrial Research for the award of a Research Studentship and an Advanced Course Studentship, respectively.

The authors are indebted to the Council of the Royal Society for the award of a grant to support this work.

RIASSUNTO (*)

Abbiamo studiato, in un vasto campo di condizioni sperimentali l'emissione di luce dei tubi di scarica al neon attraversati da particelle ionizzanti. Mostriamo che l'intensità della luce emessa da una batteria di tubi è riproducibile in modo sufficiente per potere eseguire stime accurate del numero di tubi che si accendono, in base alla quantità totale di luce emessa. Un'ovvia applicazione di questa tecnica si può fare allo studio degli sciami di raggi cosmici (sciami estesi dell'aria): la necessità di fotografare la batteria di tubi viene eliminata sostituendole la registrazione di un singolo impulso proveniente da un sistema di fotomoltiplicatori. Se usato in congiunzione con un « doposcarica » il metodo dei fotomoltiplicatori può essere usato per dare ad una batteria di tubi di scarica una qualche misura di una selezione interna di eventi, per esempio si possono far prendere fotografie solo quando molti tubi di scarica sono stati attraversati dalle particelle ionizzanti.

(*) Traduzione a cura della Redazione.

On the Application of the Nuclear Emulsion Technique to the Study of Complex Electron Conversion Spectra.

A. M. CARTACCI, M. G. DAGLIANA and L. TOCCI

Istituto Nazionale di Fisica Nucleare - Sottosezione di Firenze
Istituto di Fisica dell'Università - Firenze

(ricevuto il 6 Aprile 1961)

Summary. — In the course of an investigation on the (n, p) reactions on Ag and Br in nuclear emulsion, energy measurements on the slow conversion electrons were made by blob counting and range determination. The method has proved to be capable of yielding energy values with an uncertainty of $\pm 5\%$ for single measurements. The results on the (n, p) reactions on Ag and Br are also reported. These reactions were identified by their typical appearance in emulsion. The angular distributions of the emerging protons are given; a forward collimation is evident also if we restrict unmistakably to the Ag or Br (n, p) reactions.

1. — Introduction.

In the course of an investigation on the (n, p) reactions on the heavy elements (Ag, Br) of the emulsion we were led to measure the energy of slow electrons by blob counting and range measurements.

We report here the results because the experience we had with this kind of measurements make us feel that the method may find successful application in other cases, whenever the emulsion can be loaded

with a reasonable amount of « parent nuclei » without disturbing its sensitivity.

Our primary purpose was to get angular and energy distribution of protons

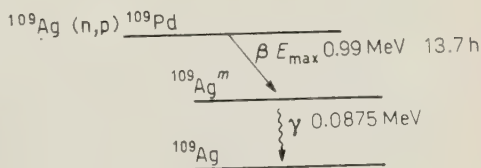


Fig. 1.

produced by (n, p) reaction in heavy elements, identifying unambiguously the target nucleus by means of the characteristic decay products which, in some cases, follow the reaction.

A suitable case appeared to be the $^{109}\text{Ag}(n, p)^{109}\text{Pd}$ reaction, which is followed by the decay shown in Fig. 1.

The typical appearance of an event of this kind is given in Fig. 2; there



Fig. 2.

is no doubt that no reaction on the light elements can simulate an event of this type. For the other heavy elements the situation is more involved; if,

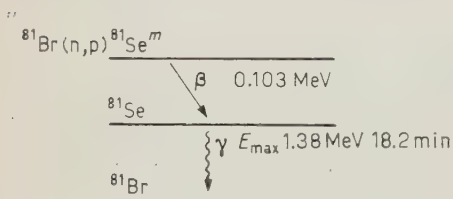


Fig. 3.

for instance, the $^{81}\text{Br}(n, p)^{81}\text{Se}$ reaction leads at least partially, to the $^{81}\text{Se}^m$ isomeric state, according to scheme of Fig. 3, a similar « proton+conversion electron + β^- particle » event could be produced.

In an attempt to distinguish between ^{81}Br and ^{109}Ag reactions we tried successfully energy measurements on the conversion electrons by blob counting and range determination. (Reactions on ^{79}Br and ^{107}Ag are not expected to give similar events.)

2. — Experimental principles of the method.

Nuclear G-5 plates were exposed to 14 MeV neutrons; development was made with an amidol-type developer 24 hours after the exposure of the plates.

As a first step blob number and range were measured for all the conversion electrons (events of the type in Fig. 2) and for an unbiased sample of other slow electrons; the blob number *vs.* range is shown in Fig. 4; the experimental points clearly cluster around a smooth curve.

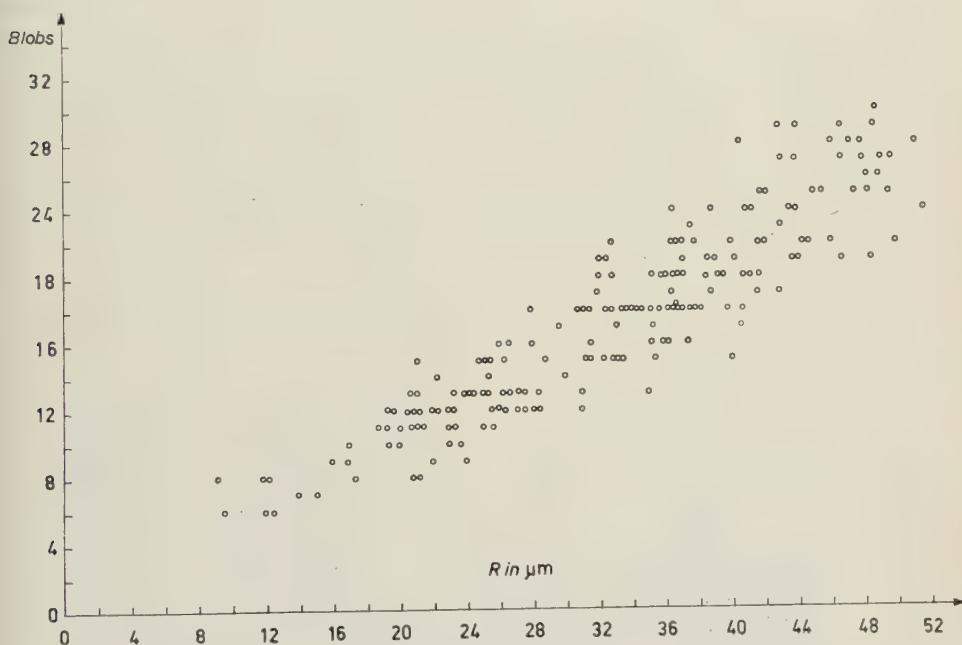


Fig. 4.

By assuming a blob-range relation of the type

$$(1) \quad B = aR^k,$$

we have found $a = 0.316$; $k = 1.142$ as the best fit by a least-square method. Eq. (1) enables us, by using existing energy-range relations, to employ blob number as a convenient parameter for energy measurements. An energy-range relation was proposed by BLUM ⁽¹⁾ and it holds in the energy region (20 ÷ 100) keV

$$(2) \quad R = 2.1 \cdot 10^{-2} E^{1.67} \quad R \text{ in } \mu\text{m}; E \text{ in keV.}$$

⁽¹⁾ J. M. BLUM: *Journ. Phys. Rad.*, **12**, 860 (1951).

More recently another relationship was proposed by DELLA CORTE and BIZZETI ⁽²⁾ for energy up to (70÷80) keV

$$(2') \quad R = 2.1 \cdot 10^{-2} E^{1.72}.$$

From (2) and (2') we obtain the blob-energy relationship (for our plates and development)

$$(3) \quad B = 3.83 \cdot 10^{-3} E^{1.96},$$

$$(3') \quad B = 3.83 \cdot 10^{-3} E^{1.91}.$$

We are now in a position to get two independent values for the energy of conversion electrons from range and blob number; the hystograms of conversion electrons, belonging to the events of type in Fig. 2, are shown in Fig. 5 and 6.

An accumulation of the electrons is clearly apparent in both hystograms around three peaks the widths of which indicate the accuracy of these two

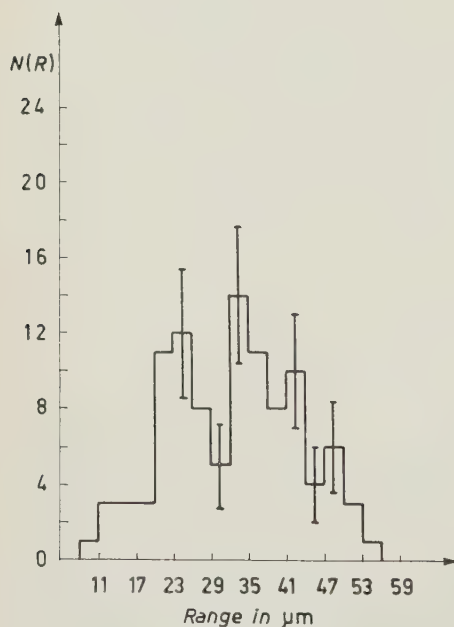


Fig. 5.

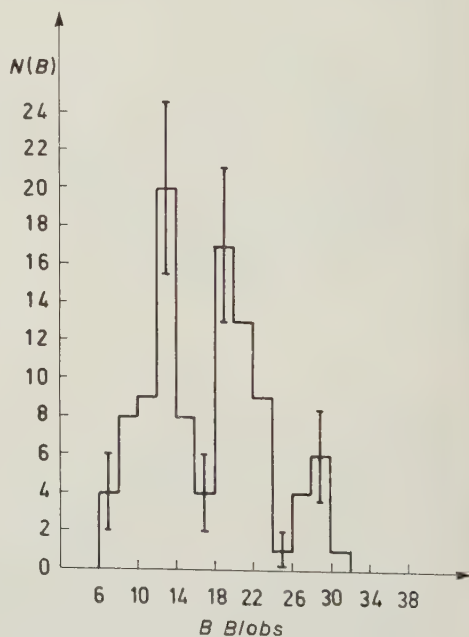


Fig. 6.

measurements (and hence the standard deviations of range and blob distributions, which we think to be normal, around some average value). We can

(2) P. G. BIZZETI and M. DELLA CORTE: *Nuovo Cimento*, **11**, 317 (1959).

now combine the two sets of data to give an unique weighted number-energy distribution, as shown in Fig. 7.

The three peaks are easily accounted for by assigning them to: 1) conversion electrons from the K -shell in ^{109}Ag decay (expected energy 62 keV); 2) $LM \dots$ shells in ^{109}Ag ($(87 \div 87)$ keV) plus ^{81}Se K -shell (90 keV); 3) $LM \dots$ shells in ^{81}Se ($(101.5 \div 103)$ keV), respectively.

The agreement with expected energy values can be considered good in view of the experimental errors and the uncertainty in the range-energy relationship. On the other hand, if the above assignment of the peaks is correct, we can plot the average ranges of the electrons in each peak against the corresponding energy, in an empirical energy-range plot (Fig. 8). The three points so obtained fit well with those obtained by several other workers ⁽³⁻⁷⁾.

The method of range and blob counting, as used in the present experiments, has proved to be capable of yielding energy values with an uncertainty of $\pm 5\%$ for single measurements. These results indicate that it is possible to make measurements on the

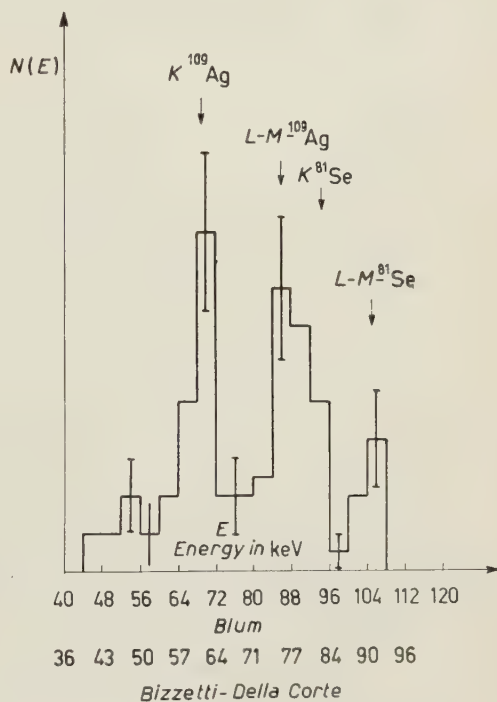


Fig. 7.

slow electrons in emulsion with a good approximation; it appears moreover that even blob counting alone provides a quick and simple method for energy measurements after a calibration has been made once for all for a given stack. The results are also satisfactory because they are obtained under very unfavourable experimental conditions owing to the high and unavoidable slow electron background which increased the difficulties in the measurements and sometimes reduced the precision owing to background electrons which occasion-

(3) M. A. S. ROSS and B. ZAJAC: *Nature*, **164**, 311, (1949).

(4) G. ALBOUY and J. TEILLAC: *Compt. Rend.*, **229**, 435 (1949).

(5) G. ALBOUY and J. TEILLAC: *Compt. Rend.*, **230**, 945 (1956).

(6) R. H. HERZ: *Phys. Rev.*, **75**, 478 (1949).

(7) J. SACTON: *Bull. Classe Sci.*, **11**, 1118 (1956).

ally crossed our conversion electrons. The present results make us confident that the method may be successfully applied to the study of complex nuclear

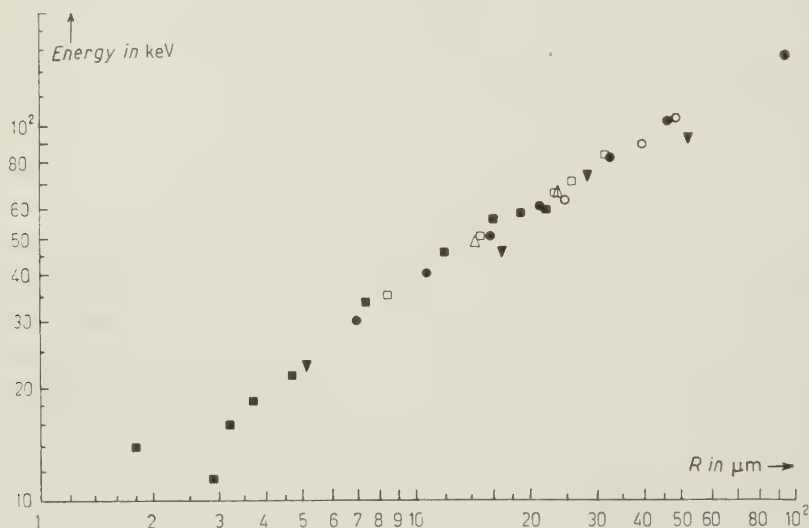


Fig. 8.

disexcitation (if with a good conversion probability) and β -decay of activated nuclei which may be introduced in emulsion in a convenient chemical form.

3. - Some results on the (n, p) reactions.

It seems now worth-while to report also on the results we obtained on the (n, p) reactions on Ag and Br because the method we have used allows to distinguish unmistakably (n, p) from (n, np) and (n, d) reactions which with the ordinary methods are undistinguishable ⁽⁸⁻¹³⁾.

(⁸) D. L. ALLAN: *Nucl. Phys.*, **6**, 464 (1958).

(⁹) D. L. ALLAN: *Nucl. Phys.*, **10**, 348 (1958).

(¹⁰) P. V. MARCH and W. T. MORTON: *Phil. Mag.*, **3**, 1256 (1958).

(¹¹) P. AVIGNON and L. ROSIER: *Compt. Rend.*, **247**, 1849 (1958).

(¹²) L. COLLI, M. PIGNANELLI, A. RYTZ and R. ZURMÜHLE: *Nuovo Cimento*, **9**, 280 (1958).

(¹³) V. V. VERBINSKY, T. HURLIMANN, W. E. STEPHENS and E. J. WINHOLD: *Phys. Rev.*, **108**, 779 (1958).

Unfortunately the present method has revealed itself too cumbersome to accumulate a statistics big enough for detailed energetic distribution of protons in the $\text{Ag}(n, p)$ and $\text{Br}(n, p)$ reactions with 14.8 MeV neutrons. However a significant result can be obtained for the angular distribution of emerging particles.

In Fig. 9 and 10 are shown some distributions respectively for events on silver and bromine and on silver only. In both cases there is evidence of

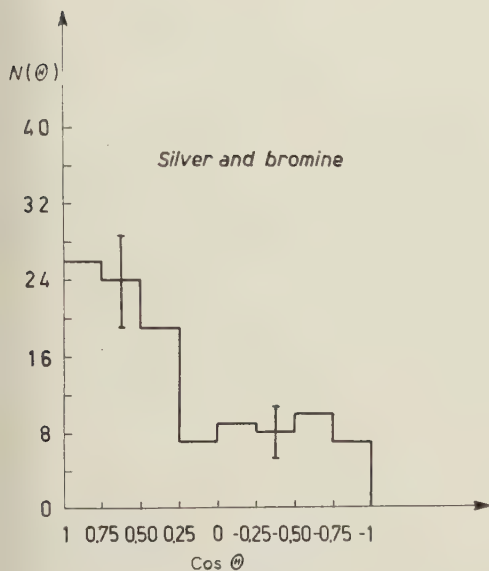


Fig. 9.

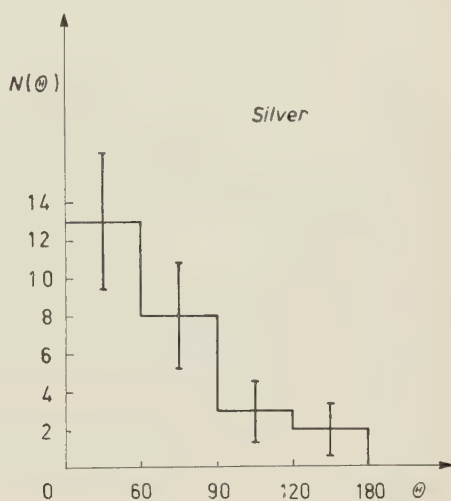


Fig. 10.

a forward collimation (a χ^2 test made on the hystogram shown in Fig. 9 gives an agreement probability with isotropic distribution less than 0.1 %).

There is therefore a direct evidence that the anisotropy in the proton angular distribution, observed by the others workers is still present when we restrict unmistakably to the Ag or Br (n, p) reactions.

* * *

We wish to thank Prof. PUPPI and Prof. PETRALIA of the University of Bologna for kindly allowing the free use of the accelerator.

Thanks are also due to Prof. FRANCHETTI for his continuous interest and to Prof. M. MANDÒ and Prof. M. DELLA CORTE for suggesting this work and for helpful discussions.

RIASSUNTO

Durante uno studio sulle reazioni (n, p) su Ag e Br in emulsione, sono state fatte misure di energia sugli elettroni di conversione per mezzo di conteggi di blob e misure di range. Il metodo si è mostrato capace di fornire il valore dell'energia con una precisione del 5% sulla singola misura. Sono dati anche i risultati ottenuti sulle reazioni (n, p) su Ag e Br. Queste reazioni erano riconosciute dal loro aspetto tipico in emulsione. Vieni data la distribuzione angolare dei protoni emessi. È evidente una collimazione in avanti.

Fotometria dei nuclei pesanti relativistici.

M. G. DAGLIANA, M. DELLA CORTE and L. TOCCI-CECCHI

Istituto Nazionale di Fisica Nucleare - Sottosezione di Firenze
Istituto di Fisica dell'Università - Arcetri (Firenze)

(ricevuto il 17 Aprile 1961)

Riassunto. — Viene studiato il profilo fotometrico delle tracce di nuclei pesanti relativistici. Un modello di traccia costituito da una parte centrale di granuli direttamente impressionati e da una parte periferica in cui l'annerimento è dovuto agli elettroni secondari viene confermato sperimentalmente. Si discute la possibilità di usare la semilarghezza fotometrica come parametro per l'individuazione della carica del nucleo pesante.

Introduzione.

La determinazione della carica dei nuclei pesanti relativistici che costituiscono una parte della radiazione cosmica primaria viene correntemente effettuata con l'osservazione della densità dei raggi δ .

Questa tecnica presenta molteplici inconvenienti dipendenti dalla ben nota difficoltà di identificare e classificare raggi δ di energia maggiore di un certo valore limite così che la determinazione della carica Z risulta fortemente dipendente dall'osservatore e richiede una lunga pratica e un controllo continuo delle convenzioni di conteggio.

È evidente che una tecnica rigorosamente oggettiva come la tecnica fotometrica può presentare un interesse notevole in questo campo di misura.

In alcuni precedenti lavori ⁽¹⁻⁴⁾ abbiamo studiato in particolare la dipen-

(¹) M. DELLA CORTE: *Nuovo Cimento*, **4**, 1565 (1956).

(²) P. G. BIZZETI e M. DELLA CORTE: *Nuovo Cimento*, **7**, 231 (1958).

(³) P. G. BIZZETI, M. G. DAGLIANA, M. DELLA CORTE e L. TOCCI: *Nuovo Cimento* **10**, 388 (1958).

(⁴) P. G. BIZZETI e M. DELLA CORTE: *Nuovo Cimento*, **11**, 317 (1959).

denza della larghezza fotometrica della traccia dai valori di Z e β della particella verso la fine del percorso. Ci proponiamo in questa nota di considerare il problema della dipendenza della larghezza fotometrica dal valore della carica per nuclei pesanti relativistici.

L'apparecchiatura e la tecnica di rilevamento del profilo fotometrico, che sono state descritte in precedenti note ^(1,2), sono qui riassunte in breve.

L'immagine della traccia si forma sul piano di una fenditura ad essa parallela dopo una riflessione su uno specchietto oscillante così che l'immagine stessa si sposta perpendicolarmente alla fenditura.

Il flusso luminoso trasmesso attraverso la fenditura incide sul catodo di un fotomoltiplicatore la cui corrente di uscita, opportunamente amplificata, pilota l'asse y di un oscillografo catodico. Lo spostamento x è pilotato da una tensione oscillante sinerona e in fase con l'oscillazione dello specchietto in modo da ottenere sullo schermo il profilo fotometrico privo di distorsioni.

Spostando micrometricamente la fenditura normalmente alla sua lunghezza, il profilo fotometrico si sposta nella direzione dell'asse x rendendo possibile una misura rapida e diretta della sua larghezza a metà altezza o ad una frazione qualsiasi di questa.

Se si vuol ottenere l'andamento dell'annerimento in funzione della distanza dall'asse, il profilo può essere disegnato per sovrapposizione su una striscia di carta trasparente, e le ordinate in un certo numero di coppie di punti equidistanti dal centro possono essere misurate. I valori ottenuti vengono mediati su un centinaio di profili corrispondenti a segmenti successivi di traccia di lunghezza pari alla lunghezza equivalente della fenditura.

1. - Schematizzazione della traccia di un nucleo pesante relativistico.

È ben noto che il numero di elettroni secondari di energia maggiore di W_0 emessi per unità di percorso da una particella di carica Z è dato da

$$(1) \quad n = k \frac{Z^2}{\beta^2} \int_{W_0}^{W_{\max}} \frac{dW}{W^2}.$$

Questa espressione non tiene conto della correzione relativistica proposta da MOTT ⁽⁵⁾ e ASKIN ⁽⁶⁾ in quanto per valori di $Z \leq 30$ questa può essere trascu-

⁽⁵⁾ N. F. MOTT: *Proc. Roy. Soc.*, A **124**, 425 (1929).

⁽⁶⁾ H. BRADT e P. PETERS: *Colston Papers* (London, 1949), p. 5.

rata essendo inferiore a qualche $\frac{0}{0}$. Quanto al valore dell'energia massima

$$W_{\max} = \frac{2mc^2\beta^2}{1-\beta^2},$$

non si commette grande errore ponendo $W_{\max} = \infty$ perchè il numero di δ diminuisce molto rapidamente con l'energia.

In questa ipotesi possiamo pensare che l'annerimento a distanza x dall'asse della traccia sia dovuto unicamente alla ionizzazione prodotta dagli elettroni secondari di energia maggiore di $W(x)$ cioè di energia tale che il loro percorso superi la distanza x .

In realtà non tutti gli elettroni secondari di energia maggiore di $W(x)$ contribuiranno alla ionizzazione a distanza x sia perchè il loro percorso è fortemente distorto dallo scattering sia perchè la direzione di emissione non è sempre perpendicolare alla direzione di moto del nucleo pesante. Poichè il range vero e la massima distanza raggiunta da un elettrone (gittata) stanno, in prima approssimazione, in un rapporto costante, possiamo pensare che la ionizzazione si mantenga proporzionale al numero di elettroni di energia $\geq W(x)$ almeno nell'intervallo di energia che ci interessa ($W(x) \leq 50$ keV).

Poichè la relazione range-energia per gli elettroni è del tipo

$$x = aw^\alpha$$

dalla (1) si trova che il numero di elettroni secondari di percorso $\geq x$ è dato da

$$n(x) = \frac{kZ^2}{\beta^2} x^{-1/\alpha},$$

e assumendo per α il valore 1.72 ⁽⁴⁾ si ottiene per la ionizzazione a distanza x

$$I(x) = K \frac{Z^2}{\beta^2} x^{-0.581} = K \frac{Z^2}{\beta^2} \varphi(x),$$

con K costante.

Quando si considerano distanze dall'asse della traccia dell'ordine di $0.5 \mu\text{m}$ si deve tener presente che oltre al contributo della ionizzazione dovuto ai δ , l'annerimento è in parte dovuto anche ai granuli impressionati direttamente dal nucleo pesante, granuli che costituiscono il « core » della traccia ⁽⁷⁾. Questo contributo è tanto meno importante quanto più la distanza dall'asse è grande e diviene trascurabile per distanze dell'ordine di 1 o $1.5 \mu\text{m}$ al massimo.

⁽⁷⁾ P. CÜER e J. P. LONCHAMP: *Compt. Rend.*, **236**, 70 (1953).

Una utile schematizzazione può esser fatta introducendo una funzione $h \cdot f(x)$ che chiameremo « ionizzazione equivalente del core » che rappresenta la ionizzazione che dovrebbe esistere a distanza x per produrre un annerimento uguale a quello prodotto dai granuli del « core ».

Questa funzione non è nota *a priori*, ma potremo scrivere che la ionizzazione totale a distanza x è

$$I_0(x) = hf(x) + K \frac{Z^2}{\beta^2} \varphi(x),$$

con h costante di proporzionalità.

Tenendo conto dell'effetto di saturazione, cioè del fatto che al crescere della ionizzazione l'annerimento A tende al valore 1, potremo porre

$$(2) \quad A = 1 - \exp \left[- hf(x) - K \frac{Z^2}{\beta^2} \varphi(x) \right].$$

2. - Risultati sperimentali.

Sono stati rilevati i profili fotometrici di 13 tracce reperite in uno stack di lastre Ilford G-5 esposte a 27 000 metri per 6 ore a 41° di latitudine (Texas flight 1956). Queste tracce sono state selezionate con i criteri normalmente adottati per individuare i primari pesanti della radiazione cosmica (lunghezza $\geq 5 \cdot 10^3 \mu\text{m}$ per lastra senza variazione apprezzabile della ionizzazione o del numero medio di δ ; angolo con la verticale $< 30^\circ$; primari pesanti di interazioni con energia visibile molto elevata, ecc.).

Il taglio del campo magnetico terrestre a 41° di latitudine corrisponde a circa 1.5 GeV/nucleone e quindi ad un valore limite di β di 0.925. Ammetteremo nel seguito che β sia lo stesso per tutti i primari esaminati.

Di ogni traccia è stato rilevato il profilo fotometrico su 100 celle successive di $50 \mu\text{m}$ di lunghezza scelte nella zona centrale dell'emulsione. Per evitare inomogeneità di sviluppo o fenomeni di corrosione sono stati scartati i primi $100 \mu\text{m}$ di spessore verso il vetro e verso l'aria.

Le dimensioni equivalenti della fenditura sul piano della lastra erano $(64 \cdot 0.29) \mu\text{m}$. L'obiettivo usato, un Leitz $\times 22$ a immersione, nelle condizioni di lavoro dava un ingrandimento 62.2. L'illuminazione era ottenuta con una lampada da 50 W con filamento a nastro survoltata per il 25%.

Come indicato nella nota (2), durante il rilevamento i profili venivano normalizzati in altezza assumendo come annerimento 0 l'annerimento a distanza $13.75 \mu\text{m}$ dall'asse.

Poichè il campo esplorato fotometricamente intorno alla traccia risultava abbastanza esteso è stato necessario correggere i profili di annerimento per

eventuali disuniformità di illuminazione. Questa correzione è stata fatta rilevando il profilo fotometrico del fondo dopo aver spostato la lastra perpendicolarmente alla traccia per un tratto di un centinaio di μm . I profili sono stati disegnati su carta trasparente come detto nella sezione precedente.

Come primo controllo dello schema proposto possiamo analizzare i profili fotometrici a distanza dall'asse maggiore di $3\ \mu\text{m}$, cioè quella parte del profilo nella quale certamente non interviene il « core » di granuli direttamente impressionati dal nucleo pesante. Per queste distanze infatti deve essere $f(x) = 0$ e quindi il rapporto

$$R(Z) = - \frac{+\ln(1-A)}{\varphi(x)} = \frac{KZ^2}{\beta^2},$$

deve risultare proporzionale a Z^2 , nell'ipotesi che β sia lo stesso per tutte le tracce.

Poichè i valori di A nell'intervallo considerato sono abbastanza piccoli, quanto abbiamo detto non dipende criticamente dalla forma della funzione di saturazione da noi tentativamente assunta come esponenziale.

I valori di $(R(Z)\beta^2/K)^{\frac{1}{2}}$, calcolati per ciascuna traccia nei punti a distanza 3.44, 4.58, 6.88 μm dall'asse assumendo per β^2/K il valore di $1.048 \cdot 10^{-2}$ sono riportati in Tabella I.

TABELLA I.

Tr. n°.	$(R(Z)\beta^2/K)^{\frac{1}{2}}$	Z	Tr. n°.	$(R(Z)\beta^2/K)^{\frac{1}{2}}$	Z
10	3.3	Z=3	15	4.98	Z= 5
4	2.83				
13	2.83				
14	2.88				
3	4.01	Z=4	6	6.4	Z= 6
8	3.90		2	5.95	
			11	6.05	
12	4.26				
			1	9.92	Z=10

Nella Fig. 1 abbiamo riportato i valori medi di $-\ln(1-A)/Z^2$ in funzione di x .

Come si vede, per distanze oltre i $3\ \mu\text{m}$ i punti cadono intorno ad una unica curva. La curva disegnata a tratto continuo rappresenta la funzione $1.048 \cdot 10^{-2}[\varphi(x) - \varphi(13.75)]$ che tiene conto della normalizzazione $A=0$ per $x=13.75\ \mu\text{m}$. Per valori di x inferiori a $3\ \mu\text{m}$ i punti sperimentali si collocano al disopra della curva poichè $f(x) \neq 0$.

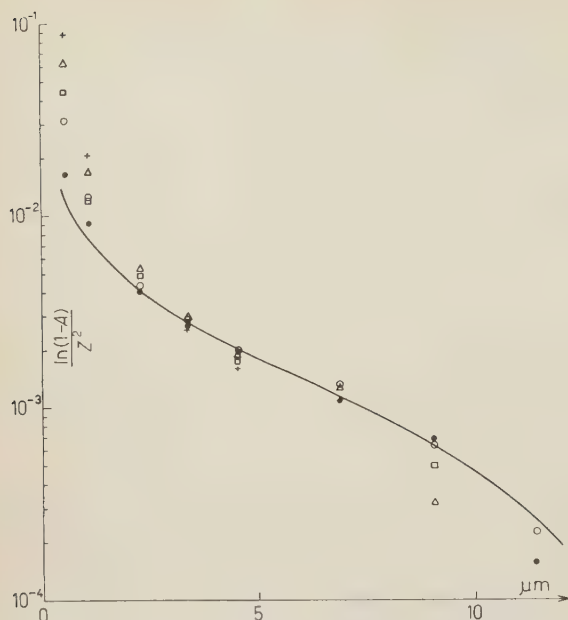


Fig. 1. - Valori di $-\ln(1-A)/Z^2$ in funzione della distanza dell'asse della traccia.

tico 153.8, quelli per $x=0.57$ e $1.14 \mu\text{m}$ con l'ingrandimento 62.2 (*).

Possiamo ora procedere oltre nel confronto fra il modello proposto e l'esperienza. Se il modello proposto è giusto, la somma

$$\ln(1-A) + K \frac{Z^2}{\beta^2} \varphi(x) = -hf(x),$$

deve risultare indipendente da Z . Il confronto è mostrato nella Tabella II. Nelle colonne 3-6 sono riportati i valori medi di $hf(x)$ per distanze crescenti dall'asse per i diversi valori di Z e per un numero di tracce in ciascun Z indicato nella colonna 2. I dati per $x=0.335$ e $0.67 \mu\text{m}$ sono stati ottenuti con ingrandimento 153.8, quelli per $x=0.57$ e $1.14 \mu\text{m}$ con l'ingrandimento 62.2 (*).

TABELLA II.

Z	no. di tracce	x in μm			
		0.335	0.570	0.670	1.14
10	1	—	0.414	0.454	0.180
6	3	—	0.659	0.324	0.186
5	1	0.89	0.504	0.228	0.132
4	3	0.961	0.765	0.306	0.149
3	5	0.956	0.659	0.280	0.116
Medie pesate		0.951	0.653	0.305	0.146

(*) Queste due coppie di valori sono ottenute con ingrandimenti differenti e quindi con diverse larghezze equivalenti della fenditura sul piano della lastra.

Si osserva che $hf(x)$ si mantiene sensibilmente costante e comunque non mostra una dipendenza sistematica da Z .

L'andamento di $hf(x)$ è riportato in Fig. 2.

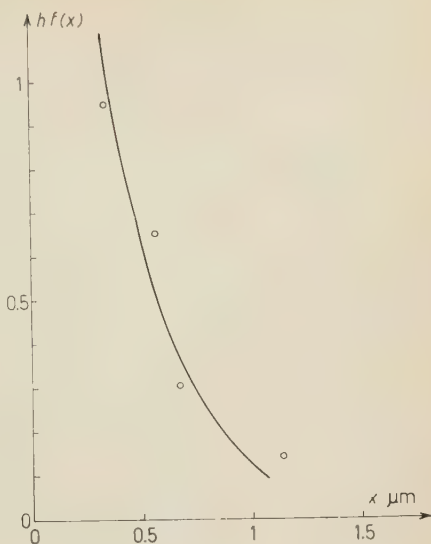


Fig. 2. - Andamento della «ionizzazione equivalente del core» in funzione della distanza dall'asse della traccia.

3. - Identificazione della carica di un nucleo pesante relativistico.

Come abbiamo visto precedentemente, lo studio dell'annerimento a distanza sufficientemente grande dall'asse della traccia può fornire un metodo per la identificazione della carica. Tale metodo però risulta piuttosto lungo e laborioso e richiede l'utilizzazione di almeno un centinaio o più di profili perchè le fluttuazioni statistiche, almeno per valori di Z relativamente piccoli, sono piuttosto sensibili.

Come abbiamo già osservato, la grandezza che viene determinata dall'analisi della « coda » del profilo è in realtà il rapporto Z/β e quindi una valutazione corretta di Z richiederebbe la conoscenza di β . Per particelle di energia ≥ 1.5 GeV/nucleone una stima significativa di β , per esempio con misure di scattering, non è possibile sulle lastre del nostro stack. L'aver ammesso $\beta = \text{cost}$ per tutte le particelle porta evidentemente un errore su Z , tanto maggiore quanto più Z è grande.

In una precedente nota ⁽⁴⁾ abbiamo esaminato la possibilità di identificare tracce di nuclei pesanti in fine percorso dalla misura diretta della larghezza del profilo fotometrico.

Per tracce relativistiche prendiamo in considerazione la semilarghezza del profilo misurata sia a metà altezza $\lambda_{0.5}$ che a un quarto dell'altezza $\lambda_{0.25}$. Abbiamo misurato questi parametri per il gruppo di tracce precedentemente identificate usando un ingrandimento ottico di 153.8 (obb. Leitz $\times 53$) ed ampiezza di oscillazione intorno all'asse della traccia di $\pm 8 \mu\text{m}$ e $\pm 13.75 \mu\text{m}$. Per ciascuna traccia i valori di λ sono stati determinati su 50 celle. Le dimen-

TABELLA III.

Te. n°.	Z	Amp. oscill. $\pm 8 \mu\text{m}$		Amp. oscill. $\pm 13.75 \mu\text{m}$	
		$\lambda_{0.5}$	$\lambda_{0.25}$	$\lambda_{0.5}$	$\lambda_{0.25}$
10	3	0.431	0.702	0.470 ± 0.006	0.695 ± 0.016
5	3	0.464	0.761	0.473 ± 0.006	0.737 ± 0.024
4	3	0.504	0.823	0.516 ± 0.005	0.798 ± 0.028
13	3	0.458	0.782	0.506 ± 0.005	0.745 ± 0.020
14	3	0.449	0.753	0.508 ± 0.006	0.740 ± 0.020
2*	3	—	—	0.500 ± 0.006	0.793 ± 0.019
4*	3	—	—	0.469 ± 0.004	0.682 ± 0.010
5*	3	—	—	0.485 ± 0.004	0.748 ± 0.023
Media — Z=	3	0.461	0.764	0.491	0.742
3	4	0.518	0.873	0.521 ± 0.007	0.848 ± 0.022
8	4	0.537	0.942	0.563 ± 0.009	1.000 ± 0.054
12	4	0.488	0.818	0.521 ± 0.007	0.829 ± 0.026
Media — Z=	4	0.514	0.878	0.535	0.892
15	5	0.531	0.904	0.541 ± 0.008	0.905 ± 0.038
3*	5	—	—	0.589 ± 0.008	1.089 ± 0.048
6*	5	—	—	0.539 ± 0.008	1.089 ± 0.048
6*	5	—	—	0.587 ± 0.009	1.105 ± 0.065
Media — Z=	5	0.531	0.904	0.572	1.033
11	6	0.664	1.191	0.711 ± 0.018	1.341 ± 0.075
6	6	0.666	1.153	0.643 ± 0.012	1.28 ± 0.064
2	6	0.665	1.147	0.645 ± 0.014	1.212 ± 0.05
7*	6	—	—	0.640 ± 0.008	1.255 ± 0.078
Media — Z=	6	0.665	1.164	0.660	1.272
1*	8	—	—	0.889 ± 0.018	1.920 ± 0.081
8*	8	—	—	0.890 ± 0.019	1.807 ± 0.073
Media — Z=	8	—	—	0.890	1.863
1	10	1.203	2.666	1.36 ± 0.036	3.032 ± 0.13
Media — Z=	10	1.203	2.666	1.360	3.032

sioni equivalenti della fenditura sul piano della lastra erano $(26 \times 0.12) \mu\text{m}$. Oltre al citato gruppo di tracce, altre 8 tracce reperite in una lastra appartenente ad un altro stack sono state misurate: queste ultime sono indicate nella Tabella III con un asterisco. I risultati sono riportati in Fig. 3 e in Tabella III. Le curve sono calcolate risolvendo graficamente la (2) per $A = 0.5$ e $A = 0.25$ nell'ipotesi che la $hf(x)$ soddisfi alla relazione

$$\ln f(x) = -ax + b.$$

I valori numerici delle costanti $a = 3.14$ e $b = 0.975$ sono stati ricavati dai dati di Tabella II (col. 3-5) (*).

Osserviamo anzitutto che un aumento dell'ampiezza di oscillazione aumenta la discriminazione specialmente per i grandi valori di Z e tale effetto è più sensibile per i valori di $\lambda_{0.25}$ che per $\lambda_{0.5}$.

Come abbiamo detto, nel rilevamento del profilo si assume come linea di base, cioè corrispondente ad $A = 0$, la linea equidistante dai punti estremi del profilo (^{1,2}). Se l'ampiezza di oscillazione è sufficientemente grande tali punti corrispondono effettivamente al fondo della lastra, ma se l'ampiezza non è abbastanza grande, in questi punti può essere sensibile l'effetto dei δ più energici ed il valore effettivo di A

risulta quindi maggiore di zero. In questo caso la normalizzazione del profilo porta necessariamente ad una riduzione della larghezza fotometrica (v. Fig. 4). Un effetto del genere è tanto maggiore quanto più grande è Z e porta come conseguenza una minore discriminazione che diviene sensibile per valori di $Z > 20$. Le semilarghezze fotometriche $\lambda_{0.5}$ e $\lambda_{0.25}$ mostrano una dipendenza da Z della forma $\lambda = Az^n - b$ con n compreso fra 2 e 3 e funzione dall'ampiezza di oscillazione.

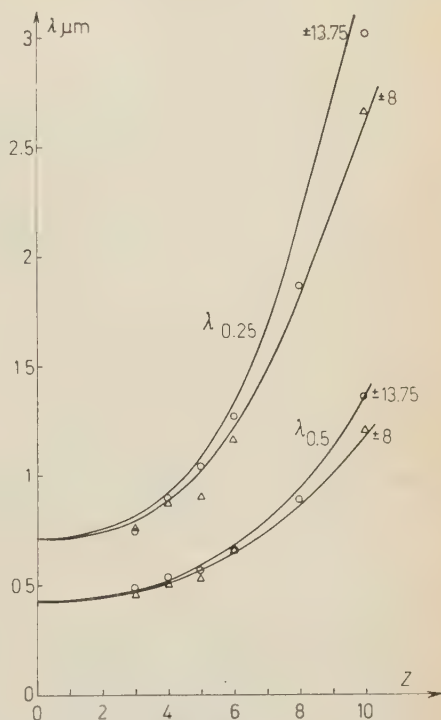


Fig. 3. - Semilarghezze del profilo fotometrico misurato a metà altezza $\lambda_{0.5}$ o ad un quarto $\lambda_{0.25}$ in funzione di Z . Ottenute con ampiezza di oscillazione $\pm 8 \mu\text{m}$ e $\pm 13.75 \mu\text{m}$.

(*) Sono stati utilizzati solo i valori ottenuti con ingrandimento 153.8 per evitare l'effetto di una diversa larghezza equivalente della fenditura.

Si osservi però che le misure di λ effettuate su tracce diverse di ugual Z presentano delle fluttuazioni in generale più grandi dell'errore statistico. Queste fluttuazioni possono esser dovute sia ad eventuali disomogeneità di sviluppo sia al fatto che particelle diverse hanno in generale un diverso β .

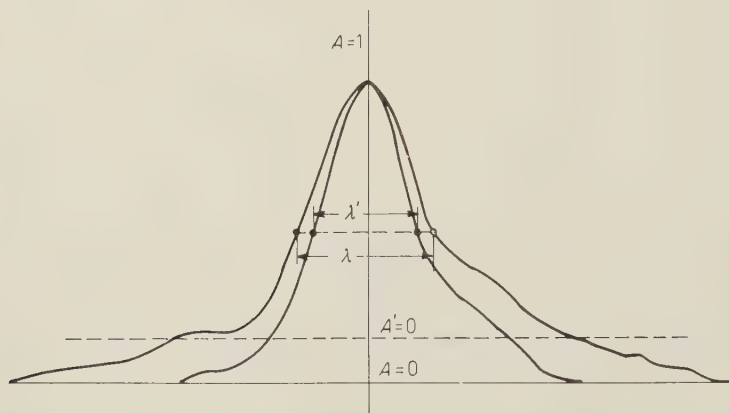


Fig. 4. - Effetto della riduzione dell'ampiezza di oscillazione sulla semilarghezza del profilo fotometrico.

Per quanto riguarda il parametro $\lambda_{0.25}$, se a prima vista questo può sembrare più adatto all'identificazione di Z , in realtà non lo è perchè è anche soggetto a fluttuazioni notevolmente più grandi, e il vantaggio della sua più rapida variazione con Z risulta quindi illusorio.

SUMMARY

The photometric profile of the tracks of relativistic heavy nuclei in nuclear emulsions has been studied. A model for the track is developed according to which the track is made up of a central part of grains directly affected by the heavy nuclei and of a peripheral part in which the darkening is due to the secondary electrons. The experimental results are in accord with this model. By measuring the darkening at a distance of more than $3.5 \mu\text{m}$ from the axis of the track a method is proposed for the identification of the charge Z of the heavy nuclei. This method appears to compete favourably with other standard methods. The possibility of using the half width as a parameter for the identification of the charge of heavy nuclei is also discussed.

A 60° Sector Type Electromagnetic Isotope Separator.

F. BISI, A. CATTONI, B. DE MICHELIS and P. PIECHELE

Istituto di Fisica del Politecnico - Milano

(ricevuto il 18 Maggio 1961)

Summary. — The paper describes a 60° sector type electromagnetic isotope separator. The separator produces ion current of the order of some milliamperes, in the range of light and intermediate masses. Some results of a few experimental separations, carried out by using zinc and magnesium, are also reported.

1. — Introduction.

An electromagnetic isotope separator has been constructed at the Institute of Physics of the Politecnico in Milan. The type chosen was similar to the one in Saclay, constructed by A. BERNAS in 1952 ⁽¹⁾; more recently, on the basis of this scheme, another separator was constructed in Beograd ⁽²⁾.

Our separator was designed to produce ion currents of the order of some milliamperes, in the range of light and intermediate masses, and to collect milligrammes of pure isotopes for nuclear research purposes.

A schematic drawing of the separator and a picture of the installation appear in Fig. 1 and 2.

⁽¹⁾ R. BERNAS: *Journ. Phys. et Rad.*, **14**, 34 (1953).

⁽²⁾ I. F. SEVARAC, B. DJ. PEROVIC, B. V. DUNJIĆ and R. M. PROTIC: *Nucl. Instr.*, **3**, 245 (1958).

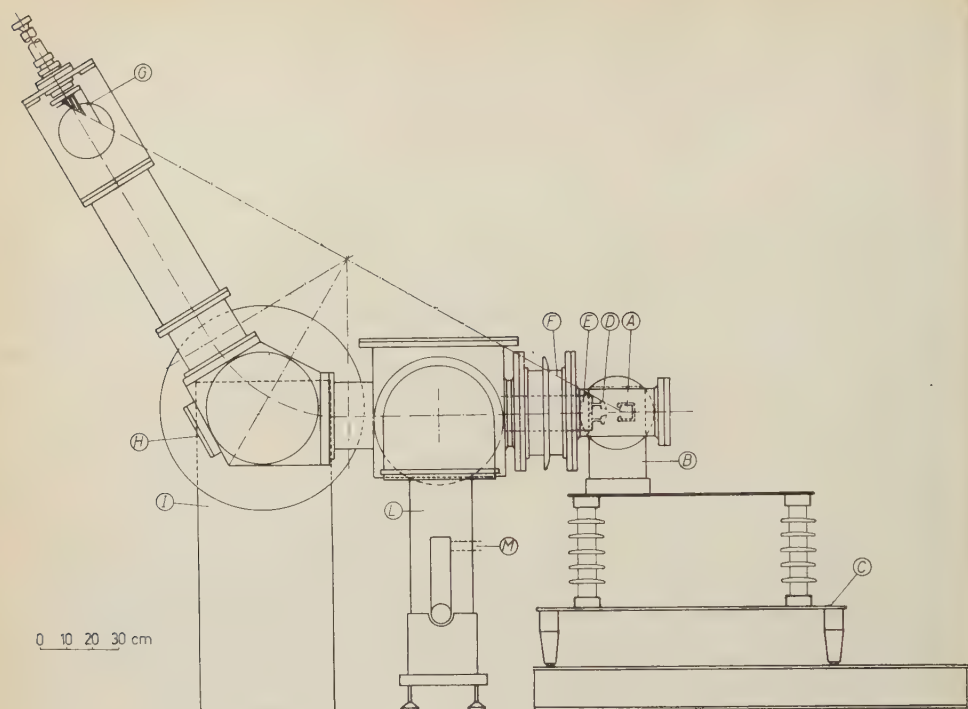


Fig. 1. - Design of the isotope separator: A) ion source; B) source magnet; C) cart; D) extraction electrode; E) aluminium tube; F) porcelain insulator; G) collector; H) glass window; I) analyzing magnet; L) diffusion pump; M) vacuum connection to the rotary pump.

2. - The magnet.

The analysing magnet has a sector angle of 60° , the radius of the main ion path is 50 cm and the gap 66 mm. The magnet is a conventional horse-shoe circuit in ARMCO iron (5500 kg). The ARMCO iron was chosen for its well-known characteristics that assure a good uniformity of magnetic properties.

The magnetic poles, cylindrical with a diameter of 40 cm, end with two pentagonal faces. Great care was taken in machining the polar faces; the tolerance on the surface was ± 0.01 mm and the same tolerance was imposed on the parallelism of the faces.

On the poles were mounted the magnetizing coils. The magnetic circuit was designed to give a maximum magnetic induction of 12 000 gauss. A D.C. generator 300 V - 40 A is used for the excitation current of the magnet. The current is stabilized at 1/10 000 by means of electronic stabilizers. For such

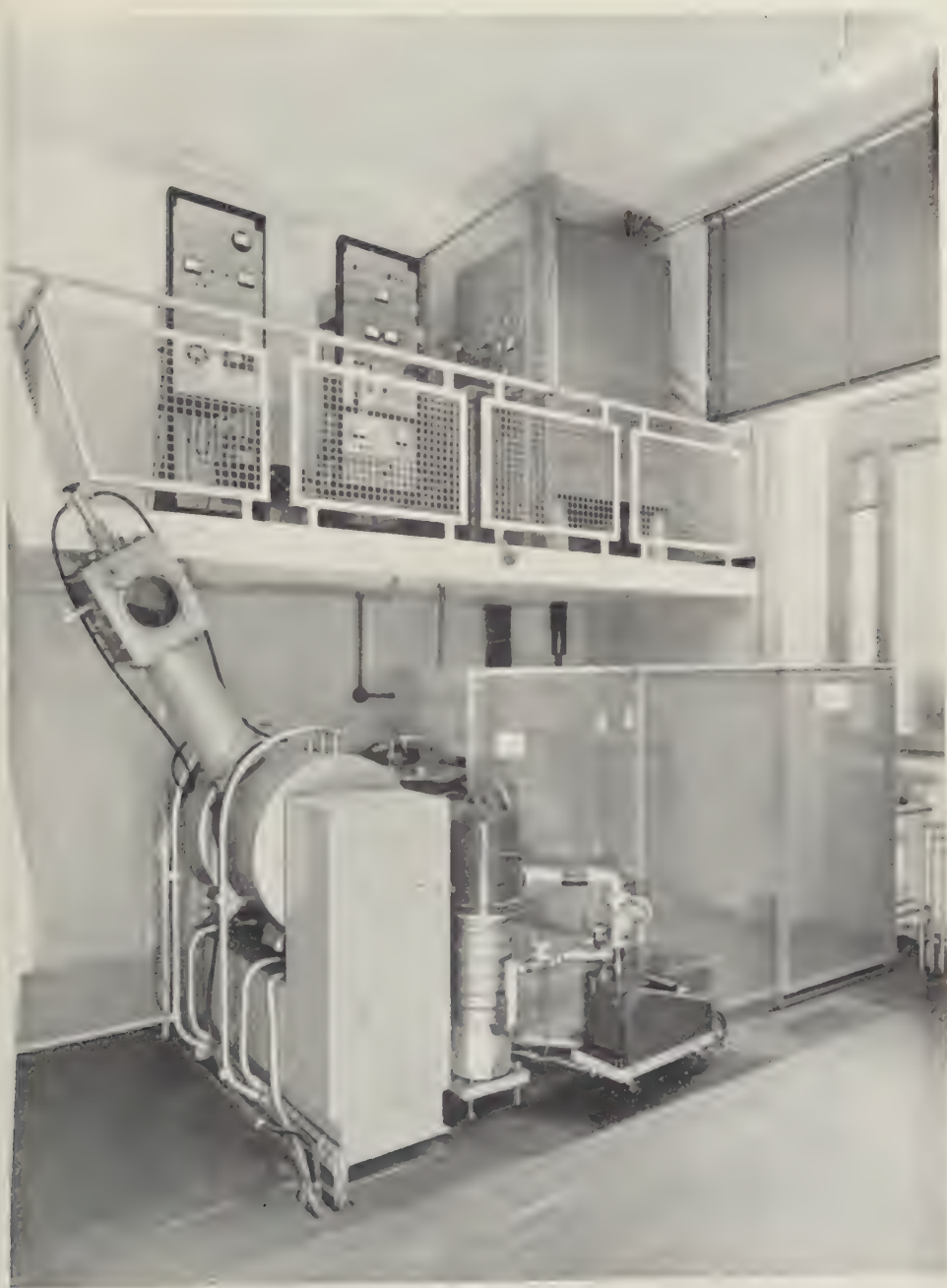


Fig. 2. - General view of the separator.

a current we chose a copper wire of rectangular section (3×2) mm, covered by electroglass. A maximum current density of about $(6 \div 7)$ A/mm² compels us to use some cooling. The 2500 turns were wound on six independent aluminium supports that were mounted on the cylindrical expansions. Eight aluminium chambers were inserted between adjacent supports and water-cooled.

Measurements of the magnetic field were made by means of a fluxometer and an exploring coil. The range of linearity between induction and excitation current is reasonably large and covers all the values of induction that we shall use in our separation work. The magnetic field proved to be satisfactorily uniform on the polar faces and the stray field distribution was found to be consistent with theoretical curves. The polar faces were so designed as to allow the insertion of iron pieces at the edges to correct the effect of stray field and to achieve a better focusing⁽³⁾.

3. — The vacuum system.

The vacuum chamber was built in stainless steel. We took care to use amagnetic material everywhere with a view to reduce losses in the magnetic circuit.

The case of the ion source, that is at high positive potential with respect to earth, is electrically insulated by means of a ceramic insulator. In the gap of the magnet, the vacuum chamber is formed by a pentagonal box in stainless steel to which the two tubes are sealed, with an angle of 210°, where the beam runs. The insertion of the box reduces the useful gap for the ion beam to 60 mm. The pentagonal box is provided with a glass window for the inspection of the source region and the study of the undeviated beams. To seal the box we used rubber seals, adequately cut; in all other part of the separator we used seals. The collectors are located in a separate demountable case at the end of the upper tube.

The evacuation of the system is achieved by means of a silicon oil pump and a rotary pump for the preliminary vacuum. The silicon oil pump is an Edwards 903 A with a pumping speed of 1500 l/s; the pump is provided with a baffle for a better ultimate vacuum. At the baffle the pumping speed is reduced to 900 l/s. The system is provided with a by-pass valve, through which the system is evacuated without using the diffusion pump.

The ultimate vacuum is around $5 \cdot 10^{-6}$ mm Hg; the operative vacuum is around $5 \cdot 10^{-5}$ mm Hg. The residual gas favours the neutralization of the space charge of the ion beam, by means of electrons produced in the residual gas by ion shocks⁽⁴⁾.

⁽³⁾ C. CASSIGNOL: *Journ. Phys. et Rad.*, **14**, 31 (1953).

⁽⁴⁾ J. KOCH: *Electromagnetic Isotope Separators and Applications of Electromagnetically Enriched Isotopes* (Amsterdam, 1958), p. 281.

The vacuum in the separator tank is measured by a Penning gauge operating in the range between $(10^{-6} \div 5 \cdot 10^{-4})$ mm Hg; absolute readings of the pressure are taken on an Edwards ionization gauge. The evacuation of the tank up to the operating pressure varies widely with the past history of the separator. When the tank is initially at atmospheric pressure a longer time is necessary for the evacuation; therefore it is essential for the continuity of the operation of the separator to limit the introduction of air to a few cases. For this reason a valve is put at the end of the upper tube, before the collector box. Thus, the extraction of the collectors and every related operation is possible without affecting the vacuum in the separator. The collector can be evacuated directly by the rotary pump. Other rather frequent operations are the change of the furnace charge and filament in the source. These operations cannot be undertaken without introducing air in the system; however, filament and furnace are so located that their change takes only a few minutes. When air is introduced in the tank, care must be taken that the graphite of the source box is not too hot.

4. - The ion source.

The ion source is a conventional hot cathode, magnetic source with radial ion extraction; a detailed description of the ion source has been given in another paper ⁽⁵⁾.

The discharge chamber is in graphite: the dimensions are $(5 \times 7 \times 14)$ cm. The source is useful both for gaseous and solid charge materials; if solid, the charge material is introduced in a graphite furnace, electrically heated, and evaporated; if the charge material is in a gaseous state, the furnace is substituted by a system for the introduction of the gas, provided with a needle valve for flow regulation.

The ions produced in the discharge are extracted from a slit of (2×50) mm. In some preliminary experiments with zinc and argon, ion currents to a maximum of 20 mA were extracted from the source.

In Table I are listed the principal electric data for the source.

TABLE I.

Arc Voltage	$(50 \div 200)$ V
Arc Current	$(0.1 \div 5)$ A
Filament heating current	$(40 \div 60)$ A
Magnetic field	$(100 \div 800)$ G
Furnace heating power	500 W

⁽⁵⁾ F. BISI and B. DE MICHELIS: *Nuovo Cimento*, **11**, 861 (1959).

The case housing the source, at high tension level, is supported by a cart on rails, to allow an easy cleaning of the parts of the source after separation and the inspection of the internals of the vacuum chamber. The upper plan of the cart is insulated at 50 kV from earth by means of four porcelain insulators. The cart is in stainless steel, and care was taken to round off all sharp edges so as to reduce corona effects.

In fully operating conditions a power of about 3 kW must be carried off the source region, so that it is necessary to cool the vacuum chamber, the coils of the source magnet and the front plate with low voltage source insulators.

The vacuum tube, the front plate, the filament supporting rods are constructed with double wall, to allow the passage of cooling water.

For cooling, a closed circulation system with a force pump and a heat exchanger is used, because the source operates at high tension level. Distilled water is used in the source cooling system to decrease current losses in the high tension supply; the water between the source and the heat exchanger at earth level flows inside a serpentine of several meters in length. The losses are thus reduced to a few μA .

5. — The extraction system.

The ions extracted from the source are accelerated at normal operating voltages of $(20 \div 30)$ kV. The high voltage supply is designed for a maximum output of 50 kV, 50 mA: the voltage is stabilized at $1/5000$ ⁽³⁾. The extraction electrode has a slit of (4×55) mm and is made of graphite. It forms a Pierce lens ⁽⁶⁾ with the front plate of the ion source; both the front plate of the ion source and the extraction electrode are cut at an angle of 47° . This extraction electrode is insulated with respect to the ground by means of three steatite insulators, 4 cm long, and is supported by an earth-grounded aluminium tube. A variable potential between 0 and -10 kV is given to the extraction electrode.

Some care was taken in the construction and mounting of the extraction electrode and its supporting tube with a view to reduce the formation of sparks in the high tension region and the deposition of metal powder of elements evaporated in the source on the insulators. All the surface in the extraction region were rounded off and a smoothed aluminium ring was forced around the graphite electrode as a cap for the steatite insulators.

The whole extraction system, formed by the accelerating electrode and the supporting tube, has three degrees of freedom; a system of shafts, vacuum sealed and easily handled by the operator during the operation of the separator, allows axial, vertical and rotational displacements around the cylindrical axis of symmetry. The alignment of the slits of the ion source and extraction

⁽⁶⁾ J. R. PIERCE: *Journ. Appl. Phys.*, **11**, 548 (1940).

electrode can be achieved by observing the source slit, visible when the filament is lightened, through the glass window in the pentagonal box. The position of the extraction electrode can be modified to reach the best conditions of focalization at the collector even during the operation.

6. - The collector.

A sketch of the collector box is given in Fig. 3.

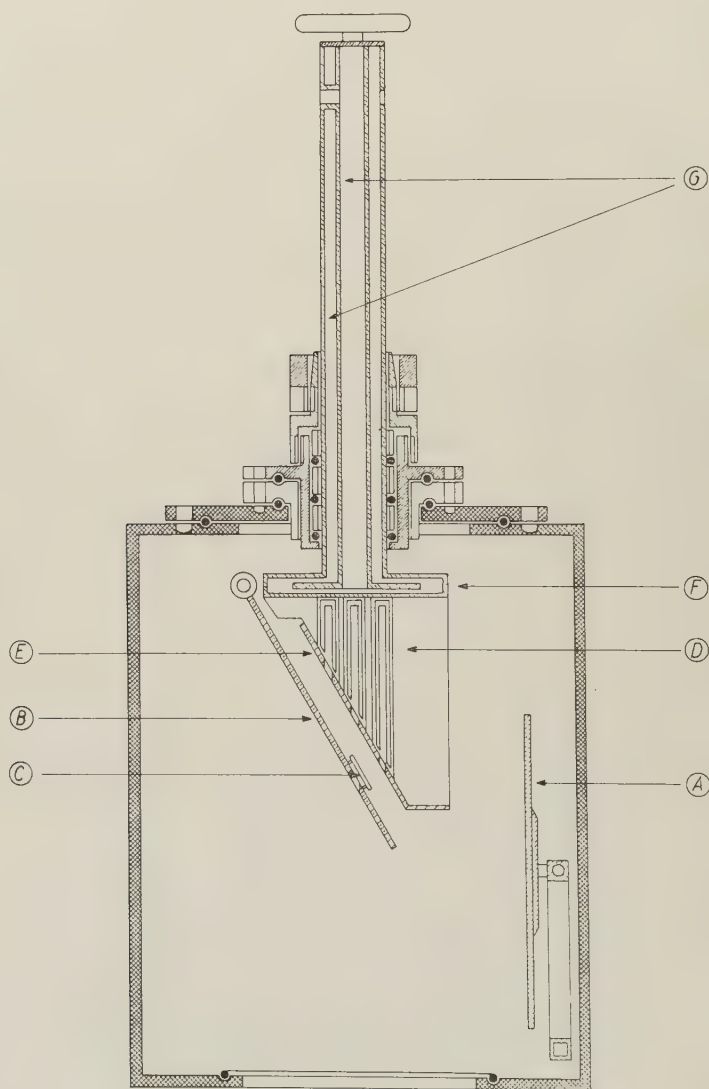


Fig. 3. - Collector box: A) valve; B) movable screen; C) measuring electrode; D) collector chambers; E) fixed screen; F) supporting plate; G) cooling tubes.

On a water cooled copper plate are mounted the collector chambers. The supporting plate with the chambers can be displaced in the axial direction until the focal plan is reached. Rotational movements are also possible. A fixed copper screen with slits at a correct distance is mounted in front of the collectors so as to reduce the contamination of collected isotopes from sputtered material and to facilitate the visual observation of the beams at the collectors.

A movable screen provided with a slit and a measuring electrode can be placed in front of the collector during the adjustment of the separator; the adjustment is accomplished by reading currents on the measuring electrode. Any contamination of the collectors is thus avoided. The screen is removed when the separation starts.

A plexiglass window on one side of the collector box allows the visual inspection of the position of the beams, when the ion current is over 100 μA .

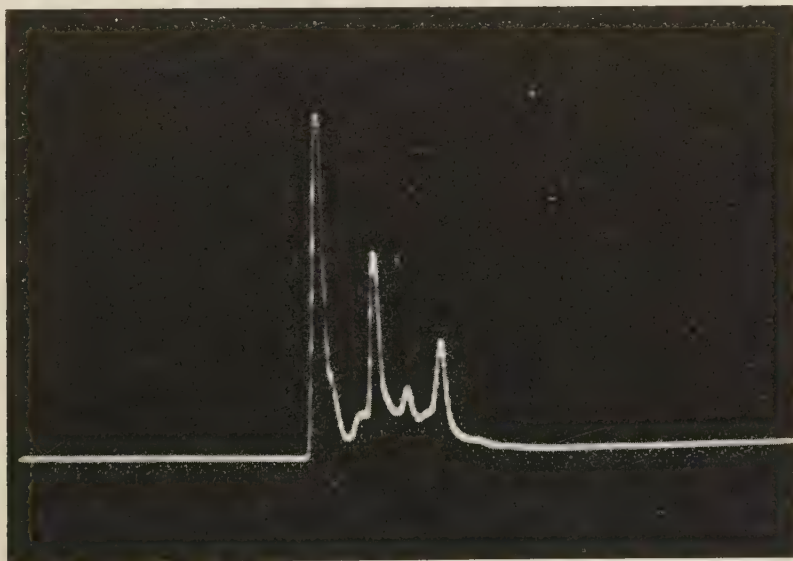


Fig. 4. — Oscillogramm of the mass spectrum of the zinc.

The collection plate is replaced by a system for recording the mass spectrum of the separated isotopes at the collector. The region of the beam is scanned by a slit moving at constant velocity on the focal plane, and the signal collected on a fixed electrode behind the slit is put on the vertical deflection plates of an oscilloscope (7).

The spectrum in Fig. 4 was taken by means of this recording system.

(7) F. BISI, A. CATTONI and B. DE MICHELIS: to be published.

7. — The experimental results.

The first separated ion beams were collected on a provisional collector screen in March 1960. The separator has since been mainly used for the study of operational characteristics. In the first experiments concerning mainly the ion beam formation, argon was used. A few experimental separations were then carried out by using zinc and magnesium.

a) Zinc. As charge material pure zinc metal in bars was used. We used zinc at the mean consumption rate of about 1 g per hour. The total charge of the furnace was about 20 g; not all this material is used in view of the increasing instability of the arc when the furnace is getting empty. So the mean life of the charge was about 15 hours. The temperature of the furnace was about 400 °C and the initial power input 400 W; this power can be gradually reduced to 200 W after the start of the discharge, due to the contribution of the additional power of the arc.

The separated isotopes were not collected, but only used for a quantitative chemical analysis. Such analysis gave a total zinc collection of 29.2 mg for a 10 hours run. For the analysis we used a colorimetric chemical method, employing dithyzon ⁽⁸⁾.

The accelerating voltage was 20 kV; large amounts of zinc condensed on the insulating supports of the extraction electrode and on other parts around the source, so that they produced after about 40 hours of operation some troubles and sparks. After such a period, cleaning of the ion source region and extraction system was necessary.

The total collector current was about 1 mA.

In Fig. 4 can be seen a mass spectrum of zinc taken on an oscilloscopic screen.

b) Magnesium. Magnesium metal was used in the furnace. The mean consumption rate of charge material was about 250 mg per hour and the input power of the furnace somewhat higher than for the zinc. The mean collector current was about 300 μ A. A quantitative analysis of the collected material gave a total collection of 2.6 mg in a 25 hours run. The low efficiency of collection was probably due to intense sputtering processes. The collector surfaces were in copper, covered by a thin oxide layer, to increase collection efficiency ⁽⁹⁾.

⁽⁸⁾ F. D. SNELL and C. J. SNELL: *Colorimetric Methods of Analysis*, vol. 2, p. 412.

⁽⁹⁾ P. S. BAKER: *Second United Nations International Conference on the Peaceful Uses of Atomic Energy*, 8, 245 (1958).

* * *

Thanks are due to Prof. G. BOLLA and Prof. E. Gatti for their help and interest in our work: we wish also to thank the Acciaierie e Ferriere Lombarde Falck for their financial and technical assistance in the construction of the magnet and S.p.A. Pirelli for financial aid in the construction of the magnetic coils.

Thanks also are due to the Consiglio Nazionale delle Ricerche for the support of this work.

RIASSUNTO

Si descrive un separatore elettromagnetico di isotopi a settore di 60° . Il separatore è progettato per lavorare prevalentemente nella zona delle masse medie e leggere ed è in grado di fornire correnti ioniche dell'ordine di alcuni mA. Vengono pure riportati i risultati di alcune separazioni sperimentali degli isotopi dello zinco e del magnesio.

Angular Distribution in $\pi \rightarrow \mu + \nu$ Decay.

E. FROTA-PESSOA and N. MARGEM

*Centro Brasileiro de Pesquisas Físicas,
Faculdade Nacional de Filosofia - Rio de Janeiro*

(ricevuto l'8 Giugno 1961)

Summary. — A study of the angular distribution of 4 132 μ -mesons resulting from π -decay at rest in nuclear emulsion is made using area scanning, looking for μ -ends. The results are compared with others obtained in the same plates with area scanning, looking for π - μ vertices. Contrasting with these previous results which gave a strong backward-forward asymmetry the present analysis gives no asymmetry. This is attributed to the strong reduction of bias against small π - μ angles in the μ -ending scanning.

1. — Introduction.

In 1957 LATTES and FREIER ⁽¹⁾ studied the angular distribution of μ -mesons resulting from the decay of π -mesons at rest in nuclear emulsions. A beam of π^+ -mesons entered a nuclear emulsion stack parallel to one of the edges. Being θ the angle between the initial direction of the μ -meson projected on the plane of the emulsion and the direction of beam the distribution function $dN/d\theta$ was measured. Instead of an isotropic distribution which should be expected for a decaying particle of spin zero a back-forward asymmetry was obtained. The referred authors attributed this asymmetry to an instrumental error rather than to a real property of the pions.

After that work many other papers appeared in most of which an asymmetry of the same nature was also observed; the origin of the asymmetry has not been settled, however. Also, most of these works suffered of the lack of sufficient statistics.

⁽¹⁾ C. M. G. LATTES and P. S. FREIER: *Proc. Padova-Venice Conf.* (1957), IV p. 17.

The purpose of this paper is to report the result of the analysis of that asymmetry in plates where a very large effect had been found in previous study by HULUBEI *et al.* ⁽²⁾ (to be referred from now on as A) with good statistics (7 526 $\pi \rightarrow \mu$ decays). The referred authors conclude that they have evidence for non-zero spin of π^+ meson. Also they suggest that «conditions of pion generation may play an essential role in different features of the π - μ -e decay chain». This might explain previous results not compatible with theirs.

Using a new method of scanning which should reduce bias against small angles no back-forward asymmetry was found in the present paper within statistical error.

2. - $\pi \rightarrow \mu$ vertex scanning.

In A as in previous works the method of area scanning was used to find the points of $\pi \rightarrow \mu$ decays. Fig. 1 shows the results of A both for μ 's and e 's (positrons). The histograms suggest angular distributions relative to the incoming beam

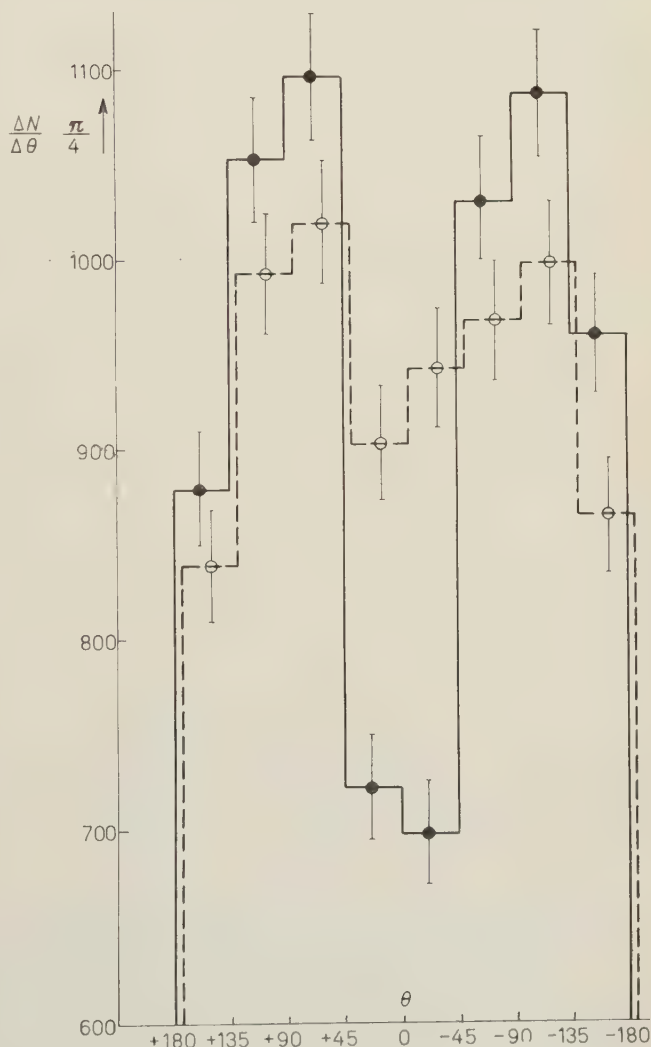


Fig. 1. - ● — 7 526 events μ -mesons (HULUBEI *et al.* ⁽²⁾); ○ --- 7526 events electrons (HULUBEI *et al.* ⁽²⁾).

⁽²⁾ H. HULUBEI, J. AUSLÄNDER, E. BALEA, E. FRIEDLÄNDER and S. TITEICA: *Proc. Second Int. Conf. Peaceful Uses of Atomic Energy*, vol. 30 (Geneva, 1958), p. 276

of the form

$$(1) \quad \frac{dN}{d\theta} = C(1 + a_1 \cos \theta + a_2 \cos 2\theta + a_3 \cos 3\theta).$$

Indeed the values of a_1 , a_2 and a_3 obtained by the minimum square method gave a good fit of the experimental distributions by eq. (1). These values are given in Table I together with the usual forward-backward asymmetry coefficient

$$b = 2(F - B)/(F + B).$$

TABLE I.

Particle	a_1	a_2	a_3	b
μ	-0.107 ± 0.016	-0.210 ± 0.018	-0.050 ± 0.022	-0.115 ± 0.023
e	$+0.036 \pm 0.016$	-0.090 ± 0.016	$+0.020 \pm 0.021$	$+0.037 \pm 0.023$

Using the same method of scanning we obtained, for 2 594 cases in one plate, the following coefficients for the μ distributions:

$$a_1 = -0.037 \pm 0.029; \quad a_2 = -0.141 \pm 0.031; \quad a_3 = -0.018 \pm 0.037$$

and

$$b = -0.040 \pm 0.039,$$

which result from Table II.

TABLE II.

θ	$(0 \div 45)^\circ$	$(45 \div 90)^\circ$	$(90 \div 135)^\circ$	$(135 \div 180)^\circ$
Number of events	565.0	706.0	707.5	615.5

These results are not compatible with isotropy.

On the other hand comparison of these results with those of A gives for $n=3$, $\chi^2=14.4$. and probability $P \simeq 0.002$. We assumed compatibility of our results with those of A, although realizing that the small probability might indicate an influence of scanners training. Thus we did not proceed to increase the statistics with this scanning method because we did not believe that this would lead to a conclusive result. Indeed we assumed that the anisotropy was real.

As to the origin of the observed anisotropy we considered then the possibilities:

a) That the anisotropy is due *only* to distortion. This is already excluded by the data of Table I as then μ 's and e 's should have the same distribution. The coefficients for μ and e are indeed not compatible. Of course the existence of some distortion effect is not excluded.

b) Existence of observational bias resulting from the fact that some $\pi \rightarrow \mu$ events might be lost due to small decay angles (due to the angular dispersion of ending π tracks these cases correspond mainly to values of θ smaller than 90°). In order to examine this possibility we devised another method of scanning which minimizes this effect if it is significant (μ -end scanning):

Instead of finding directly the points of $\pi \rightarrow \mu$ decay we looked for μ -mesons stopping in the emulsion. The μ track was then followed back to find the $\pi \rightarrow \mu$ vertex. The minimization of bias effect results from the fact that if a μ -ending is found, the π - μ vertex must be found within the μ range even if it looks as a scattering in which case it would be lost in the « π - μ vertex scanning».

3. - μ -end scanning.

The same scanners who did the previous scanning were instructed to look for all black tracks ending in the emulsion (area scanning). These tracks were followed back to see whether they corresponded to a μ resulting from a $\pi \rightarrow \mu$ decay at rest. All such black tracks with more than $400 \mu\text{m}$ (projection) in the emulsion which were not considered as a μ from a $\pi \rightarrow \mu$ decay by these scanners were registered. All these cases and the $\pi \rightarrow \mu$ decays were then revised by other scanners and, in case of disagreement, by all scanners. For 4 132 $\pi \rightarrow \mu$ final cases 5 were discarded for being obvious mistakes and 13 new cases were found.

The scanning and track following were made with obj. $25\times$ and eyepieces $15\times$. Each track was also examined with obj. $100\times$ and eyepieces $15\times$ which were used to measure depths and angles. As in the first scanning only the cases where both π and μ ended more than $20 \mu\text{m}$ (developed) from the glass or emulsion surface were accepted. A map of the plate was made and the twice counted $\pi \rightarrow \mu$ corrected. As the $\pi \rightarrow \mu$ decays were not uniformly distributed in the emulsion, the cases with projected distance less than $700 \mu\text{m}$ from the border of the scanned area were rejected in order to avoid the introduction of a preferential direction.

The angular distribution of the μ -mesons thus obtained is plotted in Fig. 2 together with the results of A for comparison. The line labelled μ in Table III

gives the values of a_1 , a_2 , a_3 and b to be compared with those of A (Table I).

We see that the forward backward asymmetry (coefficients a_1 , a_3 , b) are consistent with zero. Also the value of a_2 is reduced in relation to our π - μ vertex scanning and it is not compatible with the value in A. We conclude that these are consequences of a strong reduction of bias in the present method of scanning. The fact that 11 out of the 13 μ 's lost by the first scanners had a $\pi \rightarrow \mu$ angle smaller than 25° indicates that there is still some bias in our method against small values of θ .

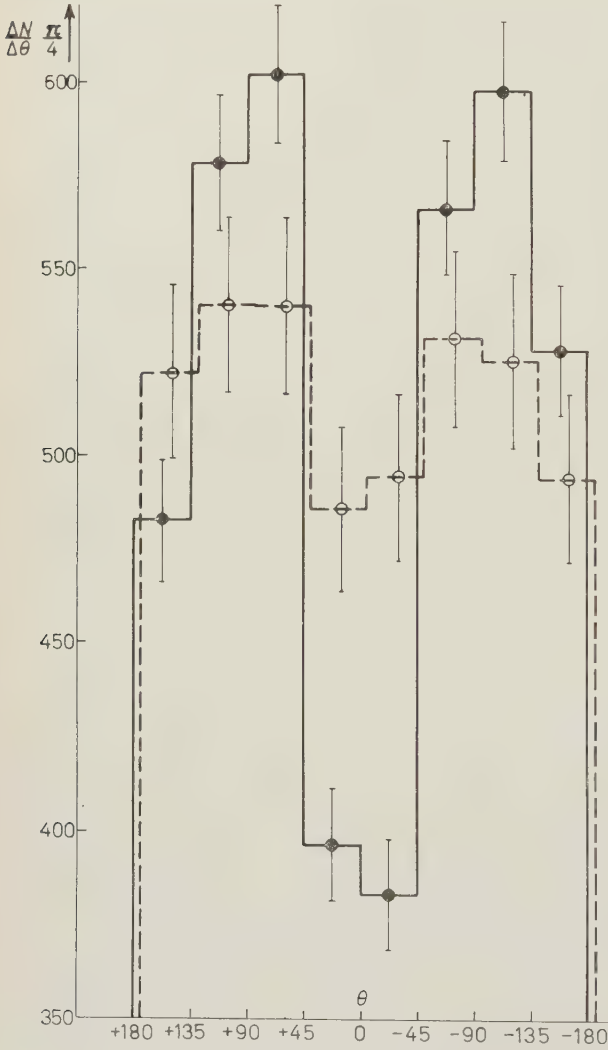


Fig. 2. — μ -mesons; ● — 7 526 events normalized to 4 132 (HULUBEI *et al.* ⁽²⁾)
○ --- 4 132 events (μ -end scan).

TABLE III.

Particle	a_1	a_2	a_3	b
μ	-0.016 ± 0.022	-0.052 ± 0.024	-0.012 ± 0.028	-0.015 ± 0.031
e	$+0.005 \pm 0.022$	-0.030 ± 0.022	$+0.014 \pm 0.028$	0.000 ± 0.031
α	$+0.003 \pm 0.024$	-0.024 ± 0.026	$+0.012 \pm 0.030$	-0.001 ± 0.033
$\alpha + e + \mu$	-0.003 ± 0.013	-0.036 ± 0.014	$+0.004 \pm 0.017$	-0.005 ± 0.018

4. - Possible distortion effects.

Although our results for the μ angular distribution are compatible with isotropy the value of a_2 (responsible for the side peaking of the angular distribution) is larger than twice the statistical error. Thus we looked for eventual distortion effects by examining also the angular distribution of the electrons from μ -decay and 3 669 α -particles from natural radioactive stars which has been determined simultaneously with the μ distribution. In Fig. 3 these distri-

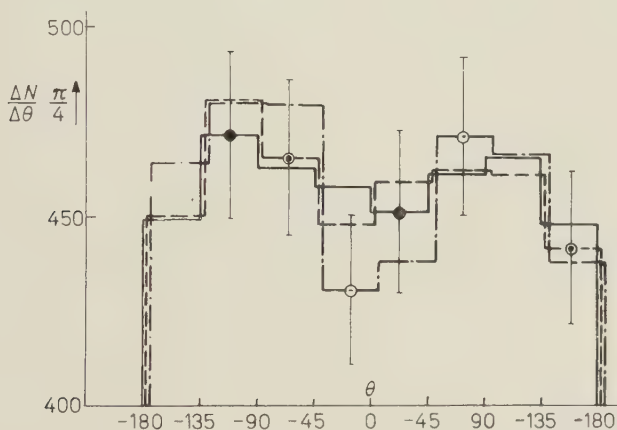


Fig. 3. — ● — 3 669 events α -particles; ○ --- 4 114 events normalized to 3 669 electrons; ○ - · - · 4 132 events normalized to 3 669 μ -mesons.

butions are compared. The 18 cases where the electron was not found correspond to μ 's stopping near the surface or glass. The values of the coefficients of eq. (1) are given in Table III also for α , e and the total distribution of α , e and μ together. The absence of back-forward asymmetry is confirmed. The a_2 values are found to be consistent with that for the μ distribution which would confirm the existence of distortion, but they are also consistent with isotropy. Improvement of the statistics is being done to find if the distortion effects exist. The value $a_2 = -0.090 \pm 0.016$ for electrons in A might be an indication that distortion effects exist and are larger in other plates of the stack.

* * *

We are thankful to the HULUBER group for the permission for using three of their plates and to Professor LATTES who encouraged us to work on the $\pi \rightarrow \mu$ decay angular distribution.

We are thankful to Miss C. Z. BILBAO, Mrs. T. L. FERREIRA, Miss L. R. GIL, Miss E. V. VAZ and Mrs. C. M. P. WÖHRLE who helped us in the scanning.

RIASSUNTO (*)

Si è eseguito uno studio della distribuzione angolare di 4132 mesoni μ risultanti da decadimenti π a riposo in emulsione nucleare usando l'esplorazione per area con ricerca delle terminazioni dei μ . Si confrontano i risultati con quelli di altri ricercatori ottenuti con le stesse lastre usando l'esplorazione per area, con ricerca dei vertici π - μ . In contrasto con questi risultati precedenti che indicavano una forte asimmetria indietro-avanti, la presente analisi non rivela asimmetria. Si attribuisce il fatto alla forte riduzione, nell'esplorazione con ricerca delle terminazioni μ , del bias a favore dei piccoli angoli π - μ .

(*) Traduzione a cura della Redazione.

A Study of Uniform Isothermal Processing of Nuclear Emulsions (*).

D. KNIFFEN

*Department of Physics, Washington University - St. Louis, Mo. (**)*

(ricevuto il 13 Giugno 1961)

Summary. — Nuclear emulsions exposed to the 1.86 GeV/c positive particle beam at the Berkeley Bevatron were developed using a variety of methods. It was found that an isothermal procedure at 10 °C could give satisfactory uniformity of development with depth. Data are also presented on the grain size, background grain density and distortion for the different methods used.

1. — Introduction.

The development and use of the thick ($\geq 400 \mu\text{m}$) nuclear emulsion presented emulsion workers with new problems in their processing procedures. The time required for the diffusion of the developer through the entire thickness of the emulsion was no longer negligible in relation to the required developing time and hence one could no longer obtain satisfactory development using normal photographic procedures. The undesirable result was that non-uniform development with depth was obtained. In 1948, DILWORTH, OCCHIALINI and PAYNE suggested as a solution to the non-uniformity, the now conventional two-cycle « temperature development ». The essential feature of this technique is the application of a two-stage development in which the first stage consists of soaking the emulsion in cold (5 °C) developer in order that the developer may penetrate the thickness of the emulsion at a temperature at which the

(*) Work performed under a programme sponsored by the Air Force Office of Scientific Research, the U.S. Army Research Office (Durham) and the National Science Foundation.

(**) Present address: N.A.S.A. Goddard Space Flight Center, Greenbelt, Md.

developer is relatively inactive. Then the emulsion is removed from the cold developer and placed on a «hot plate» where it is maintained at a temperature of $(25 \div 30)^\circ\text{C}$, allowing the development to take place in a more uniform manner. Refinements on this procedure have been reported by various groups⁽¹⁻⁹⁾.

In spite of the increased uniformity of development obtained with the temperature cycle and its wide acceptance and use, this process still presented serious disadvantages. The emulsion gelatin, which merely serves to hold the silver halide in suspension, has strains introduced into it during manufacture. As the temperature of the emulsion is raised during the hot stage of the temperature cycle development, the emulsion softens, allowing these strains to be released and causing relative displacement of the emulsion layers subsequent to exposure. This causes distortions in the particle tracks⁽¹⁰⁾ which are very annoying and make multiple scattering measurements quite difficult and sometimes impossible. Distortions are also produced by large and/or rapid changes in pH or osmotic pressure and by excessive shock or handling during the processing.

As a solution to the problems of the temperature cycle development, HERZ and EDGAR⁽¹⁰⁾ suggested an alternative procedure in which all of the steps were performed at the same temperature, but they recognized that this isothermal procedure had the disadvantage of offering a low signal-to-background ratio near the surface of the emulsion.

The most successful attempts at isothermal development were those introduced by YAGODA⁽¹¹⁾ and MARGUIN⁽¹²⁾. These methods replaced temperature variations with pH variations and have produced quite successful results with emulsion with thickness up to 2 mm. The disadvantage of these latter procedures was the complexity of operation for large batches of emulsions to

(1) C. C. DILWORTH, G. P. S. OCCHIALINI and R. M. PAYNE: *Nature*, **163**, 102 (1948).

(2) C. C. DILWORTH, G. P. S. OCCHIALINI and L. VERMAESEN: *Bull. Cent. Phys. Nuc. Univ. Libre Bruxelles*, No. **13** a, (1950).

(3) A. D. DANTON, A. R. GATTIKER and W. O. LOCK: *Phil. Mag.*, **42**, 396 (1951).

(4) A. BONETTI, C. C. DILWORTH and G. P. S. OCCHIALINI: *Bull. Cent. Phys. Nuc. Univ. Libre Bruxelles*, No. **13b**, (1951).

(5) A. J. HERTZ: *Journ. Sci. Instr.*, **29**, 60 (1952).

(6) A. J. HERTZ: *Journ. Sci. Instr.*, **29**, 15 (1960).

(7) C. C. DILWORTH, G. P. S. OCCHIALINI and E. SAMUEL: *Bull. Cent. Phys. Nuc. Univ. Libre Bruxelles*, No. **2**, (1948).

(8) M. J. WILSON and S. VANSELOW: *Phys. Rev.*, **75**, 1144, (1949).

(9) D. LAL, Y. PAL and B. PETERS: *Proc. Ind. Acad. Sci.*, A **38**, 277 (1953).

(10) A. J. HERZ and M. E. EDGAR: *Proc. Roy. Soc., Lond.*, A **66**, 115 (1953).

(11) H. YAGODA: *Rev. Sci. Instr.*, **26**, 263 (1955).

(12) G. MARGUIN: *Sci. Ind. Phot.*, **28**, 321 (1957).

a degree which is unnecessary for satisfactory development of the more common thicknesses ($(400 \div 600) \mu\text{m}$). Indeed many elaborate processes might be and have been devised which would yield satisfactory results on a small scale, but this was not a solution to the problem for those who must process large quantities of emulsion. Nonetheless, one must certainly consider the merits of an isothermal procedure which will at the same time give an acceptable noise-to-background ratio at all depths, and this experiment was conducted in search of such a procedure.

2. - Experimental procedure.

2'1. *Exposure of the plates.* - The plates used in this experiment were fourteen of a total stack of fifty-six Ilford G-5, $600 \mu\text{m}$, glassbacked emulsions, exposed to a beam at the Berkeley Bevatron, the particulars of which are given in Table I. It can be seen that the proton tracks should exhibit grain densities corresponding approximately to the plateau value, whereas pion tracks will have grain densities about seven percent lower.

TABLE I. - *Berkeley bevatron beam data (approximate).*

	Proton	Pion
Relative abundance	80%	20%
Momentum (GeV/c)	1.86	1.86
$p\beta$ (GeV/c)	1.65	1.86
$\gamma - 1$	1.22	12.2

The complete stack was exposed to the beam at an angle to give tracks of about 1 cm length in each emulsion. The energy is sufficient to allow the approximation that no energy is lost by the particles as they traverse the stack and hence any variations in grain density must be attributed to the development or other treatment of the plates.

2'2. *Development procedure.* - This experiment was prompted by the knowledge that emulsion distortions are reduced upon lowering development temperature and by results obtained in this laboratory showing low scattering noise in a stack of emulsions processed isothermally by GUSS and FICHEL⁽¹³⁾.

(13) D. E. GUSS: *Ph. D. thesis Washington University* (1960).

Realizing that a minimum of changes should be made in the processing procedure over those previously used in this laboratory so that cause and effect could be more accurately determined, it was decided that variations should be made only in developer composition, developing time and development temperature. The temperature was varied only to provide a basis for comparison with the isothermal procedure.

Table II presents the various procedures used. In all cases the first stage of the development was preceded by a 3 h water soak which was initiated

TABLE II. — *Development procedures.*

Plate	1st dev. stage	2nd dev. stage	3rd dev. stage	Stop bath
5	Dev. + 1KBr	Developer (3 h)	Dev. + 1KBr (1 h)	(4 h)
5'	Same as 5			
6	Dev. + 1KBr	Developer (4 h)	Dev. + 1KBr (2 h)	(2 h)
6'	Dev. + 2KBr (2 h)	Developer (4 h)	Dev. + 2KBr (2 h)	(2 h)
7	Dev. + 2KBr (1 $\frac{1}{2}$ h)	Developer (3 h)	Dev. + 2KBr (1 $\frac{1}{2}$ h)	(4 h)
7'	Same as 7			
8	Dev. (Circ.) (6 h)	—	—	(2 h)
8'	Same as 8			
9	Dev. (Circ.) (3 h)	Hot plate (24 °C) (1 h)	—	(2 h)
9'	Dev. + Borax (Circ.) (6 h)	—	—	(2 h)
10	Developer (3 h)	Hot plate (24 °C) (1 h)	—	(4 h)
10'	Developer (3 h)	Hot plate (24 °C) (2 h)	—	(3 h)
11	Developer (6 h)	—	—	(2 h)
11'	Dev. + Borax (6 h)	—	—	(2 h)

KEY TO ABBREVIATIONS

<i>Abbreviation</i>	<i>Content of developer</i>
Dev. + 1 KBr	Basic developer + 0.8 g/l KBr
Dev. + 2 KBr	Basic developer + 1.6 g/l KBr
Dev. + (Circ.)	Basic developer with circulation
Dev. + Borax (Circ.)	Basic developer + 5 g/l Borax with circulation
Dev. + Borax	Basic developer + 5 g/l Borax

at room temperature and cooled gradually to that of the first development stage, preventing the application of severe thermal shock. All subsequent steps of the procedure were performed at a temperature of 10 °C.

The basic developer consisting of

3.8 g/l Amidol ,
6.7 g/l Sodium Sulfite ,

and demineralized water to make one litre, is referred to as the « developer » or as just « Dev » in Table II.

The stop bath consisted of a one-half percent solution of glacial acetic acid, using demineralized water for dilution. The developer sequence of (Developer+KBr) — (Developer) — (Developer+KBr), as suggested by P. H. FOWLER (1955, private communication), was used in an attempt to reduce development activity during the in-diffusion and out-diffusion processes, with the symmetry of the situation serving as a balance to provide uniform development with depth. Borax was used to adjust and buffer pH values, to investigate the effect of such adjustments on distortion. Circulation was introduced in an effort to further reduce penetration time of the developer. The primary purpose of the hot plate procedures was to provide a basis for comparison with such methods.

Following the stop bath the procedure for all plates was the same. Each was placed in a fixing solution consisting of 400 g/l sodium thiosulfate, 40 g/l sodium bisulfite and tap water. Because of the small number of plates being developed in tanks containing thirty-five litres of solution, the fixer was not replenished, but it was continuously recirculated. Fixation was continued for clearing time plus about one day. In each case this amounted to a total of about four days.

At this point the plates were removed from the darkroom and dilution was begun at the rate of about 1.5 l/h. The completion of dilution was simultaneous with the beginning of the washing stage, which was allowed to continue for several days. Total dilution and washing time amounted to about one week.

At the completion of the washing stage, the plates were bathed in a series of four solutions maintained at 10 °C and containing:

- (i) 6 % glycerine: 3 h;
- (ii) 33% alcohol and 6% glycerine: 3 h;
- (iii) 67% alcohol and 6% glycerine: 3 h, and
- (iv) 95% alcohol and 6% glycerine: 3 h.

The remainder of the solutions consisted of tap water for dilution.

The plates were allowed to finish drying in air. Once they were completely dry, the surfaces were cleaned of dirt and excess silver deposit by rubbing with surgical cotton soaked with alcohol. The surfaces of plates 8, 8' and 9', which had remained in circulating developers for the full 6 h development, were so heavily coated with silver that the deposit could not be removed, even with vigorous rubbing, which should otherwise be avoided.

3. - Basic measurements and analysis.

The first step taken in the measurement of grain density was to scan the emulsion roughly, searching for a track which appeared to be a beam track as denoted by its direction and near minimum ionization. Once a track was found, rough scattering measurements were made, following the method of FOWLER ⁽¹⁴⁾ to determine if this was indeed a beam track. The second difference, second overlap method of noise elimination was utilized.

Since the tracks under investigation were only about 1 cm in length, $p\beta$ measurements, based on the second overlap on second differences, were determined on the basis of only about ten independent readings, on the average, giving a statistical uncertainty of about 25% in the measurement of $p\beta$. Assuming that one is working with a proton track, as would be expected in eighty percent of the cases, tracks were accepted if the measured $p\beta$ was in the range $(1.2 \div 2.1)$ GeV/c. Thus it can be seen, with these limits, that the $p\beta$ values for protons and pions were not resolvable. However, this was not necessary for the measurement of grain density variations with depth was the primary objective of the analysis.

Once a track was accepted, the grain density was determined using the method of FOWLER and PERKINS ⁽¹⁵⁾.

The choice of gap size is of some importance and should be discussed. Experimentally, it is found that a B/H ratio of about four is optimum where B is the blob density and H the gap density for gaps greater than or equal to the chosen gap size. Higher values give insufficient statistics on the number of gap counts while lower values provide insufficient sensitivity to variations in grain density. In this experiment, the blob density was based on a count of five hundred blobs, in most cases, and, initially, an optimum gap length of $7.2 \mu\text{m}$ was chosen. Later a change was made to a gap length of $6.0 \mu\text{m}$ in an effort to increase statistics. Spot checks showed that the new gap length gave results consistent with those obtained using the earlier one.

The measurement of background was made with a rectangular grid eyepiece reticle by means of which the number of background grains within a rectangle could be counted as they appeared in focus while the focus was being varied toward increased emulsion depth. In this manner one can obtain a rough estimate of the number of background grains per unit volume. This was done throughout the entire depth of the emulsion, dividing the depth into thirds to get an estimate of the variation of background with depth.

⁽¹⁴⁾ P. H. FOWLER: *Phil. Mag.*, **41**, 169 (1950).

⁽¹⁵⁾ P. H. FOWLER and D. H. PERKINS: *Phil. Mag.*, **46**, 587 (1955).

The final measurement, that of curvature distortion, was made using the method of MAJOR ⁽¹⁶⁾.

4. - Presentation of the data.

In Figs. 1-9 the results of the grain density measurements are presented. The results in each emulsion are based on three or four tracks, depending on the consistency. In each case, grain counting was initiated at the glass surface

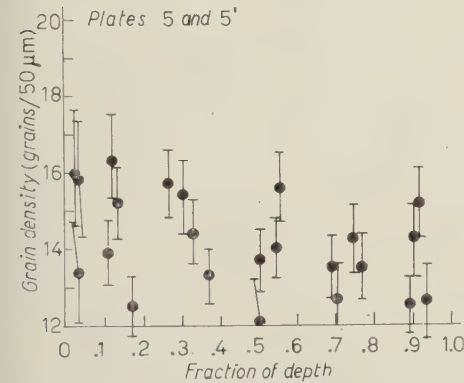


Fig. 1a.

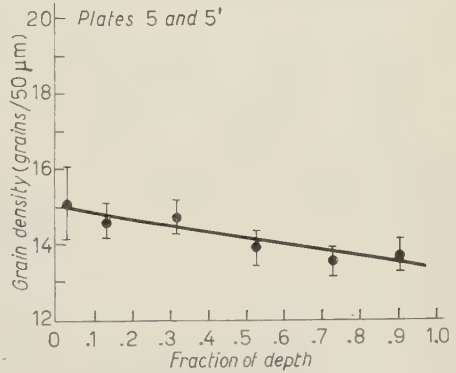


Fig. 1b.

and the results tabulated after each five hundred blob count. In general, then, the blob counts are fewer and hence the statistics not as good for the point

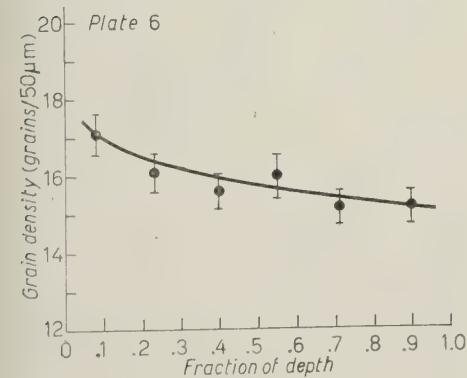


Fig. 2.

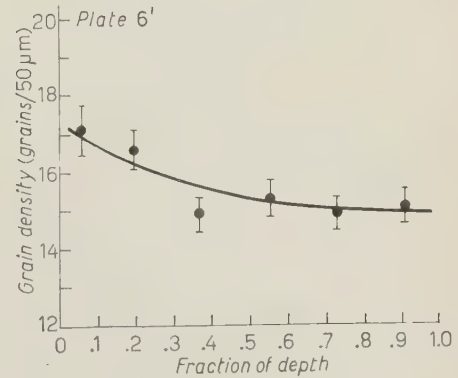


Fig. 3.

nearest the air surface as they are for the points representing lower depths in the emulsion. Nevertheless this procedure was adopted since it had the

⁽¹⁶⁾ J. V. MAJOR: *British Journ. Appl. Phys.*, 3, 309 (1952).

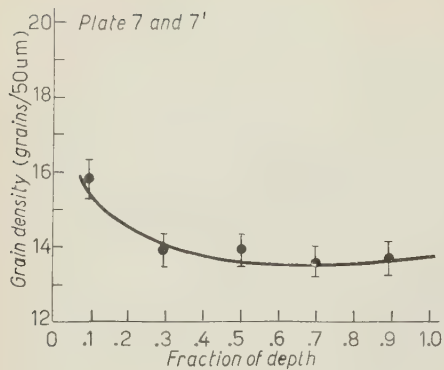


Fig. 4.

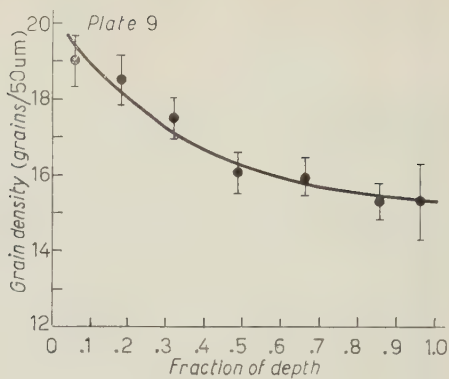


Fig. 5.

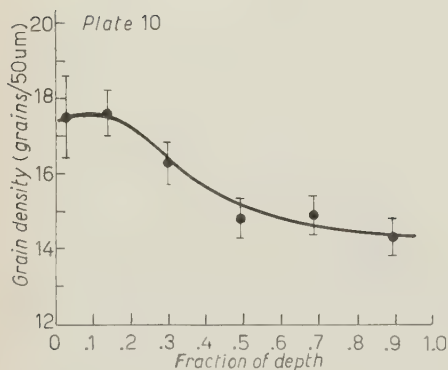


Fig. 6.

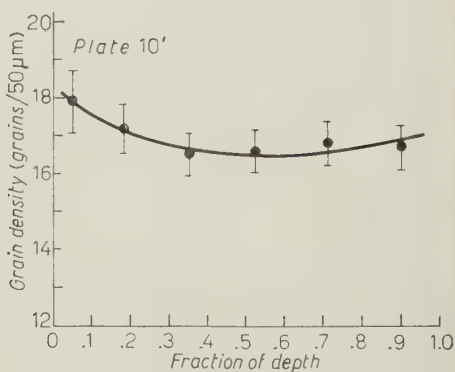


Fig. 7.

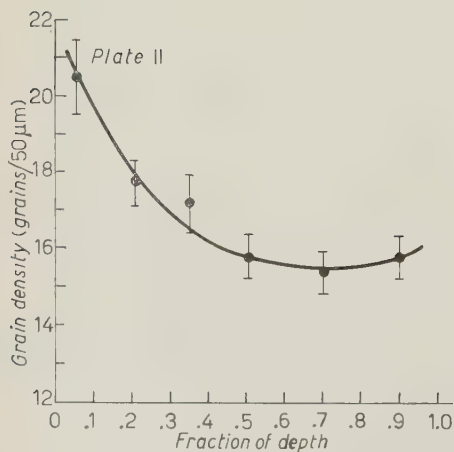


Fig. 8.

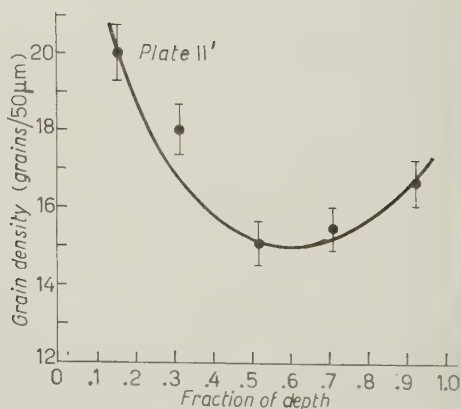


Fig. 9.

desirable property of yielding a point nearer the air surface, the position of particular interest.

Fig. 1*a* shows the results of each point for each track separately to show the dispersion encountered in one emulsion. By grouping the points which

TABLE III. — *Background grain density measurements.*

Plate	Upper third		Middle third		Lower third	
	Background (grains/1000 μm^3)	Ratio	Background (grains/1000 μm^3)	Ratio	Background (grains/1000 μm^3)	Ratio
5 and 5'	$3.2 \pm .2$	4.6	$2.4 \pm .2$	5.8	$2.6 \pm .2$	5.3
6	$6.0 \pm .4$	2.8	$3.0 \pm .2$	5.3	$3.3 \pm .3$	4.6
6'	$6.8 \pm .4$	2.4	$4.4 \pm .3$	3.5	$4.5 \pm .3$	3.3
7 and 7'	$5.5 \pm .2$	2.7	$2.9 \pm .2$	4.7	$3.2 \pm .2$	4.2
9	$9.6 \pm .4$	1.9	$3.8 \pm .3$	4.2	$3.2 \pm .3$	4.8
10	$9.7 \pm .3$	1.8	$4.3 \pm .3$	3.5	$3.4 \pm .3$	4.2
11	$14.1 \pm .6$	1.3	$5.2 \pm .3$	3.0	$3.7 \pm .3$	4.4
11'	$18.4 \pm .6$	1.1	$5.4 \pm .3$	2.8	$4.4 \pm .4$	3.6

lie roughly in the same depth interval, one obtains the results presented in graph 1*b*. This procedure has been adopted in presenting the results for the remaining plates, since it was felt that this gave a clearer picture of the grain density variations. The dispersion observed in plates 9-11' was not as severe as that in plates 5-7'.

It will be noticed that results for plates 8, 8' and 9' are omitted. Due to the heavy surface deposit, mentioned previously, and associated fogging which seemed to penetrate quite deeply into the depth of the emulsion, the clarity was entirely too poor to permit any type of measurement.

The grain densities shown should be slightly below those corresponding to the plateau as explained in Section II and they will thus lie, on the average,

TABLE IV. — *Distortion measurements.*

Plate	Distortion (covans)
5 and 5'	19 ± 6
6	46 ± 14
6'	49 ± 16
7 and 7'	17 ± 5
9	43 ± 13
10	33 ± 11
10'	59 ± 18
11	22 ± 7
11'	30 ± 9

about ten percent above minimum values. The difference from minimum, then, is not significant.

In Table III the results of the background measurements are listed, according to depth. In each case the adjoining column gives the ratio of track grain density to background grain density. Thus, of course, high values in this

TABLE V. - *Grain sizes.*

Plate	α , approximation to the average grain diameter (μm)
5 and 5'	.69
6	.81
6'	.85
7 and 7'	.72
9	.75
10	.83
10'	.80
11	.80
11'	.73

column are more desirable. The errors listed are based on the total number of grains counted, N , in each case, and are computed from $100/(N)^{\frac{1}{2}}$ percent. For plates 5 and 5' and 7 and 7', the values from the two plates are averaged.

The measurements of distortion are presented in Table IV. The data given are based on ten tracks in each plate. The plate was divided roughly into five imaginary columns and two closely located tracks were measure in each column. The errors are computed as in Table III where, in this case, N is the number of tracks measured, 10. Though the statistics are not good, the relative results between the various processing methods are probably meaningful.

It may sometimes be desired to control the grain size during development

TABLE VI. - *pH values.*

Solution	pH value
Demineralized water	$7.2 \div 7.9$
Developer (Basic)	6.5
Developer + 1 KBr	6.5
Developer + 2 KBr	6.4
Developer + Borax	6.9
Stop Bath	3.5
Fixer	4.6
Tap Water	$8.0 \div 9.4$

depending upon the nature of the experiment being undertaken. For this reason the values of α , an approximation to the average diameter of the grains in the developed emulsion, are given in Table V (¹⁵). However, since there is no universally optimum grain size, this aspect of the experiment was not pursued further.

Due also to the importance of pH in processing for minimum distortion, the pH values of the various solutions used in this experiment are presented in Table VI.

5. - Analysis of the results.

A satisfactory processing procedure must give favorable results in all three of the criteria used in the analysis of the plates in this experiment. A study of the results which appear in Section 4 shows quite conclusively that the isothermal procedure, using a developer with potassium bromide added, is the most satisfactory of those used here. However, there seems to be a variation of the desirable characteristics with changes in development time. The unfortunate aspect of this result is the apparent increase in distortion for increased development time, as revealed by the results obtained for plates 5-7'. The distortions observed in plates 5 and 5' and 7 and 7' are quite low; however, an increased development time of only 2 h using the same developer in plates 6 and 6' yielded almost a three-fold increase in distortion. This would place severe limits in the use of development time variations as a control on the magnitude of the grain density. Changing the development time also seems to vary the grain density gradient and the track to background density ratio. This aspect is particularly important since emulsion sensitivity may vary to rather large extremes from one batch to another, and hence quite different development times might be required to give proper grain densities to meet the requirements of the specific experiment. The result is a restriction on temperature as a control on grain density, even though it may be more desirable to stick to one temperature from the standpoint of reducing distortions.

It is obvious from the grain density curves that variations are not entirely eliminated in any of the cases considered. It should be noted, however, that the grain density scale in the figures is expanded to an extent that variations in grain density appear exaggerated. Even the most extreme of the gradients in the potassium bromide developers produced only about fifteen percent variations between grain density extremes in an emulsion. This is an improvement over many procedures in use at present, the low distortions being considered.

It is not surprising that the most serious distortions occur for the processing method which uses a 2 h «hot plate» cycle. It appears on the basis

of the results that an 1 h «hot plate» stage is not undesirable from a distortion standpoint, but this reduction in time leaves one with severe grain density gradients. Actually it appears that the additional hour serves to boost the grain density in the lower regions of the emulsion while having little or no effect on the grain density at the air surface.

Most of the additional results obtained are consistent with those one might expect. Increased development in plates 6 and 6' produces an increase in the average grain density over that of the lesser development time of plates 5, 5', 7 and 7' using the same developer. Also plate 10' with a 2 h hot stage shows a higher grain density than plate 10 using the same developer, but with only a 1 h hot stage.

From the standpoint of background, plate 11, using the same developer as 10 and 10', but with only an isothermal development exhibits considerably higher background grain density in the upper regions of the emulsion especially. This apparently is more than compensated for by the addition of potassium bromide as in plates 5-7'. It appears in the case of the latter plates, however, that too much potassium bromide has the effect of increasing the background grain density again. Also, increased development time increases background in these plates, as one would expect.

The only difference in the treatment of plates 9 and 10 was the application of circulation to the developer in the case of the former. As was expected the results show that this causes an increase in the distortion. No advantages were gained from this procedure.

The purpose of the addition of borax in the developer used for plate 11' was merely to adjust the pH in an effort to reduce the distortion. Apparently, the distortion, either by virtue of the pH change, or some other unknown variation, was increased, along with an increase in the background grain density, over the similar development without borax used in plate 11. For this reason, on the basis of these results, there appears to be no need or justification for adding borax to the developer.

6. - Conclusions.

On the basis of the results presented here it is safe to conclude that the optimum development procedure among those considered in this experiment is an isothermal one using a developer which contains potassium bromide in the amount of about 0.8 g/l in addition to the basic amidol developer described in Section 2. There is still a need for improvement, however. Even though the uniformity of development with depth is excellent for the potassium bromide developers, there is still an additional advantage to be obtained from absolutely constant grain density with depth. This would obviate the need

for any normalization of grain densities and would also make photoelectric determinations much more useful and simple to apply.

On the basis of the results obtained in this experiment, a stack of emulsions was processed using the potassium bromide developer, but the time was varied to adjust the grain density to the value desired for the particular experiment involved. The grain density obtained was far removed from the expected value and hence this emphasized the necessity of processing a series of test plates before each new emulsion batch is processed to determine the correct procedure to obtain the desired results. However, the advantage now is that one can be more certain of obtaining the most desirable results using small variation in the optimum development reported here.

If one adopts the isothermal procedure, an additional advantage is obtained. The rate of development at the lower temperature is sufficiently low that there is no need to bring the development to a rapid stop at the end of the development stage. This removes the need for a stop bath and eliminates the very large change in pH incurred in going from the developer into the stop bath. Direct application of the fixer would wash all of the developer out of the emulsion within thirty minutes, and at such low temperatures and long development time, this additional exposure to developer would be insignificant. This type of procedure should produce a minimum of distortion for it now allows an isothermal procedure with a nearly constant pH throughout.

It is the final conclusion of this experiment, therefore, that the most favorable results can be obtained with an isothermal development at a temperature of approximately 10 °C and containing a developer with the following composition:

Amidol	3.8 g/l
Sodium Sulfite	6.7 g/l
Potassium Bromide	0.8 g/l

and demineralized water to make one litre.

It should be noted here that no attempt has been made at spurious scattering determinations. The assumption was made that the isothermal procedure was satisfactory on the basis of the results of FICHEL and GUSS⁽¹³⁾. Actual analysis of this aspect of the processing procedure would have involved an additional beam exposure, since longer and higher energy tracks would be needed. An analysis of spurious scattering effects in various processing procedures has been made by JUDEK⁽¹⁷⁾. However, the particle energies used in that work are unfortunately so low that the scattering signal actually swamps the noise and thus subtraction of the theoretical sagitta of the multiple Coulomb scattering from the measured mean sagitta to obtain the mean sagitta

(17) B. JUDEK: *Nuovo Cimento*, **16**, 834 (1960).

of spurious scattering is statistically meaningless. JUDEK also shows that the processing methods under investigation yield a noise which increases rapidly with cell-size, which is also a crucial factor of any emulsion process designed to reduce distortions. Thus it would appear that the procedure outlined in the last paragraph is the most acceptable one for the purposes discussed here.

* * *

I wish to express my gratitude to Dr. M. W. FRIEDLANDER for his helpful advice and constant interest. I am also grateful to Dr. D. KEEFE and the University of California Radiation Laboratory for the Bevatron exposure. I wish finally to thank Dr. M. G. K. MENON of the Tata Institute, Bombay, for his interesting and informative discussion of the results.

This work has been supported by the Air Force Office of Scientific Research, the U. S. Army Research Office (Durham) and the National Science Foundation.

RIASSUNTO (*)

Ho sviluppato, usando svariati metodi, emulsioni nucleari esposte nel Bevatrone di Berkeley al fascio di particelle positive da 1.86 GeV/c. Ho trovato che un procedimento isotermico a 10 °C può dare uno sviluppo soddisfacentemente uniforme in profondità. Presento anche dei dati sulla dimensione dei granuli, sulla densità dei granuli di fondo e sulla distorsione per i diversi metodi usati.

(*) Traduzione a cura della Redazione.

Waveforms and Pulse-height Distributions of the Grid Pulses from Gridded Ionization Chambers.

I. OGAWA

Department of Physics, Rikkyo University - Tokyo

(ricevuto il 26 Giugno 1961)

Summary. — An improved pulse-height formula for the grid pulses from a gridded ionization chamber is derived on the basis of a waveform analysis. It is found that the original formula proposed by BOCHAGOV *et al.* becomes insufficient for an accurate work, when the drift time t_2 of electrons in the grid-collector space is not negligible in respect to the drift time t_1 in the cathode-grid space. It is shown that the negative pulse-height of grid pulses due to particles emitted from the collector or the grid is very small compared to those due to particles from the cathode, provided that $t_2 \ll t_1$. Distortion in pulse-height distributions, caused by the finite thickness of the source as well as by the finite band-width of the amplifier, is also investigated analytically.

1. — Introduction.

BOCHAGOV, VOROB'EV and KOMAR ^(1,2) showed, in 1956, that the pulses extracted from the grid of a gridded ionization chamber may be conveniently used as a signal containing information on the orientation of tracks of α -particles emitted from the cathode of the chamber. This method has been made more complete with the use of a double-grid chamber by OGAWA and DOKE ⁽³⁾, who succeeded in obtaining a high resolution of about 2% in energy

⁽¹⁾ B. A. BOCHAGOV, A. A. VOROB'EV and A. P. KOMAR: *Izv. Akad. Nauk SSSR, Ser. Fiz.*, **20**, 1455 (1956).

⁽²⁾ B. A. BOCHAGOV, A. A. VOROB'EV and A. P. KOMAR: *Zh. Tekhn. Fiz.*, **27**, 1575 (1957).

⁽³⁾ I. OGAWA and T. DOKE: *Journ. Phys. Soc. Japan*, **16**, 1025 (1961).

even when pulses are extracted simultaneously from both the grid and the collector.

BOCHAGOV *et al.* ^(1,2) demonstrated that the method is applicable to the « electronic collimation » of α -particles. In addition, they pointed out the advantage of the method when applied to the measurement of α - γ angular correlation. OGAWA ⁽⁴⁾ attempted to extend the method to the measurement of angular distributions of nuclear reactions. Furthermore, DOKE ⁽⁵⁾ confirmed the possibility of discriminating the background with the help of grid pulses.

The method is based on the fact that the negative amplitude V_g of a grid pulse becomes a linear function of $\cos \theta$, where θ is the angle of direction of an α -particle with respect to the normal to the cathode. BOCHAGOV *et al.* ^(1,2) gave the following expression for V_g :

$$(1) \quad V_g = (Q_0/C_g) \cdot \{1 - (R^*/d_1) \cos \theta\},$$

where Q_0 denotes the total charge of the ions, C_g the capacity of the grid system, and d_1 the separation between the grid and the cathode, while R^* is a quantity representing a length close to the range R of the particle.

For a mere explanatory demonstration of the method, formula (1) with $R^* = R$ is accurate enough to analyse the observed pulse-height distribution. However, for a more precise measurement, it is necessary to prepare an explicit expression for R^* as a function of pertinent parameters and to examine whether R^* is really independent of $\cos \theta$ or not. Moreover, the effect of finite band-width of the amplifier, must be taken into account.

In view of the versatility of the method, the author carried out a waveform analysis of the grid pulses in a more general manner than BOCHAGOV *et al.*, and succeeded in deriving an improved pulse-height formula, together with a few approximate expressions giving the distortion effect of the source thickness and the amplifier band-width on the pulse-height distribution.

2. - Derivation of the improved pulse-height formula.

We consider the waveform of a pulse extracted from the grid of an ordinary (*single-grid*) ionization chamber as shown schematically in Fig. 1. We assume that the collector is grounded or directly connected to a power supply. This implies that we neglect the effect of electrostatic induction between the grid and the collector.

⁽⁴⁾ I. OGAWA: *St. Paul's Review of Arts and Science*, No. 10 (1961).

⁽⁵⁾ T. DOKE: Private conversation.

The results to be obtained with the above assumption should hold accurately for a *double-grid* chamber, in which the screen grid plays the same rôle as the collector in a single-grid chamber, as far as grid pulses are concerned.

According to an elementary consideration, a point charge q_0 at any position (x, y, z) in the chamber generally gives rise to a signal voltage

$$(2) \quad v = \varphi \cdot q_0 / C_g,$$

on the grid G , where C_g denotes the capacity of the G -system, while φ is the potential at (x, y, z) when G is kept at the unit potential and all other conductors (the collector C , the cathode K and the vessel) are grounded.

Therefore, the instantaneous value $V(t)$ at any time t of the signal voltage from G is calculated from the formula

$$(3) \quad V(t) = (1/C_g) \iiint \{ \varrho^-(x, y, z, t) + \varrho^+(x, y, z, t) \} \cdot \varphi \cdot dx dy dz,$$

where $\varrho^-(x, y, z, t)$ and $\varrho^+(x, y, z, t)$ are the charge density of electrons and ions, respectively, and $dx dy dz$ designates the volume element at (x, y, z) . The integration is to be carried out over the entire volume of the chamber.

If we take the z -axis along the symmetry axis of the chamber, with the origin on K , as is shown in Fig. 1, then we have

$$(4) \quad \begin{aligned} \varphi &= \varphi(z) \simeq z/d_1, & \text{for } 0 < z < d_1 \\ &= (d_1 + d_2 - z)/d_2, & \text{for } d_1 < z < d_1 + d_2 \end{aligned}$$

in the effective space, where d_1 , d_2 are the distances between K - G , G - C , respectively. It is tacitly assumed that the diameter of the electrodes is sufficiently greater than d_1 and d_2 .

For φ given by (4), (3) may be rewritten as

$$(5) \quad V(t) = (1/C_g) \cdot \int_0^{d_1+d_2} (\varrho_z^- + \varrho_z^+) \cdot \varphi(z) dz,$$

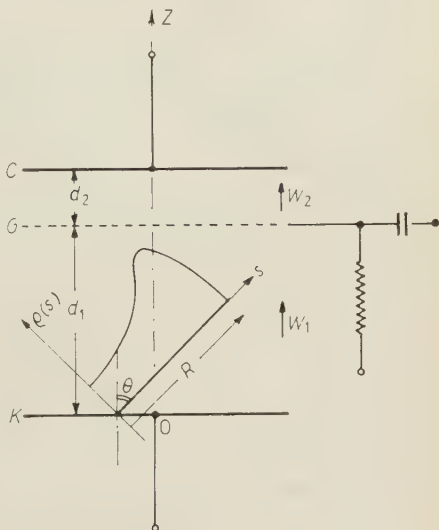


Fig. 1. - Schematic view of a single-grid ionization chamber.

where

$$(6) \quad \varrho_z^\pm = \varrho_z^\pm(z, t) \equiv \iint \varrho^\pm(x, y, z, t) dx dy.$$

Let us apply (5) to the case illustrated in Fig. 1. An α -particle or proton is supposed to be emitted at the time $t = 0$ from K with an angle θ to the z -axis. Let $\varrho(s)$ be the linear charge density of the ions produced along the track at the position s , where s is the distance from the origin of the track. We assume that the range R of the particle is smaller than d_1 .

Then, denoting by w_1 and w_2 the drift velocity of electrons in the space K - G and G - C , respectively, we obtain, after some calculation, the following expressions for ϱ_z^\pm :

I) For ions:

$$(7a) \quad \begin{cases} \varrho_z^+ = \varrho(z/\cos \theta)/\cos \theta & \text{for } 0 < z < R \cos \theta, \\ = 0 & \text{for } R \cos \theta < z. \end{cases}$$

II) For electrons:

i) During the period: $0 < t < t_0 \equiv (d_1 - R \cos \theta)/w_1$

$$(7b) \quad \begin{cases} \varrho_z^- = 0 & \text{for } 0 < z < w_1 t, \\ = -\varrho(z - w_1 t/\cos \theta)/\cos \theta & \text{for } w_1 t < z < w_1 t + R \cos \theta, \\ = 0 & \text{for } w_1 t + R \cos \theta < z. \end{cases}$$

ii) During the period: $t_0 < t < t_1 \equiv d_1/w_1$

$$(7c) \quad \begin{cases} \varrho_z^- = 0 & \text{for } 0 < z < w_1 t, \\ = -\varrho(z - w_1 t/\cos \theta)/\cos \theta & \text{for } w_1 t < z < d_1 \end{cases}$$

iii) During the period: $t_1 < t$

$$(7d) \quad \varrho_z^- = 0 \quad \text{for } 0 < z < d_1.$$

iv) During the period: $t_0 < t < t_0 + t_2$, $t_2 \equiv d_2/w_2$

$$(7e) \quad \begin{cases} \varrho_z^- = -\frac{w_1}{w_2} \varrho \left[\frac{1}{\cos \theta} \left\{ \left(d_1 + \frac{w_1}{w_2} (z - d_1) \right) - w_1 t \right\} \right] \cdot \frac{1}{\cos \theta} & \text{for } d_1 < z < \\ & < d_1 + w_2(t - t_0), \\ = 0 & \text{for } d_1 + w_2(t - t_0) < z < d_1 + d_2. \end{cases}$$

v) During the period: $t_0 + t_2 < t < t_1 + t_2$

$$(7f) \quad \varrho_z^- = -\frac{w_1}{w_2} \varrho \left[\frac{1}{\cos \theta} \left\{ \left(d_1 + \frac{w_1}{w_2} (z - d_1) \right) - w_1 t \right\} \right] \cdot \frac{1}{\cos \theta}$$

for $d_1 < z < d_1 + d_2$.

In the calculation, the motion of ions is neglected. t_0 is evidently the time when the column of the electrons reaches the G -plane. In computing ϱ_z^- for $d_1 < z < d_1 + d_2$, we made use of the relation

$$\varrho_{z2}^-(d_1, t) = (w_1/w_2) \cdot \varrho_{z1}^-(d_1, t),$$

where ϱ_{z1}^- and ϱ_{z2}^- denote $\varrho_z^-(z, t)$ defined by (6) in the space K - G and G - C , respectively.

Substituting (4) and (7a ~ f) into (5) and carrying out the integration, we arrive at the following expressions for $V(t)$:

I) For $0 < t < t_0$:

$$(8a) \quad V(t) = - (Q_0/C_g) \cdot (t/t_1).$$

II) For $t_0 < t < [t_1, t'_0]_{\text{Min}}$, where $[t_1, t'_0]_{\text{Min}}$ denotes the minor of t_1 and

$$t'_0 \equiv t_0 + t_2:$$

$$(8b) \quad V(t) = -\frac{Q_0}{C_g} \left[1 - \frac{t_1 + t_2}{t_2} \cdot \frac{Q_2}{Q_0} \cdot \frac{\bar{X}_2}{d_1} \cos \theta - \frac{1}{Q_0} \left\{ Q_1 - Q_2 \cdot \left(\frac{t_1}{t_2} \right) \right\} \left(1 - \frac{t}{t_1} \right) \right].$$

III) For $t_1 + t_2 < t$:

$$(8c) \quad V(t) = (Q_0/C_g) \cdot (\bar{X}/d_1) \cos \theta.$$

In (8a ~ c), Q_0 , \bar{X} , Q_1 , Q_2 and \bar{X}_2 are defined as follows:

$$\begin{aligned} Q_0 &= \int_0^R \varrho(s) \, ds, \\ \bar{X} &= \left\{ \int_0^R \varrho(s) s \, ds \right\} / Q_0, \\ Q_1 &= \int_0^{s_1} \varrho(s) \, ds, \\ Q_2 &= \int_0^R \varrho(s) \, ds, \\ \bar{X}_2 &= \left\{ \int_{s_1}^R \varrho(s) s \, ds \right\} / Q_2, \end{aligned}$$

where

$$s_1 \equiv (\bar{d}_1 - w_1 t) / \cos \theta.$$

The expression of $V(t)$ for $[t_1, t_0']_{\text{Min}} < t < t_1 + t_2$ is not given here since it is rather lengthy but not very important.

For protons or α -particles, $\varrho(s)$ assumes the form of a Bragg curve. For any analytical expression of $\varrho(s)$ approximating this curve, $V(t)$ given by (8a \sim c) always shows a negative maximum at a time t_m in the period $t_0 < t < [t_1, t_0']_{\text{Min}}$. The negative amplitude V_g of the grid pulse is thus calculated from (8b) to be

$$(9) \quad V_g = (Q_0/C_g) \cdot \{1 - (1 - \delta) \cdot (R/\bar{d}_1) \cos \theta\},$$

where

$$(10) \quad \delta \equiv (1/R) \cdot \int_{s_m}^R \varrho(s) \cdot (R - s) ds \bigg/ \int_{s_m}^R \varrho(s) ds,$$

with $s_m \equiv (\bar{d}_1 - w_1 t_m) / \cos \theta$. t_m is determined from the equation $\dot{V}(t_m) = 0$ derived from (8b). In general, δ becomes a function of $\vartheta \equiv t_2/t_1$,

For the simplest approximation

$$(11) \quad \begin{cases} \varrho(s) = \text{const} = Q_0/R & \text{for } 0 < s < R, \\ = 0 & \text{for } s > R, \end{cases}$$

(10) leads to

$$(12) \quad \delta = (1/2)\vartheta/(1 + \vartheta) = (1/2)/\{1 + (t_1/t_2)\} \quad (*).$$

For another case where $\varrho(s)$ assumes a little more realistic form

$$(13) \quad \begin{cases} \varrho(s) = (2/3) \cdot (Q_0/R) \{1 - (s/R)^{-1/3}\} & \text{for } 0 < s < R, \\ = 0 & \text{for } s > R, \end{cases}$$

(10) gives

$$(14) \quad \delta = (5/8) \cdot \{\vartheta/(1 + \vartheta)\}^{3/2} = (5/8)/\{1 + (t_1/t_2)\}^{3/2}.$$

(*) Note added in proof. - (Cf. T. DOKE, M. TSUKUDA and I. OGAWA: *Journ. Appl. Phys. Japan* **27**, 573 (1960)): KOROLEV and KOCHAROV have independently obtained the same result as (12) by assuming (11) throughout the calculation; G. A. KOROLEV and G. E. KOCHAROV: *Izv. Akad. Nauk. SSSR, Ser. Fiz.* **24**, 357 (1960).

It is thus concluded that ϑ , and hence $R^* \equiv R \cdot (1 - \delta)$, is independent of $\cos \theta$.

Fig. 2 shows an example of pulse-shapes given by (8a ~ c) with (11). Fig. 3 is the plot of δ vs. ϑ relation given by (12) and (14). Fig. 3 also gives

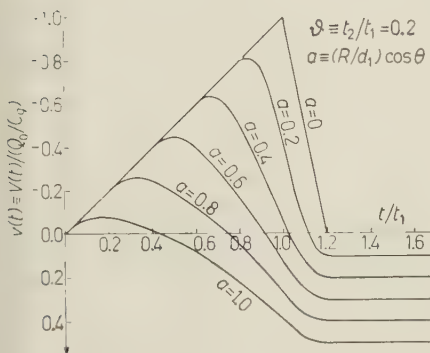


Fig. 2. — Typical waveforms of grid pulses given by (8) with (11) for $\delta \equiv t_2/t_1 = 0.2$.

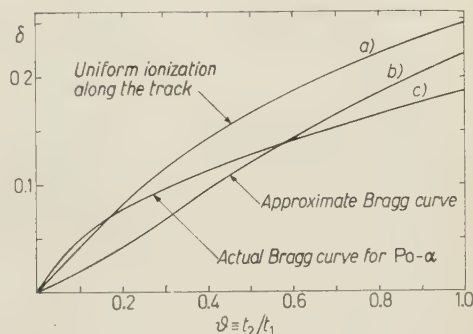


Fig. 3. — δ vs. ϑ relation for different shapes of $\varrho(s)$. δ is the fractional correction to the range R in the pulse-height formula.

the result of graphical integration of (10) for an experimental Bragg curve observed on Po- α -particles. All the curves shown in Fig. 3 have been found to be in a better agreement with the experimental results, as compared with the approximation $\delta = 0$ or $R = R^*$.

3. — Grid-pulses due to particles from other than the cathode.

DOKE⁽⁵⁾ recently succeeded in a new method of low-background counting with a double-grid chamber. The method is based on the fact that the grid pulses due to particles originated from the grid, the collector and the guard ring around it are essentially of the opposite (positive) polarity as compared to those due to particles from the cathode. It is the purpose of this section to examine how exactly the above statement holds under various operating conditions, in particular, when ϑ is not negligible to unity.

In the simplest case where $\varrho(s)$ assumes the expression (11) and ϑ is negligibly small, the positive charge Q^- on the grid G induced by the electrons as a whole increases only while the entire column of the electrons lies between the grid G and the cathode K (see Fig. 4). Such a configuration of electrons never occurs when the ionizing particle is emitted from the grid or the collector C' , with the exception of the initial moment for the particle emitted from G toward K .

Drift of an electron column crossing or leaving G toward C *always* results in a decrease in Q^- and hence contributes to the *positive* increase of the grid voltage $V(t)$. The positive ions merely bring a positive contribution independent

of t to let $V(0) = 0$ during the collection time of electrons. Therefore, it is concluded quite generally that the particles originated from G , C , or the space between G and C never produce any negative grid pulse at all. In addition, any particle crossing or reaching G from the K - G space will also never give a negative pulse.

Particles from G or C are usually due to radioactive contamination or proton recoils from the hydrogenous deposit on those electrodes. Thus it is possible to discriminate those background particles by counting only *negative* grid pulses.

For $\varrho(s)$ given by (13) but ϑ still assumed to be negligible to unity, the above statement must be slightly modified. Slightly negative grid pulses may arise when the particles are emitted from G toward K . It can be shown that the negative pulse-height $V_g^{(-)}$ becomes greatest when $R \cos \theta = d_1$, where θ is now the angle of the track

Fig. 4. Calculation of the negative amplitude of a grid pulse due to a particle from the grid.

with respect to the normal to the grid-plane. The maximum value $V_m^{(-)}$ is calculated to be

$$(15) \quad V_m^{(-)} = 0.058 \cdot (Q_0/C_g).$$

This is fairly small compared to the pulse-heights to be measured (or used) due to the particles of the same energy emitted from the cathode with a range not very close to d_1 , and is easily discriminated by a shallow bias voltage.

Even when ϑ cannot be ignored against unity, the negative pulse-height, if any, caused by the particles from G or C , is fairly small compared to Q_0/C_g , so far as ϑ is considerably smaller than unity. In fact, for $\varrho(s)$ given by (11), the greatest possible (negative) pulse-height $V_m^{(-)}$, as induced by such a particle as shown in Fig. 4, turns out, after some calculation, to be

$$(16) \quad V_m^{(-)} = (Q_0/C_g) \cdot (1/2) \cdot \vartheta / (1 + \vartheta),$$

while for $\varrho(s)$ as given by (13):

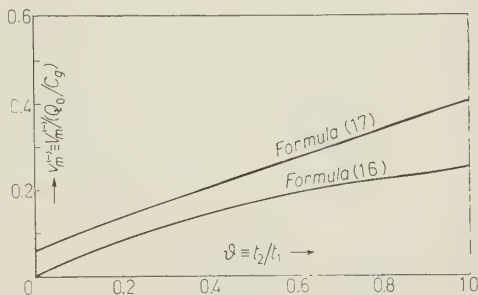
$$(17) \quad V_m^{(-)} = (Q_0/C_g) [(1 + \vartheta) \Theta^{2/3} - (2/5)(1/\vartheta) \{ (\Theta + \vartheta)^{5/3} - \Theta^{5/3} \} + (2/5)(\Theta^{5/3} - 1)],$$

where

$$\Theta = \Theta(\vartheta) \equiv \vartheta / \{ (1 + \vartheta)^{3/2} - 1 \}.$$

In the limit when $\vartheta \rightarrow 0$, (17) tends to (15). (16) and (17) are plotted in Fig. 5. As is evident from the graph, $V_m^{(-)}$ is much smaller than Q_0/C_g for $\vartheta \lesssim 0.4$.

Fig. 5. — Maximum negative amplitude $V_m^{(-)}$ divided by (Q_0/C_g) of a grid pulse due to a particle from other than the cathode. Two different shapes are assumed for $\varrho(s)$.



4. — Effect of finite thickness of the source on the pulse-height distribution.

Formula (1) or (9) implies that the pulse-height distribution of grid pulses due to monoenergetic particles from the cathode represents the angular distribution of the particles in terms of $\cos\theta$. In particular, when the particles are emitted isotropically, the distribution will be of a rectangular shape ranging from $V_{g, \min} = (Q_0/C_g) \cdot \{1 - (R^*/d_1)\}$ to $V_{g, \max} = Q_0/C_g$.

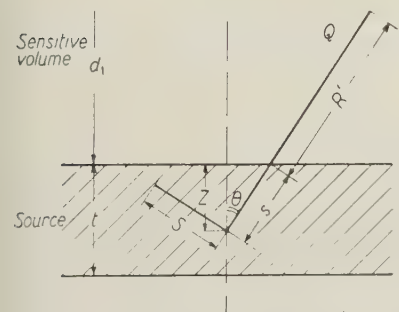


Fig. 6. Geometry for calculating the effect of finite thickness of the source on the pulse-height distribution.

In practice, however, there are various effects which may distort the pulse-height distribution: 1) Finite thickness of the source; 2) Finite band-width of the amplifier; 3) Non-uniformity of the electric field in the chamber; 4) Electron attachment; 5) Noise; 6) Energy and range straggling of the particles. This section deals with 1) in some detail.

Let us consider a source with uniform thickness t . (We follow the traditional notation; there may be no confusion with the time.) t is supposed to be negligibly small compared to the source diameter. Let S denote the range of the particle in the source, and z the depth measured from the surface. We assume, for simplicity, $\varrho(s)$ to be constant both in the gas and the source. Further we assume that $\delta = 0$, so that $R^* = R$.

Then, referring to Fig. 6, we obtain the following expression for the pulse-

height V_g :

$$(18) \quad \begin{cases} V_g = \frac{Q_0}{C_g} \cdot \left(1 - \frac{z}{S \cos \theta}\right) \cdot \left\{1 - \frac{R}{d_1} \left(1 - \frac{z}{S \cos \theta}\right) \cos \theta\right\} & \text{for } \cos \theta > z/S, \\ = 0 & \text{for } \cos \theta < z/S, \end{cases}$$

by merely replacing Q_0 and R^* of (1) by $Q' = \{1 - (z/S \cos \theta)\}Q_0$ and $R' = \{1 - (z/S \cos \theta)\}R$, respectively. In (18), Q_0 , R is the quantity of ions and the range in the gas for a particle with $z=0$.

With the abbreviations

$$(19) \quad v \equiv V_g/(Q_0/C_g), \quad \xi \equiv \cos \theta, \quad \eta \equiv z/S, \quad \alpha \equiv R/d_1,$$

(18) may be rewritten as

$$(20) \quad \begin{cases} v = \{1 - (\eta/\xi)\} \cdot \{1 - \alpha(\xi - \eta)\} & \text{for } \xi > \eta \\ = 0 & \text{for } \xi < \eta \end{cases}$$

An example of a set of contours for v given by (20) is shown in Fig. 7.

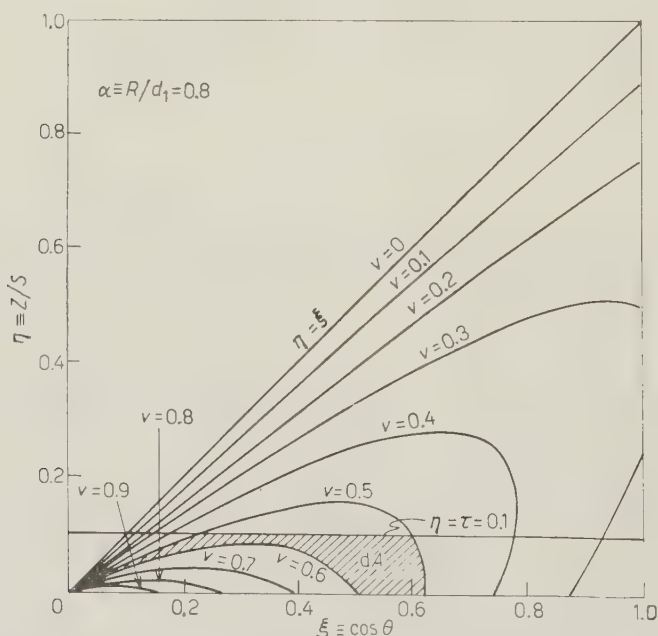


Fig. 7. - Contours for the «reduced» pulse-height $v \equiv V_g/(Q_0/C_g)$ given by (20). Abseissa indicates $\cos \theta$, while ordinate represents the depth of emitting point measured in S , the range of the particle in the source.

Suppose that the α -particles are monoenergetic and emitted isotropically. Then the number of particles dN emitted per unit time from the layer $z \sim z + dz$ into the solid angle $d\Omega = 2\pi \sin \theta d\theta$ is evidently proportional to $dz d\Omega \propto \alpha - d\xi d\eta$ by (19). Accordingly, we may obtain the pulse-height distribution $n(v)$ by computing the infinitesimal area dA in the graph like Fig. 7 as a function of v .

Let $\tau \equiv t/S$. For $0 < \tau \ll 1 - (1/2\alpha)$ with $1 > \alpha > \frac{1}{2}$, the above method leads to the following approximate expression for $n(v)$:

$$(21) \quad \left\{ \begin{array}{ll} n(v) = n_0 \cdot (\alpha\tau/2)/(1-v)^2 & \text{for } 0 < v < v_0 = 1 - \alpha, \\ = n_0 \cdot \left\{ \frac{v - v_0}{v_1 - v_0} + \frac{\alpha\tau}{2} \cdot \frac{1}{(1-v)^2} \right\} & \text{for } v_0 < v < v_1 \equiv v_0 + (2\alpha - 1)\tau, \\ = n_0 \cdot \left\{ 1 + \frac{\alpha\tau}{(1-v)^2} \right\} & \text{for } v_1 < v < v_2 \equiv 1 - \sqrt{2\alpha\tau}, \\ = n_0 \cdot \frac{3}{4\alpha\tau} \cdot (1-v)^2 & \text{for } v_2 < v < 1, \\ = 0 & \text{for } 1 < v, \end{array} \right.$$

where n_0 is a constant. (21) is plotted in Fig. 8 for $\alpha = 0.8$.

As is seen from Fig. 8, the finite thickness of the source generally produces a peak at the right end of the pulse-height distribution. It should be observed that even a fairly thin source with $\tau = 1\%$ or less may show an appreciable distortion in the pulse-height distribution. Fig. 9 gives an example

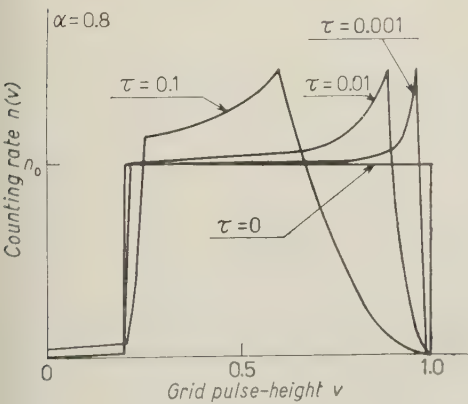


Fig. 8. — Distortion in the pulse-height distribution caused by the finite thickness of the source.

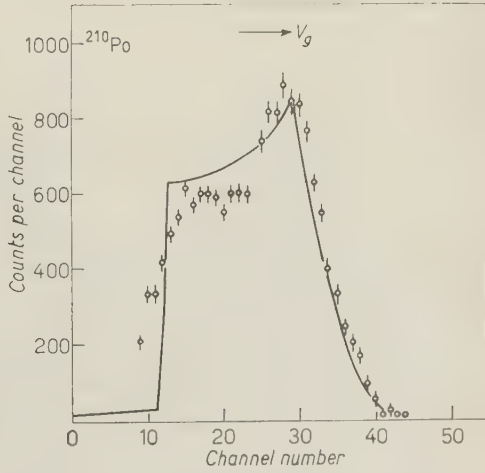


Fig. 9. — Distorted pulse-height distribution actually observed with a thick source of ^{210}Po in comparison with a theoretical curve of the best fit (solid line).

of distorted distribution observed with a thick source of ^{210}Po , together with a theoretical curve for $\alpha = 0.744$, $\tau = 0.072$ (the best fit).

The layer covering the source, and the roughness and curvature of the surface, may also cause similar effect.

5. - Effect of finite bandwidth of the amplifier on the pulse-height distribution.

We shall investigate analytically how the differentiating and integrating time constant T_1 and T_2 of the amplifier should be chosen to minimize the distortion in the pulse-height distribution of the output pulses due to non-linearity.

In practical applications, the pulse-height distribution to be measured is usually due to particles of a selected energy. We therefore limit our discussion to the case where both Q_0 and R^* may be regarded as a constant in (1) and (8). Thus we consider, for simplicity, «reduced» input pulses $v(t) \equiv -V(t)/(Q_0/C_g)$ given by

$$(22) \quad \begin{cases} v(t) = t/T & \text{for } 0 \leq t \leq t_0, \\ = (t/T) - \{1 + (\alpha/2)\xi\} \{(t - t_0)/(T - t_0)\} & \text{for } t_0 \leq t \leq T, \\ = -(\alpha/2)\xi & \text{for } T \leq t, \end{cases}$$

where

$$(22a) \quad \alpha \equiv R/d_1, \quad \xi \equiv \cos \theta, \quad t_0 \equiv T \cdot (1 - \alpha\xi), \quad T \equiv \bar{d}_1/w_1.$$

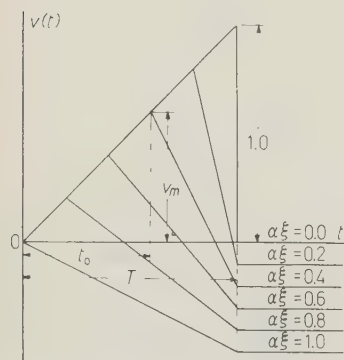


Fig. 10. - Approximate waveforms of grid pulses as given by (22), introduced for calculating the non-linearity of the amplifier.

(22) may be looked upon as a rectilinear approximation of (8) (or Fig. 2) with $t_2 = 0$, as is evident from the plot given in Fig. 10. For (22), the «reduced» pulse-height $v_m \equiv V_g/(Q_0/C_g)$ is given by

$$(23) \quad v_m = v(t_0) = t_0/T = 1 - \alpha\xi.$$

4.1. Case when $T_2 = 0$: pure clipping. - Let us denote by $u(t)$ the («reduced») output waveform. Then, for the period $0 \leq t \leq t_0$, $u(t)$ satisfies the differential equation

$$(24) \quad \dot{u} + (u/T_1) = \dot{v}(t) = 1/T.$$

Solving (24) under the initial condition $u(t) = 0$

and substituting $t = t_0$, we obtain the following expression for the « reduced » output pulse-height u_m :

$$u_m = u(t_0) = x_1 \cdot \{1 - \exp[-(t_0/T)/x_1]\}, \quad x_1 \equiv T_1/T.$$

Hence, by (22a), we get the u_m vs. v_m relation as

$$(25) \quad u_m = x_1 \cdot \{1 - \exp[-v_m/x_1]\},$$

(25) is plotted in Fig. 11 for various values of x_1 .

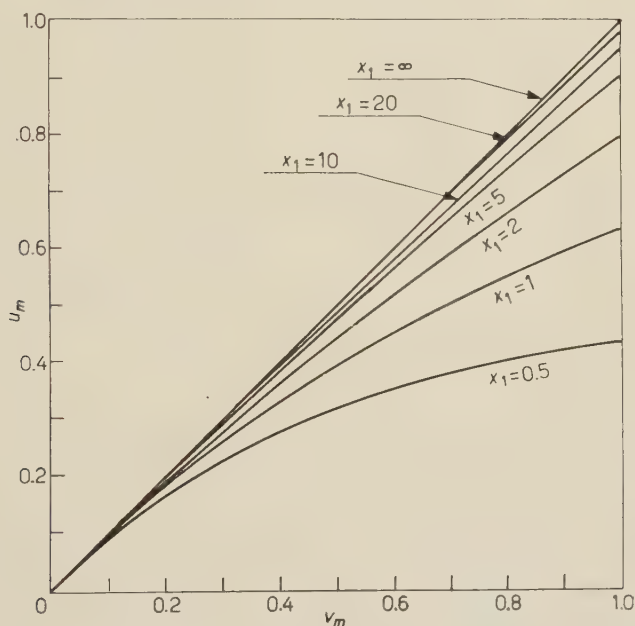


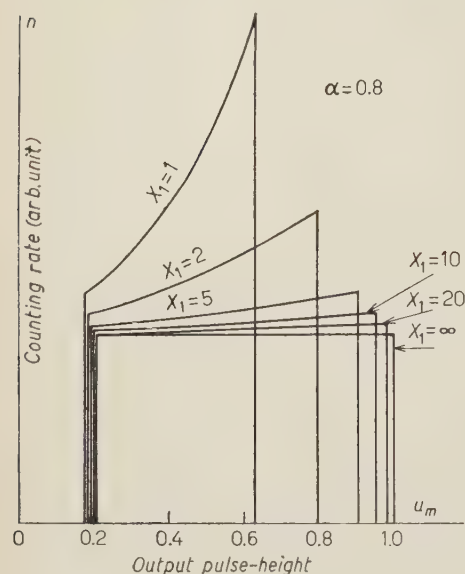
Fig. 11. — Non-linearity caused by the effect of pure clipping.

It is seen from the figure that u_m generally shows a trend of saturation toward larger v_m , unless $T_1 = \infty$. This implies that the pulse-height distribution $n(u_m)$ due to isotropic α -particles will be peaked toward the right.

Let $d\Omega$ denote the infinitesimal solid angle of emission with equal $\cos\theta$. Then $n(u_m) \propto d\Omega/du_m \propto -(d\xi/dv_m) \cdot (dv_m/du_m) = (1/\alpha) \cdot (dv_m/du_m)$. Hence we get from (25) the explicit expression for $n(u_m)$:

$$(26) \quad \begin{aligned} n(u_m) &= 0 & \text{for } 0 < u_m < u_1 \equiv x_1 \cdot \{1 - \exp[-v_0/x_1]\}, \\ &= n_0/\{1 - (u_m/x_1)\} & \text{for } u_1 < u_m < u_2 \equiv x_1 \{1 - \exp[-1/x_1]\}, \\ &= 0 & \text{for } u_2 < u_m, \end{aligned}$$

where $v_0 \equiv 1 - \alpha$ and $n_0 = \text{constant}$. Fig. 12 shows the plot of (26) for a few values of $x_1 \equiv T_1/T$.



The relative amount $\delta_2 \equiv \{n(u_2) - n(u_1)\}/n(u_1)$ of the right-hand peak turns out to be

$$(27) \quad \delta_2 = \exp[\alpha T/T_1] - 1$$

by (26). If $x_1 \gg 1$ (hence $T_1 \gg T$), then $\delta_2 \simeq \alpha \cdot (T/T_1)$. Fig. 13 gives the graphical plot of the relation (27). It is concluded from the figure that T_1 should be chosen as large as possible compared to T .

Fig. 12. — Distortion in the pulse-height distribution due to the effect of finite clipping time (time constant of differentiation) T_1 .

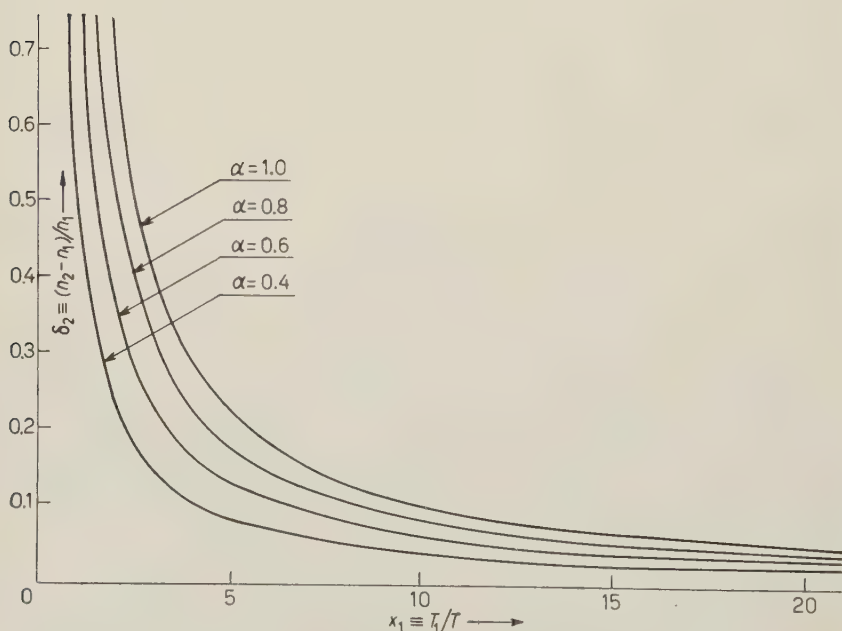


Fig. 13. — The relative amount δ_2 of the peak in the pulse-height distribution due to finite T_1 as a function of $\alpha/x_1 \equiv (R/d_1) \cdot (T/T_1)$.

4.2. *Case when $T_1 = \infty$: pure rise-time effect.* — First we solve the differential equation for $u(t)$:

$$T_2 \cdot \dot{u} + u = v(t),$$

with $v(t)$ given by (22) under the initial condition $u(0) = 0$ together with the condition of continuity in $u(t)$ at $t = t_0$. Then, computing for u_m , we obtain, after some calculation, the following expression for the u_m vs. v_m relation:

$$(28) \quad u_m = kv_m - (k-1) \cdot x_2 \cdot \log \frac{k \exp [v_m/x_2] - 1}{k-1},$$

where

$$(28a) \quad k = (1/2) + (1 - v_m)^{-1}.$$

The plot of (28), given in Fig. 14, shows that all the curves are downward convex near the origin unless $x_2 = 0$. This means that the pulse-height dis-

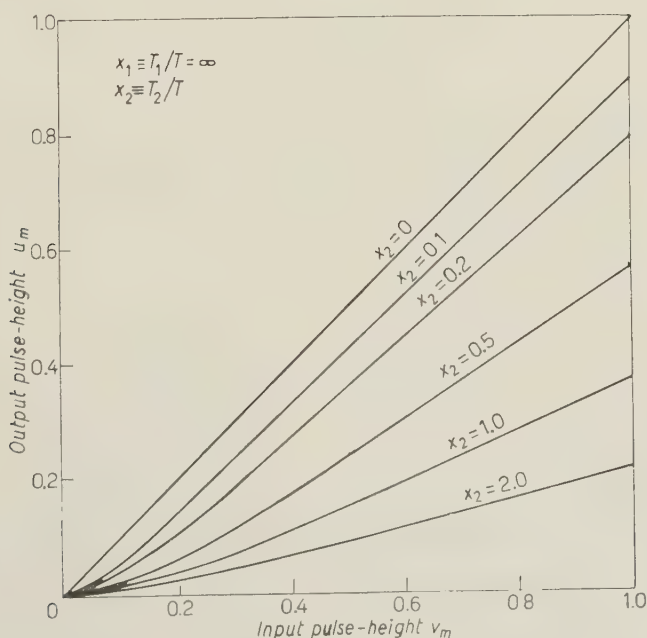


Fig. 14. — Non-linearity due to finite rise-time (integrating time constant) T_2 . $x_2 = T_2/T$.

tribution $n(u_m)$ for isotropic particles will be more or less peaked leftwards unless $T_2 \ll T$. It should be noted, however, that all the u_m vs. v_m curves are fairly rectilinear for $v_m \gtrsim 1/e = 0.37$, say, even when $x_2 \simeq 1$.

It follows that we may well use such a large $T_2 (\simeq T)$ without any appreciable distortion in $n(u_m)$, so far as we limit $\alpha \equiv R/d_1$ to be less than $1 - (1/e) = 0.63$, say. Although the use of such a large T_2 is advantageous for the improvement of signal-to-noise ratio, it is to be remembered that the extrapolated straight line from the quasi-linear portion of a u_m vs. v_m curve generally passes somewhat below the origin.

In the case where $t_2 \ll t_0$ (hence $x_2 \ll 1 - \alpha$), the relative magnitude δ_1 of the left-hand peak defined by $\delta_1 = \{n(u_{\min}) - n(u_{\max})\}/n(u_{\max})$ is approximately calculated from (28) to be

$$(29) \quad \delta_1 \simeq A \cdot x_2,$$

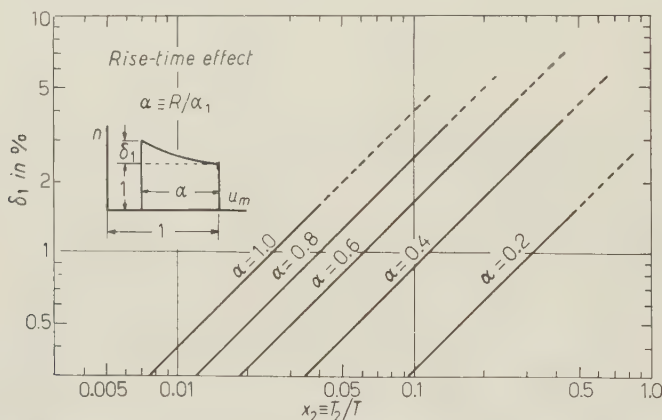


Fig. 15. Relative peaking δ_1 in the pulse-height distribution due to finite rise-time.

where

$$(29a) \quad A \equiv A(\alpha) = \frac{1}{\alpha^2} \left\{ \log \left(\frac{2 + \alpha}{2 - \alpha} \right) + \left(\frac{2 + \alpha}{2 - \alpha} \right) - 1 \right\} - \frac{1}{2}.$$

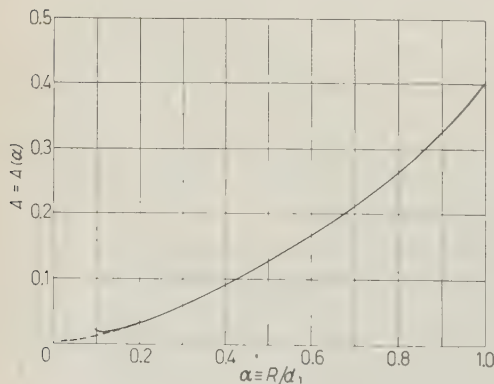


Fig. 16. — The function $A(\alpha)$ vs. α .

In the definition of δ_1 , $u_{\min} \equiv u_m(1 - \alpha)$ and $u_{\max} \equiv u_m(1)$, respectively. (29) and (29a) are plotted in Fig. 15 and Fig. 16.

4.3. General case: $T_1 < \infty$, $T_2 > 0$. — Provided that the differentiating and integrating circuits in the amplifier are quite independent and do not impose any electrical loading on each other, the output, pulse-shape $u(t)$ may

be computed from the following simultaneous equations:

$$(30) \quad \begin{cases} \dot{u}^* + (u^*/T_1) = \dot{v}(t), \\ \dot{u} + (u/T_2) = u^*/T_2, \end{cases}$$

where $u^*(t)$ denotes the intermediate pulse-shape after a mere differentiation.

Solving (30) for $u(t)$ and computing its maximum value u_m with respect to t , we get

$$(31) \quad u_m = x_1 \left[\frac{\{k \exp [v_m/x_1] - 1\}^{x_1/(x_1-x_2)}}{\{k \exp [v_m/x_2] - 1\}^{x_2/(x_1-x_2)}} - (k-1) \right] (*),$$

where $x_1 \equiv T_1/T$, $x_2 \equiv T_2/T$ and $k = (1/2) + \{1/(1-v_m)\}$.

If $T_1 = T_2 (\equiv T_0)$, then (31) takes the form

$$(32) \quad u_m = x_0 \left[\{k \exp [v_m/x_0] - 1\} \exp \left[\frac{-k(v_m/x_0) \exp [v_m/x_0]}{k \exp [v_m/x_0] - 1} \right] - (k-1) \right],$$

where $x_0 \equiv T_0/T$. Furthermore, if $x_0 = 1$, then (32) goes over into

$$(33) \quad u_m = (k \exp [v_m] - 1) \exp \left[\frac{-k v_m \exp [v_m]}{k \exp [v_m] - 1} \right] - (k-1).$$

Fig. 17 gives the plot of these results for various combinations of (x_1, x_2) . From Figs. 11, 14 and 17, it is concluded that a fairly good linearity may be

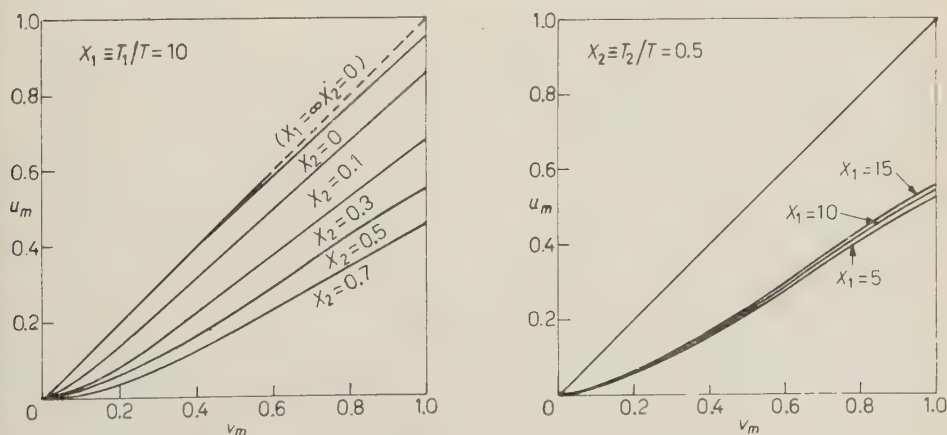


Fig. 17. - Non-linearity for $T_1 > T > T_2$, as calculated from (31).

(*) *Note added in proof.* - An expression very similar to (31) has been obtained independently by KOROLEV and KOCHAROV (*loc. cit.*) for a waveform slightly different from (22).

obtained even if we make $T_1 \geq T$, $T_2 \simeq T$, provided that α is considerably smaller unity. For α closer to unity, the condition for sufficient linearity may be simply written as $T_1 \gg T \geq T_2$.

* * *

The author would like to express his sincere gratitude to Professor E. TAJIMA for reading the manuscript and for many valuable comments. He is indebted to Assistant Professor T. DOKE for some of the basic ideas underlying the present calculation. He is also grateful to Professor T. TOYODA for helpful remarks on the calculation of amplifier linearity. Finally he wishes to thank Miss Y. ISHIBE for her aids in numerical computations.

RIASSUNTO (*)

Sulla base di un'analisi della forma d'onda si deriva una formula perfezionata dell'altezza dell'impulso per gli impulsi di griglia di una camera di ionizzazione a griglia. Si trova che la formula originale proposta da BOCHOGOV *et al.* diventa insufficiente in un lavoro accurato, quando il tempo di permanenza, t_2 , degli elettroni nella zona griglia-collettore non è trascurabile rispetto al tempo di permanenza, b_1 , nella zona catodo-griglia. Si dimostra che l'altezza negativa degli impulsi di griglia dovuti a particelle emesse dal collettore o dalla griglia, è molto piccola rispetto a quelle dovute a particelle provenienti dal catodo, purchè $t_2 \ll t_1$. Si studia analiticamente anche la distorsione nelle distribuzioni delle altezze degli impulsi, generata dallo spessore finito della sorgente e dall'ampiezza finita della banda dell'amplificatore.

(*) Traduzione a cura della Redazione.

Spettrometro a scintillazione con riduzione del contributo Compton.

C. MANDUCHI, G. NARDELLI e M. T. RUSSO-MANDUCHI

Istituto Nazionale di Fisica Nucleare - Sezione di Padova
Istituto di Fisica dell'Università - Padova

(ricevuto il 3 Luglio 1961)

Riassunto. — Si descrive uno spettrometro a scintillazione per raggi γ , costituito da un cristallo di NaI(Tl) contenuto in un cilindro di plastico scintillatore in anticoincidenza: il sistema è in grado di ridurre sensibilmente gli effetti relativi a radiazione non integralmente assorbita nel cristallo. Lo spettrometro descritto si dimostra vantaggioso nella risoluzione di spettri γ con eventi a frequenza relativamente bassa, che per la loro energia possono essere confusi nella distribuzione Compton di raggi γ con energia e frequenza più elevate. L'applicazione dello spettrometro appare inoltre conveniente quando non è possibile una collimazione della radiazione γ , e nello studio di correlazioni angolari.

1. - Introduzione.

Negli spettrometri a scintillazione per raggi γ l'interpretazione della distribuzione in ampiezza degli impulsi elettrici conseguenti a radiazioni mono-energetiche è generalmente complicata, per i diversi processi secondari che accompagnano l'assorbimento dei fotoni nel cristallo.

Diversi sono i metodi proposti per ridurre l'importanza relativa di tali processi. Spettrometri costituiti da più cristalli in coincidenza ⁽¹⁾, in grado di distinguere eventi relativi a processi di diffusione Compton o produzione di coppie, consentono una migliore risoluzione. Tuttavia essi presentano lo svantaggio di un'efficienza generalmente bassa, e la loro applicazione è limitata a quelle energie per le quali la sezione d'urto del processo considerato è sufficientemente elevata.

L'impiego di cristalli di NaI(Tl) di notevoli dimensioni ⁽²⁾ ha il vantaggio

⁽¹⁾ R. HOFSTADTER e J. A. MCINTYRE: *Phys. Rev.*, **78**, 619 (1950); J. K. BAIR e F. G. MAIENSCHIN: *Rev. Sci. Instr.*, **22**, 343 (1951).

⁽²⁾ P. R. BELL, in K. SIEGBAHN: *β - and γ -Ray Spectroscopy* (Amsterdam, 1955), pp. 138, 155.

di diminuire il contributo spettrale relativo all'effetto Compton, consentendo una ragguardevole estensione dell'analisi spettrometrica. Sussistono tuttavia problemi, quali lo studio di correlazioni angolari e la spettrometria ad alta risoluzione, per i quali è necessario ricorrere a cristalli di dimensioni ridotte. Per diminuire il contributo Compton è peraltro conveniente impiegare uno schermo scintillatore in anticoincidenza. Nello spettrometro di ALBERT ⁽³⁾ il cristallo rivelatore era circondato da frammenti di NaI(Tl) in bagno di olio: ROULSTON e NAQVI ⁽⁴⁾ hanno invece adottato come schermo un cilindro di scintillatore plastico, introducendo nel sistema la sorgente in esame, con conseguente limitazione dell'attività di questa e delle possibili applicazioni del dispositivo.

Al fine di migliorare le prestazioni spettrometriche di un cristallo di di-

mensioni relativamente piccole, è stato messo a punto uno spettrometro per raggi γ analogo, in linea di principio, al sistema proposto da ROULSTON e NAQVI, ma che da questo si differenzia per alcune caratteristiche inerenti essenzialmente alle dimensioni ed all'efficienza del plastico scintillatore, all'elettronica ed alla geometria del dispositivo.

2. - Dispositivo sperimentale.

Lo spettrometro è illustrato in Fig. 1. Esso è costituito da un cristallo di NaI(Tl) per l'analisi spettrometrica, contenuto in un cilindro di plastico scintillatore. I fotoni relativi alla radiazione γ che non ha ceduto integralmente la sua energia al cristallo, possono interagire con lo scintillatore

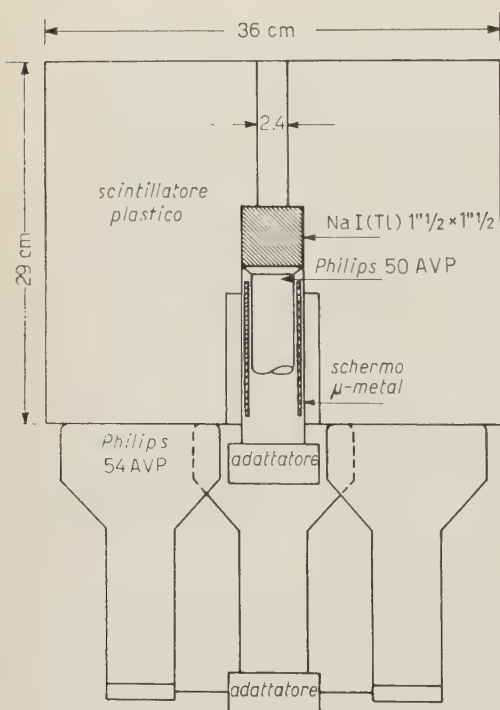


Fig. 1.

plastico; gli impulsi elettrici corrispondenti alle scintillazioni rivelate da tre fotomoltiplicatori sono posti in anticoincidenza con i segnali del fotomoltiplicatore connesso col cristallo, che pertanto vengono eliminati.

⁽³⁾ R. D. ALBERT: *Rev. Sci. Instr.*, **24**, 1096 (1953).

⁽⁴⁾ K. I. ROULSTON e S. I. H. NAQVI: *Rev. Sci. Instr.*, **27**, 830 (1956).

Il cristallo impiegato è un cilindro di NaI(Tl) di tipo commerciale, con diametro e altezza di 3.75 cm, montato su un fotomoltiplicatore 50 AVP selezionato. Il fotomoltiplicatore, provvisto di schermo magnetico, è contenuto in un cilindro di alluminio a pareti sottili, solidale col cristallo.

Lo scintillatore plastico è costituito da un cilindro di polistirolo, in cui sono disciolti in percentuale opportuna p-terfenile e POPOP: il diametro esterno del plastico è di 36 cm e l'altezza di 29 cm, mentre la cavità cilindrica superiore ha un diametro di 2.4 cm e quella inferiore di 7.5 cm. Per la costruzione dello scintillatore plastico è stato impiegato un procedimento di polimerizzazione particolarmente semplice: l'efficienza di scintillazione, rispetto ad altri plastici commerciali di normale impiego, risulta superiore di circa il 10%. La superficie laterale del plastico è rivestita di una vernice bianca diffondente, e sulla base superiore è disposta una pellicola di plastica previamente metallizzata con un sottile strato di argento; alla base inferiore sono connessi otticamente tre fotomoltiplicatori 54 AVP.

Il sistema è contenuto in un cilindro di alluminio a tenuta di luce; uno schermo di piombo, di 3 cm di spessore, può essere installato attorno e sopra il dispositivo.

La frequenza elevata delle scintillazioni nel plastico, in conseguenza delle sue dimensioni, richiede un dispositivo elettronico con tempi risolutivi brevi (Fig. 2). È stato pertanto predisposto un circuito di coincidenza con tempi

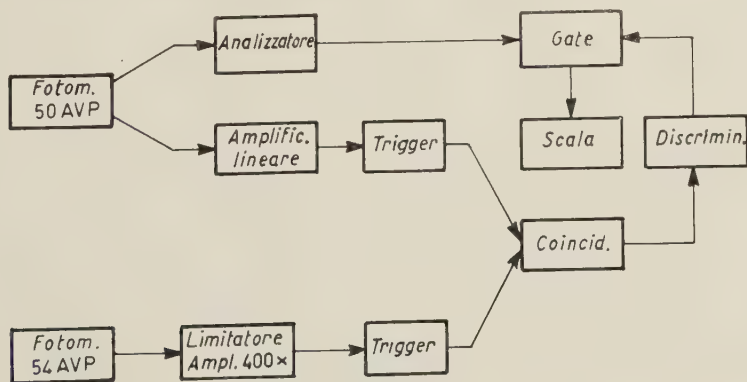


Fig. 2.

risolutivi variabili da $80 \cdot 10^{-9}$ a $150 \cdot 10^{-9}$ s, al quale sono inviati i segnali relativi al plastico e al cristallo, tramite circuiti a scatto in grado di fornire impulsi di 15 V, con tempo di salita di $8 \cdot 10^{-9}$ s, per segnali d'ingresso di ampiezza superiore a 20 mV. Gli impulsi relativi al plastico scintillatore sono prelevati agli anodi dei fotomoltiplicatori 54 AVP connessi in parallelo, ed amplificati, previa livellazione, mediante un amplificatore rapido di tipo convenzionale; gli impulsi relativi al cristallo sono prelevati all'ultimo dinodo del fotomoltiplicatore 50 AVP, ed amplificati, previo adattamento, mediante un ampli-

cattore lineare. L'anodo del fotomoltiplicatore fornisce gli impulsi per l'analisi spettrometrica, effettuata per mezzo di un analizzatore monocanale; i segnali dell'analizzatore sono inviati ad un contatore di impulsi tramite un circuito di anticoincidenza, che risponde solo allorché un impulso dell'analizzatore non è accompagnato da un segnale del discriminatore connesso al circuito di coincidenza.

3. - Analisi di alcuni spettri gamma.

Allo scopo di mettere in evidenza alcune prestazioni dello spettrometro descritto, sono stati registrati gli spettri γ di diversi nuclidi. Le sorgenti sono state fornite dal Centro di Radiochimica di Amersham (U.K.).

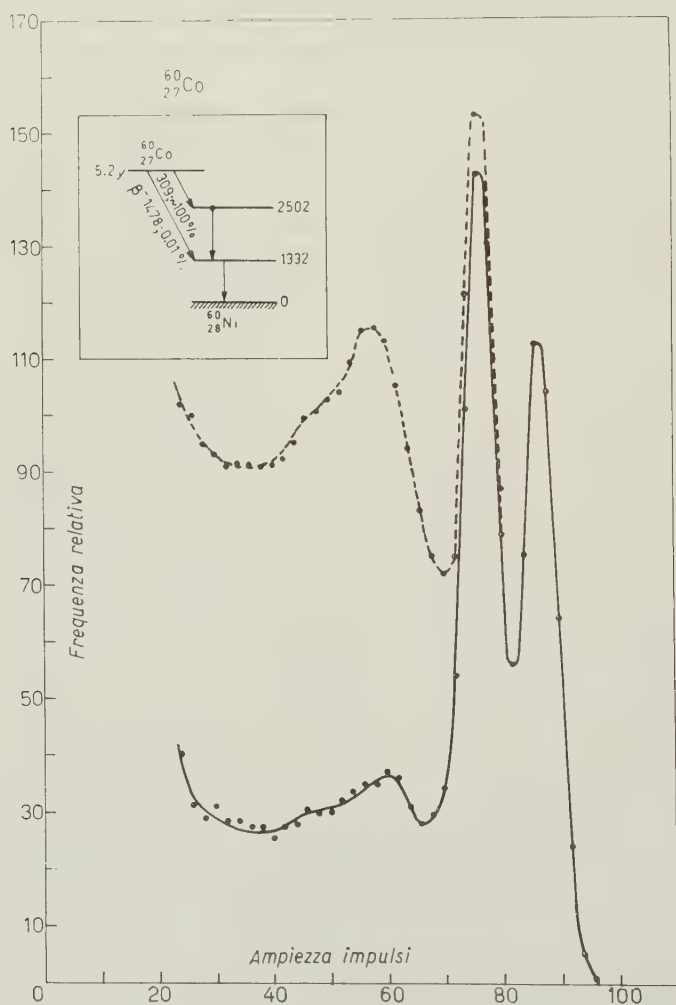


Fig. 3.

La collimazione dei raggi γ è stata effettuata mediante un foro di 0.8 cm di diametro lungo l'asse di un cilindro di piombo: risulta tuttavia che una diversa collimazione non modifica i risultati spettrometrici del sistema in anticoincidenza, mentre può variare in modo apprezzabile lo spettro relativo al cristallo semplice.

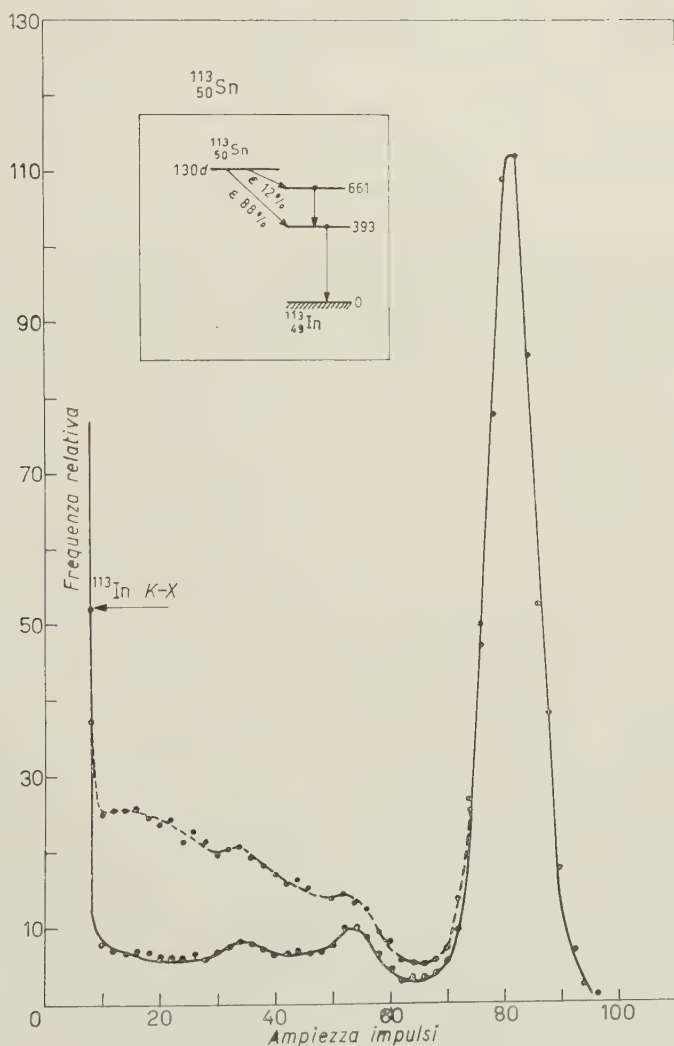


Fig. 4.

In Fig. 3 è riportato lo spettro del ^{60}Co : il picco fotoelettrico rimane invariato con il plastico in anticoincidenza, mentre il contributo Compton appare ridotto di circa il 70%.

La Fig. 4 illustra lo spettro del ^{113}Sn , il quale decade in $^{113}\text{In}^m$ per cattura elettronica. Lo stato isomerico del ^{113}In decade allo stato fondamentale con emissione di un fotone di 392 keV, o mediante conversione interna; è tuttavia possibile mettere in evidenza un picco a 258 keV, generalmente confuso nella

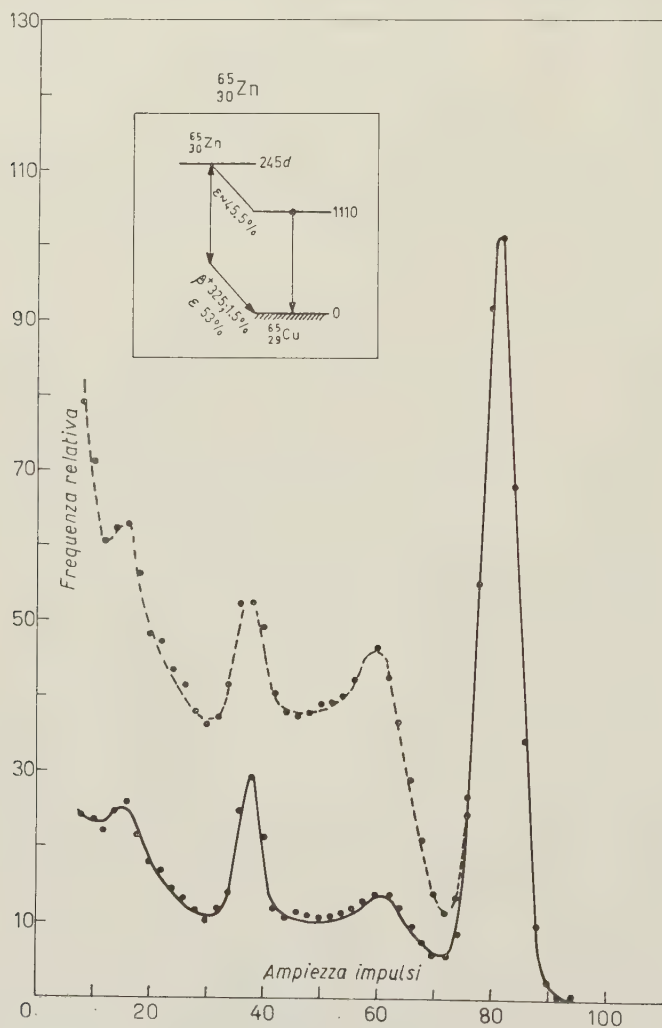


Fig. 5.

distribuzione Compton, corrispondente ad un livello eccitato di 650 keV del ^{113}In , in accordo con recenti risultati sperimentali ⁽⁵⁾.

Un vantaggio notevole dello spettrometro descritto è evidente in Fig. 5.

⁽⁵⁾ S. B. BURSON, H. A. GRECH e L. C. SCHMID: *Phys. Rev.*, **115**, 188 (1959).

Lo spettro del ^{65}Zn presenta un picco a 511 keV, che corrisponde all'emissione di positoni nella transizione allo stato fondamentale del ^{65}Cu ; lo scintillatore in anticoincidenza, sopprimendo parzialmente la distribuzione Compton relativa ai raggi γ di 1.114 MeV, permette una migliore definizione del contributo dei positoni nel processo di decadimento.

S U M M A R Y

A spectrometer has been designed in which a small NaI(Tl) crystal is surrounded by a large plastic phosphor: the output from the crystal is put in anticoincidence with the output from the plastic. This system reduces the Compton contribution in the scintillation spectrum, and enables certain spectral features to be identified.

Una camera a fissione per il controllo dell'intensità di un fascio neutronico collimato.

G. P. FELCHER, F. GAZZARRINI e G. POLETTI

Laboratori C.I.S.E. - Segrate (Milano)

(ricevuto il 3 Agosto 1961)

Riassunto. — Si descrive la costruzione di una camera a fissione a strato di uranio da utilizzare come « monitor » in un fascio strettamente collimato di neutroni uscenti da un reattore. Si discute l'influenza della pressione del gas di riempimento e della tensione di polarizzazione sul comportamento della camera. Si descrive un metodo di deposizione elettrolitica dell'uranio che presenta notevoli vantaggi sui procedimenti di preparazione di strati sottili di uranio reperibili nella letteratura.

1. — È usuale, in esperienze compiute con un fascio collimato di neutroni proveniente da un reattore, interporre sul fascio stesso un rivelatore, il quale dia una risposta proporzionale all'intensità istantanea del flusso neutronico, in modo da poter tener conto di eventuali fluttuazioni di intensità del fascio. Un simile rivelatore deve evidentemente avere come principali caratteristiche un assorbimento neutronico molto basso, onde non diminuire in misura sensibile l'intensità del fascio che lo attraversa, una alterazione pressochè nulla delle condizioni di collimazione ed una buona discriminazione tra neutroni e radiazioni γ . Inoltre è desiderabile che presenti caratteristiche di riproducibilità assai buone, dal momento che deve essere usato anche in esperienze molto prolungate. La sensibilità infine deve potersi variare entro limiti abbastanza ampi ed il conteggio deve essere il più possibile indipendente dalla tensione applicata e dalla polarizzazione del discriminatore. Il problema viene generalmente risolto interponendo nel fascio di neutroni un contatore proporzionale a BF_3 , di piccole dimensioni tale da coprire la minore area possibile. Tuttavia una camera a fissione, che intercetti completamente il fascio e che

soddisfi ai requisiti sopra indicati, presenta un certo numero di vantaggi sul contatore a BF_3 , e la sua utilizzazione appare raccomandabile in problemi di questo genere ⁽¹⁾.

Infatti, se è vero che la sensibilità di un contatore a fissione è circa 100 volte minore di quella di un contatore a BF_3 , ciò non interessa nella maggior parte dei casi, mentre è vero che la discriminazione tra neutroni e radiazioni γ sta nello stesso rapporto 1:100 a vantaggio però del contatore a fissione.

È noto inoltre che soprattutto in presenza di alti flussi γ , come nel caso da noi considerato, i contatori proporzionali a BF_3 subiscono un rapido deterioramento, che altera in modo drastico le caratteristiche di conteggio. Ciò non accade per una camera a fissione, il cui funzionamento riproducibile può protrarsi per lungo tempo e la cui manutenzione risulta molto più semplice, data l'assenza di gas corrosivi ⁽²⁾.

Un altro vantaggio del contatore a fissione sta nel fatto che esso richiede per il suo funzionamento una tensione di operazione molto minore; non essendovi amplificazione nel gas, lo spettro degli impulsi in uscita risulta, in un campo di tensioni opportunamente scelto, praticamente indipendente dalla tensione applicata.

È stata pertanto costruita una camera di ionizzazione a fissione a strato di uranio, il cui funzionamento è apparso estremamente soddisfacente e riproducibile nel corso di parecchi mesi.

2. - La camera a fissione, del tipo a elettrodi affacciati, è interamente costruita in anticorodal, mentre le parti isolanti sono costruite in teflon. Un passante Stupakoff assicura l'isolamento elettrico fra l'elettrodo a tensione e le « pareti » della camera, che vengono collegate a massa.

L'elettrodo ricoperto con materiale fissile, circolare con un diametro di 8 cm, funziona da catodo. La separazione fra gli elettrodi è di 0.5 cm, in modo da avere un volume totale sensibile di circa 25 cm³.

Poichè l'elettrodo collettore è ad alta tensione, si è reso necessario associare al contatore un circuito di disaccoppiamento degli impulsi. Tale disaccoppiatore ha una costante di tempo di differenziazione RC dell'ordine di 10^{-2} s, in modo tale da non alterare nè la forma nè i tempi caratteristici di salita e di discesa degli impulsi. Il segnale così prelevato dalla camera viene fatto passare attraverso un preamplificatore veloce a basso rumore di fondo e quindi inviato ad una catena di conteggio convenzionale.

Al fine di ridurre al minimo l'attenuazione del fascio neutronico, le pareti della camera in corrispondenza all'elettrodo coperto di uranio sono state assottigliate fino a raggiungere uno spessore di 0.5 mm di anticorodal; lo spessore

⁽¹⁾ L. SANI e F. ZANCHI: CNEN-37 (1960).

⁽²⁾ Y. M. MCKENZIE: *Nucleonics*, **17**, 1, 60 (1959).

del piattello ricoperto di uranio, costruito in alluminio nichelato elettroliticamente è stato anch'esso portato a 0.5 mm.

In tali condizioni l'attenuazione totale dell'intensità del fascio da parte della camera di ionizzazione è risultata del 2% circa. (La sezione d'urto totale dell'anticorodal è di circa 2 barn).

3. - La preparazione dello strato di uranio, depositato su di un supporto metallico, costituisce in genere la parte più critica nella costruzione di una camera a fissione. È noto infatti che strati di uranio depositati con varie tecniche si deteriorano in modo drastico nel corso di pochi giorni: ciò è ovviamente fonte di irriproducibilità nelle misure.

La scelta del supporto metallico è ancora determinata dalla condizione di minima attenuazione del fascio di neutroni: sono stati pertanto sperimentati l'alluminio, alcune leghe leggere e l'acciaio inossidabile, poichè quest'ultimo, per le sue caratteristiche meccaniche, può essere più facilmente ridotto in spessore (fino a circa 0.3 mm). Questi appaiono essere materiali particolarmente adatti allo scopo poichè hanno sezioni d'urto totali basse per neutroni lenti.

Sono state descritte preparazioni di strati di uranio ⁽³⁻⁵⁾ facendo evaporare sul sostegno metallico una soluzione titolata di un sale di uranio e fissando in seguito il residuo con un opportuno legante. Le prove effettuate hanno però mostrato che durante l'evaporazione l'uranio non si deposita in modo uniforme e che spesso il legante (nel nostro caso una soluzione di araldite in acetone) non riesce a fissare completamente la polvere ricca di uranio, determinando in tal modo una contaminazione del contatore.

Simili inconvenienti poterono essere evitati mediante procedimenti di deposizione elettrolitica. La preparazione di strati di uranio su acciaio inossidabile non presenta problemi, essendo possibile preparare in tal caso strati uniformi ed aderenti con rese elevate, fino a spessori dell'ordine di 0.33 mg/cm² ⁽⁶⁾.

Tuttavia va tenuto conto del fatto che l'attenuazione del fascio neutronico dovuto ad uno spessore di 0.3 mm di acciaio inossidabile è valutabile al 3 % circa, mentre quella dovuta ad uno spessore di 0.5 mm di alluminio è pari al 6% circa. Si è ritenuto utile quindi un tentativo di depositare strati di uranio su alluminio e su leghe leggere seguendo i procedimenti descritti nella letteratura ^(7,8)

⁽³⁾ U. FACCHINI, M. FORTE, A. MALVICINI e T. ROSSINI: *Nucleonics*, **14**, 9, 126 (1956).

⁽⁴⁾ S. SCIUTI e D. PROSPERI: *Proc. Second Intern. Conf. Peaceful Uses Atomic Energy*, P/1398 (1959), p. 568.

⁽⁵⁾ C. L. GARAVELLI: C.N.G.-51 (1960).

⁽⁶⁾ F. CIANFLONE, F. GAZZARRINI e C. TRIULZI: CISE-86 (1961).

⁽⁷⁾ L. KOCH: *Journ. Nucl. Energy*, **2**, 110 (1955).

⁽⁸⁾ C. WILSON e A. LANGER: *Nucleonics*, **11**, 8, 48 (1953).

Il metodo descritto da Koch non ha dato risultati nè riproducibili nè soddisfacenti, non ottenendosi un deposito sufficientemente aderente. Vi è inoltre da notare che la criticità delle condizioni sperimentali, la bassissima resa ($5 \div 10$)% nelle migliori condizioni) e la notevolissima concentrazione di uranio el bagno elettrolitico rendono tale metodo di scarsa praticità.

WILSON e LANGER consigliano di ricoprire il supporto di alluminio con un sottile strato di zinco e di effettuare quindi la deposizione elettrolitica dell'uranio sullo zinco. Anche in questo modo i risultati non appaiono soddisfacenti: i depositi sono poco aderenti e la resa del processo è assolutamente irriproducibile. Inoltre in varie occasioni si è notata la presenza di zinco nel bagno elettrolitico: infatti in presenza di una soluzione di ossalato di ammonio lo zinco manifesta una tendenza a passare in soluzione formando un complesso.

Non apparve d'altra parte possibile depositare l'uranio direttamente su alluminio anche dopo avere sottoposto la superficie a vari trattamenti, quali l'eliminazione totale dello strato di ossido mediante energico decapaggio con soda caustica e la passivazione mediante ebollizione in acqua distillata.

Prove orientative indicarono però la possibilità di ottenere strati soddisfacenti su nichel, suggerendo che il problema poteva essere risolto ricoprendo la superficie di alluminio con un sottilissimo strato di nichel, dell'ordine di qualche micron. Varie prove effettuate su alluminio nichelato elettroliticamente confermarono questo fatto e diedero risultati del tutto soddisfacenti e riproducibili.

È stata costruita una cella in cui il piattello su cui si effettuava il deposito copriva completamente il fondo. Ciò era necessario al fine di rendere quanto più uniforme possibile il deposito e di aumentare al tempo stesso il rendimento del processo.

La superficie del piattello, lucidata a specchio meccanicamente, veniva completamente sgrassata mediante strofinatura con cotone imbevuto di una soluzione di SnCl_2 e poi lavata con acqua distillata fino a completa bagnabilità.

Il bagno elettrolitico era costituito da una soluzione di 0.1 M di ossalato di ammonio, che veniva mantenuta costantemente in agitazione dalla rapida rotazione dell'elettrodo di platino (circa 200 giri/min), che fungeva da anodo. La temperatura del bagno era mantenuta a 85°C mediante termostato e la densità di corrente era 0.05 A/cm^2 . Poichè la deposizione di uranio in presenza di ossalato di ammonio avviene in ambiente alcalino, veniva aggiunto idrato ammonico fino a raggiungere un valore del pH pari a $8 \div 9$. Si portava a temperatura e si faceva passare corrente per circa 15 min con una densità di 0.025 A/cm^2 . Si interrompeva quindi il passaggio della corrente, si aggiungeva l'uranio in quantità opportuna, prelevandolo da una soluzione titolata di nitrato di uranile, e si riportava al pH indicato mediante aggiunta di idrato ammonico. Un'ora di elettrolisi era generalmente sufficiente per ottenere strati

uniformi ed aderenti di spessore fino a 0.4 mg/cm^2 con rese elevate. La quantità di uranio depositata veniva poi calcolata *a posteriori* misurando l'attività α della sorgente.

4. - Per determinare le migliori condizioni di lavoro del contatore, sono state fatte misure variando la pressione del gas di riempimento e la tensione di alimentazione.

Le curve sotto riportate sono state ottenute interponendo la camera sul fascio di neutroni termici proveniente da uno dei canali del reattore L 54 del CESNEF. Lo strato fissile impiegato era di 0.1 mg/cm^2 di uranio arricchito al 20% nell'isotopo ^{235}U e la potenza del reattore di 500 W, corrispondente ad un flusso di circa $3 \cdot 10^4$ neutroni/ $\text{cm}^2 \text{ s}$ nelle nostre condizioni di misura. Nella camera era stato fatto un vuoto dell'ordine di 10^{-5} mm di Hg ed era stato poi immesso argon purificato mediante circolazione su lega Ca-Mg. Nelle misure descritte la pressione è stata fatta variare tra 1 e 4 atmosfere e la tensione tra 300 e 1200 V.

In Fig. 1 sono riportate le curve di taglio ottenute a varie pressioni del gas di riempimento del contatore per una tensione di alimentazione costante. Tali curve mostrano che una pressione piuttosto bassa ha l'effetto di migliorare la discriminazione tra impulsi di fissione ed impulsi provenienti dalla attività α dell'uranio. Di conseguenza aumenta il conteggio dovuto a fissioni in corrispondenza del pianerottolo di lavoro, mentre il pianerottolo stesso diminuisce in pendenza ed aumenta in estensione.

La Fig. 2 mostra le curve di taglio ottenute a pressione costante per vari valori della tensione di alimentazione.

Dall'esame delle curve sperimentali si conclude che le migliori condizioni di funzionamento del contatore si ottengono per $T = 300 \text{ V}$ e $p = 760 \text{ mm Hg}$. La curva corrispondente è riportata in Fig. 1.

In tali condizioni il tempo di salita degli impulsi nella camera è di circa $0.5 \mu\text{s}$, sufficientemente breve cioè per permettere la collezione dei soli elettroni. Nelle presenti condizioni di lavoro il pile-up degli impulsi è totalmente trascurabile.

Per uno strato fissile di 0.1 mg/cm^2 di uranio arricchito al 20% nell'isotopo ^{235}U , la sensibilità del contatore è risultata uguale a $2.5 \cdot 10^{-4}$. Con un simile strato la camera qui descritta raggiunge pienamente il suo scopo per flussi di neutroni termici compresi tra 10^3 e 10^8 neutroni/ $\text{cm}^2 \text{ s}$. Per flussi istantanei al di fuori di questo intervallo si possono agevolmente ottenere conteggi convenienti variando lo spessore dello strato di uranio, o l'arricchimento dell'uranio stesso.

Data la relativamente piccola differenza di potenziale da applicare agli elettrodi, è stata adottata una alimentazione a pile.

Numerose misure di fondo e di stabilità del contatore, eseguite a lunghi intervalli di tempo, hanno mostrato che il fondo è praticamente inesistente e la stabilità del tutto soddisfacente.

È stato inoltre verificato sperimentalmente che interponendo il

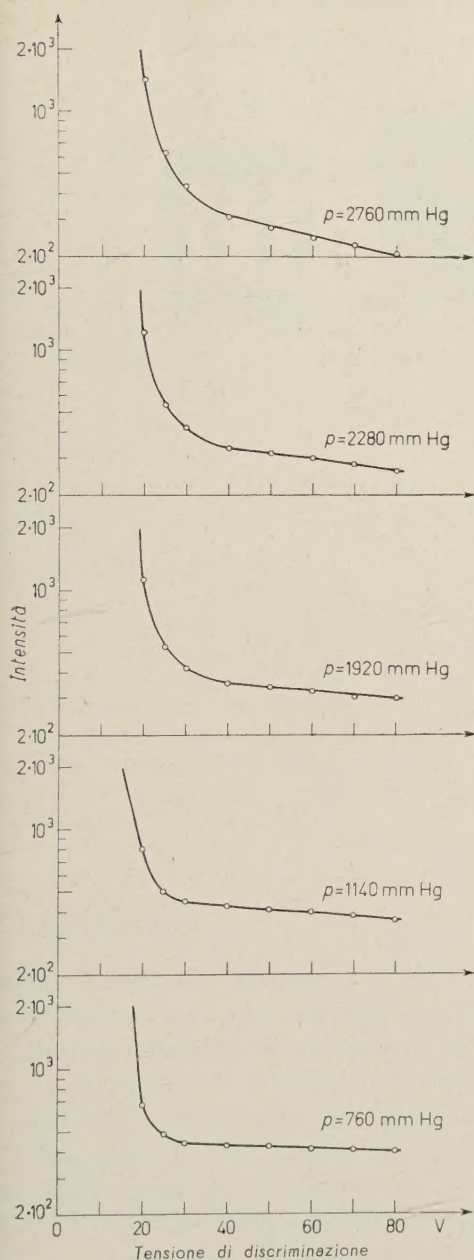


Fig. 1. — Influenza della pressione del gas di riempimento. Le curve sono state ottenute con una tensione di alimentazione costante $T=300$ V.

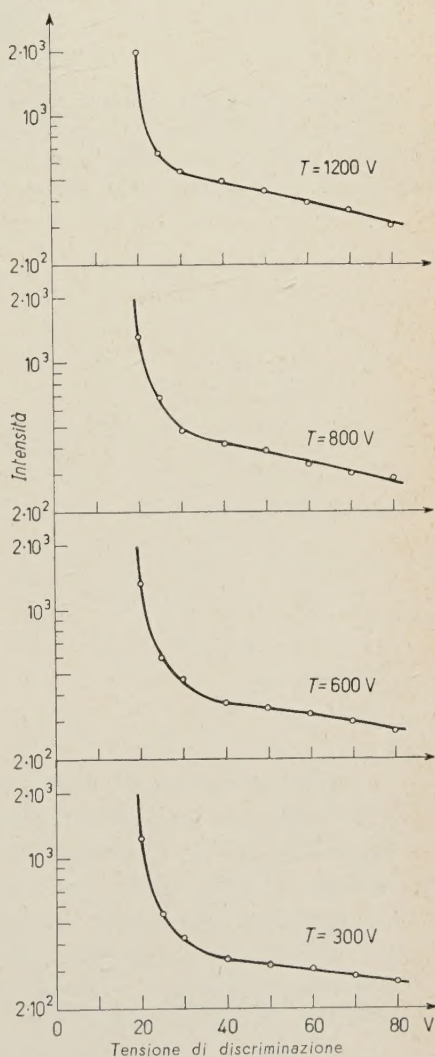


Fig. 2. — Influenza della tensione di polarizzazione. Le curve sono state ottenute con una pressione costante del gas di riempimento $p=2280$ mm Hg.

suddetto contatore in un fascio neutronico strettamente collimato (divergenza angolare dell'ordine di $20'$), la collimazione non risulta sensibilmente alterata.

SUMMARY

A thin layer fission chamber, which is to be used as a monitor in a collimated slow neutron beam from a reactor, is described. The influence of the pressure of the filling gas and of the voltage is discussed. A description of the electrodeposition of thin layers of uranium is also given.

PROPRIETÀ LETTERARIA RISERVATA

Direttore responsabile: G. POLVANI

Tipografia Compositori - Bologna

Questo fascicolo del *Supplemento* è stato licenziato dai torchi il 29-VII-1961